REPORT DOCUMENTATION PAGE		READ INSTRUCTIONS BEFORE COMPLETING FORM
1. REPORT NUMBER	2. GOVT ACCESSION NO. AD-A087563	3. RECIPIENT'S CATALOG NUMBER
4. TITLE (and Subtitle) Centrifugal Modelling of Transient Water Flow in Earth Embankments		5. TYPE OF REPORT & PERIOD COVERED Final Report 7 May 80
		6. PERFORMING ORG. REPORT NUMBER
7. AUTHOR(s) Kenneth Wylie Cargill		8. CONTRACT OR GRANT NUMBER(s)
9. PERFORMING ORGANIZATION NAME AND ADDRESS Student HQDA, MILPERCEN (DAPC-OPP-E) 200 Stovall Street Alexandria, VA 22332		10. PROGRAM ELEMENT, PROJECT, TASK AREA & WORK UNIT NUMBERS
11. CONTROLLING OFFICE NAME AND ADDRESS HQDA, MILPERCEN, ATTN:DAPC-OPP-E 200 Stovall Street Alexandria, VA 22332		12. REPORT DATE 7 May 80
		13. NUMBER OF PAGES 161
14. MONITORING AGENCY NAME & ADDRESS(If different from Controlling Office)		15. SECURITY CLASS. (of this report) Unclassified
		15a. DECLASSIFICATION/DOWNGRADING SCHEDULE

LEVEL

16. DISTRIBUTION STATEMENT (of this Report)

Approved for public release; distribution unlimited.

17. DISTRIBUTION STATEMENT (of the abstract entered in Block 20, if different from Report)

18. SUPPLEMENTARY NOTES

19. KEY WORDS (Continue on reverse side if necessary and identify by block number)

Geotechnical, Earth Embankment, Transient Flow, Centrifugal Modelling, Phreatic Surface, Water Flow, Pore Pressures

20. ABSTRACT (Continue on reverse side if necessary and identify by block number)

This thesis examines the phenomenon of transient water flow in earth embankments as modelled in a geotechnical centrifuge. The theory and equations governing transient water flow are presented and current solution techniques are outlined. It is hypothesized that better solutions are obtainable through centrifugal modelling of the process. In order to interpret→

DD FORM 1 JAN 73 1473 EDITION OF 1 NOV 65 IS OBSOLETE

the experimental results, theoretical scaling relations for
quantities pertinent to transient water flow are developed
through consideration of the basic independent variables
governing the flow. Testing was conducted on a 10-g ton
centrifuge in a container specially constructed for the
test series. Acceleration levels of 25 g, 37.5 g, and 50 g
were used. Pore pressures were measured and recorded during
the transient rise and fall of the headwaters by four miniature
pressure transducers. From these data, histories of total
head as a function of time and equipotentials during
headwater rise and drawdown are plotted. Steady state flow
rates are also measured. Analysis of the data leads to the
conclusion that theoretical scaling relations are valid and
that this method does indeed give a better understanding
of the phenomenon of transient flow and may be useful in
design practice.

Accession For

NTIS GRA&I	☑
DDC TAB	☐
Unannounced	☐
Justification	

By

Distribution/

Availability Codes

Dist	Avail and/or special
A	

Centrifugal Modelling of Transient Water Flow
in Earth Embankments

Captain Kenneth W. Cargill
HQDA, MILPERCEN (DAPC-OPP-E)
200 Stovall Street
Alexandria, VA 22332

Final Report   7 May 1980

Approved for public release; distribution unlimited.

A thesis submitted to University of Colorado, Boulder,
Colorado, in partial fulfillment of the requirements
for the degree of Master of Science.

CENTRIFUGAL MODELLING OF

TRANSIENT WATER FLOW IN EARTH

EMBANKMENTS

by

Kenneth Wylie/Cargill

B.C.E., Georgia Institute of Technology, 1971

9) Final rpts   *11) 7 May '8*

12) 178

A thesis submitted to the Faculty of the Graduate

School of the University of Colorado in partial

fulfillment of the requirements for the degree of

Master of Science

Department of

Civil, Environmental, and Architectural Engineering

1980

391171

This Thesis for the Master of Science Degree by

Kenneth Wylie Cargill

has been approved for the

Department of

Civil, Environmental, and Architectural Engineering

by
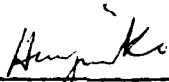
_____
Hon-Yim Ko
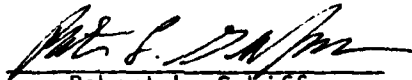
_____
Robert L. Schiffman

Date ___May 7, 1980___

Cargill, Kenenth Wylie (M.S., Civil Engineering)

Centrifugal Modelling of Transient Water Flow in Earth Embankments

Thesis directed by Professor Hon-Yim Ko

This thesis examines the phenomenon of transient water flow
in earth embankments as modelled in a geotechnical centrifuge.
The theory and equations govening transient water flow are pre-
sented and current solution techniques are outlined. It is hypo-
thesized that better solutions are obtainable through centrifugal
modelling of the process. In order to interpret the experimental
results, theoretical scaling relations for quantities pertinent to
transient water flow are developed through consideration of the
basic independent variables governing the flow. Testing was con-
ducted on a 10-g ton centrifuge in a container specially constructed
for the test series. Acceleration levels of 25 g, 37.5 g, and 50 g
were used. Pore pressures were measured and recorded during the
transient rise and fall of the headwaters by four miniature pres-
sure transducers. From these data, histories of total head as a
function of time and equipotentials during headwater rise and draw-
down are plotted. Steady state flow rates are also measured.
Analysis of the data leads to the conclusion that theoretical
scaling relations are valid and that this method does indeed give
a better understanding of the phenomenon of transient flow and may
be useful in design practice.

This abstract is approved as to form and content.

Signed   _Hon-Yim Ko_

Faculty member in charge of thesis

ACKNOWLEDGEMENTS

I would here like to recognize and thank those people who have so greatly contributed to the successful completion of this research and writing.

To Professor Hon-Yim Ko whose professional expertise and guidance were so instrumental in the accomplishment of this work, I will be eternally grateful. To my wife Pat and sons, Kevin and Ethan, I thank you for your understanding during the past year and will try to be more available during the coming year. In the experimental portion of this research, the assistance of Myoung Mo Kim deserves special recognition, and in bringing it to final typed form I thank all the secretaries of the CE Department and especially Liz Stimmel for the final typing. Acknowledgement is also given to the United States Bureau of Reclamation for financial support to the research.

TABLE OF CONTENTS

LIST OF TABLES

LIST OF FIGURES

CHAPTER I

INTRODUCTION

Of all the engineering disciplines, the one most often referred to as an art is Geotechnical Engineering. Among geotechnical engineers, the activity most often referred to as an art is earth embankment design. The reason for this is that nature's materials and nature's forces are the principal ingredients of any earth embankment, and as is often said, nature is sometimes unpredictable. Yet, we are able to construct earth dams hundreds of feet in height with every confidence that they will perform satisfactorily and safely through the worst of natural occurrences. Our ability to do this results from years of successful and sometimes not so successful experience with similar earth dams. Laboratory testing and quality control in the field have taken a lot of the uncertainties out of material selection and placement, but when it comes to predicting how these materials will respond or change under the influence of nature's forces, we find ourselves having to generalize and idealize to a large extent. The most common and one of the most devastating of these natural forces is transient water. Even with all the experience and confidence developed through the years, the occasional failure which is invariably caused by transient water in some manner reminds us that more experience is needed but not at the expense of more failure.

There has been considerable experience gained in many areas of the geotechnical field through full scale testing and laboratory simulation. However, experience on the effects of transient water flow through earth embankments by such testing programs is practically non-existent due to the great expense of full scale tests and the fact the phenomenon cannot be simulated by normal laboratory methods. The purpose of the research this paper represents is to develop a procedure whereby laboratory experience can be gained on transient water flow by modelling the phenomenon in a centrifuge and to investigate the effects of this flow through some simple soils.

The use of a geotechnical centrifuge in testing soil structures is continually gaining in popularity. It is the only method outside of full scale tests which permits proper representation of body forces. These forces play a predominant role in many soil problems and in the representation of flow through an embankment they are the only forces of any consequence. Therefore, if meaningful laboratory experience is to be gained, it will have to result from centrifugal testing.

This paper is organized to first examine the theoretical basis for predicting transient water flow through soil. As will be shown, this basis contains so many idealizing assumptions that it is practically useless for anything more than academic problems. Regardless of this, there has been attempts to solve real problems and some of these methods are examined.

Any intepretation of the results from centrifuge testing requires an understanding of the scaling relationships between model and the prototype it represents. These relationships are developed for quantities pertinent to the transient flow problem by consideration of the basic problem variables. The influence each variable has on a scaling relation is shown to facilitate analysis of experimental results.

The testing apparatus and procedure is next described. The main component of the system is a 10-g ton geotechnical centrifuge with swinging baskets. The sample container was specially constructed for the testing program, but measuring and monitoring equipment are all standard shelf items. A test series basically involves testing the same sample at different g levels while monitoring pore water pressures at different points in the sample. Each test consists of three phases; a rising headwater, steady state flow, and then headwater drawdown. Four different soils are used in each series of tests.

The results of each test are pore pressure histories for each point monitored. These pressures are converted to heads and added to the elevation heads of the monitoring points. The total head is then plotted on a time scale for use in determining equipotential distributions during the three phases of the test which are also plotted. These figures are consolidated in the appendix for easier reference. Flow rates were also measured during steady state flow. The results of the testing program are then used to develop scaling relations for comparison with the theoretical relationships developed earlier.

CHAPTER II

THE TRANSIENT PHREATIC SURFACE IN EARTH EMBANKMENTS

The transient phreatic surface phenomenon in earth embankments
is a complex problem. An analytical solution for real embankment
shapes and boundary conditions normally encountered in practice
has not yet been formulated. But most embankment failure, ranging
from minor toe sloughing to a catastrophic breach, usually occurs
during the rise or fall of the phreatic surface, and thus predic-
tion of its occurrence and effects is most important for success-
ful embankment design.

A survey of the literature reveals that the most common method
of solving the unsteady flow problem for engineered embankments is
through a succession of steady-state solutions [1,3,10][1]. Since
even steady-state solutions to flow through a porous medium require
many simplifying assumptions and idealized boundary conditions, one
is never really sure that predicted behavior will match field
behavior or even come close. Accepting the fact that the limita-
tions on numerical or graphical solutions are here to stay, one
can only conclude that an improvement in our ability to predict
transient (and steady-state) behavior in real embankments will only
come about through an improvement in our ability to model the
phenomenon.

---

[1]Throughout this paper, numbers in brackets refer to references
in the bibliography.

The purpose of this chapter is to review the theory of fluid flow in porous media and some solutions, both analytical and approximate, to very simple problems. There will also be a discussion of modelling used in the past and what future trends in modelling should entail.

Theoretical Basis

To gain a better understanding of fluid flow through porous media, a rigorous though simple-minded development of the governing equations will be given in this section. The development following that of Aravin and Numerov [1] is based on balance laws, the continuity equation and Darcy's law. It is convenient in the derivations to assume only a two-phase system, liquids and solids. Any gases present are considered either free to escape or an integral part of the solid structure. The inclusion of surface tension forces is an unwarranted complication at this time.

The Balance Laws

Consider an elemental soil cube of dimensions dx, dy, and dz as shown in Figure 1 with all open spaces in the solid structure completely filled by the liquid. The sum of all forces acting on this mass is equal to its inertia. Then for the entire cube of soil and water

$$\Sigma F_i = F_I = ma \tag{1}$$

where the F_i's are all internal and external forces and F_I is the resulting inertial force. Let us now specify that the solid soil
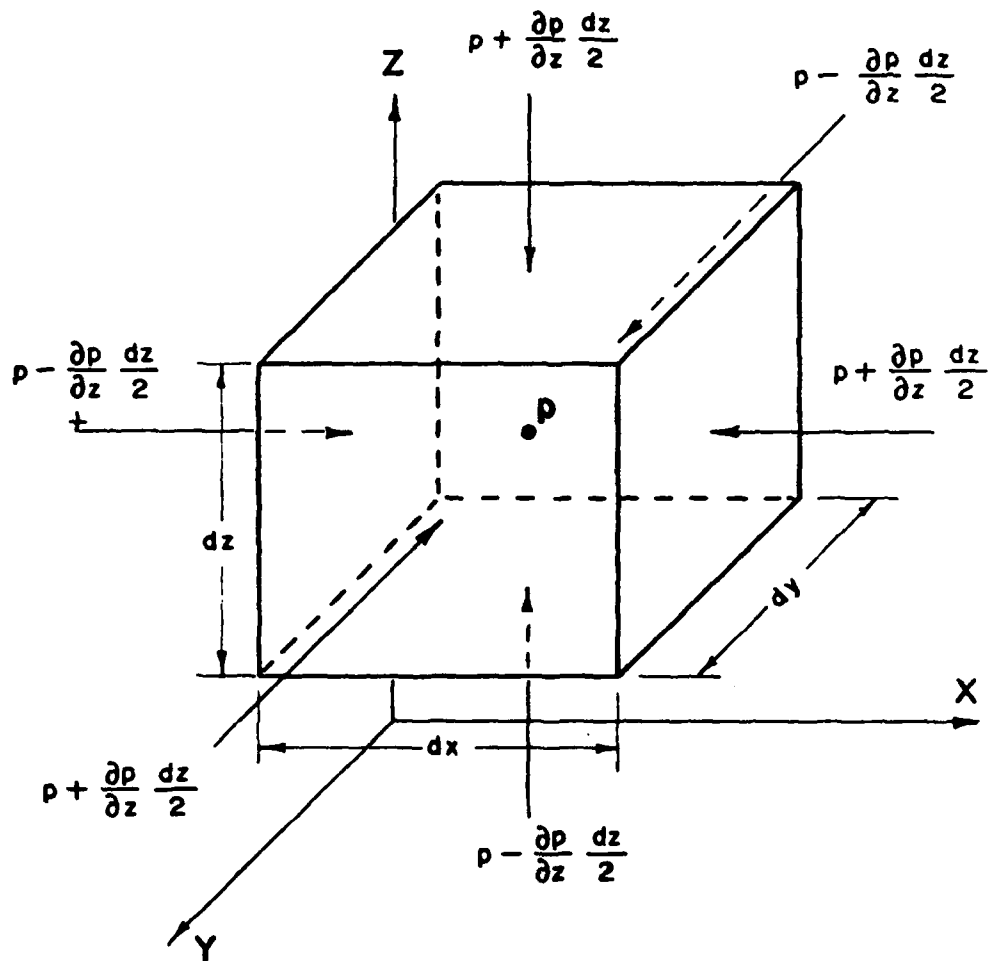
Figure I. Elemental cube of saturated soil volume
below the free water surface.

particles are incompressible and rigidly fixed in space. A balance
law can then be written in terms of the fluid phase with due regard
for forces exerted on the fluid by the rigidly fixed solid
particles.

The principal forces acting on the liquid phase are pressure
forces, body forces, and drag forces. By considering the contribu-
tion of each in the three orthogonal directions, a set of balance
equations can be formulated. For now drag forces will be vaguely
described as the reactions to seepage forces.

If the hydrodynamic pressure at the center of the cube is p,
then the pressure exerted on the +x face of the cube is

$$p + \frac{\partial p}{\partial x} \frac{dx}{2} \; . \tag{2}$$

When a section through a porous soil structure is cut, the face
will contain both solid and open areas. Defining porosity, n, of
a volume to be the ratio between the volume of the voids to total
volume, we assume that n also defines the area of voids to total
area for any typical section. This makes the area over which the
fluid pressure acts on the +x face n·dy·dz. The fluid component
of the pressure force on this face is then

$$n \left(p + \frac{\partial p}{\partial x} \frac{dx}{2} \right) dy \, dz \; . \tag{3}$$

Likewise the pressure force on the -x face is

$$n \left(p - \frac{\partial p}{\partial x} \frac{dx}{2} \right) dy \, dz \tag{4}$$

and similar expressions can be written for the other faces.

If one considers the solid particle stresses to be transmitted through point contacts between the particles, then there is also a component of the pressure force on each face equal to the fluid pressure over the area of the solids. On the +x face this would be

$$(1-n) \left(p + \frac{\partial p}{\partial x} \frac{dx}{2} \right) \, dy \, dz \qquad (5)$$

and similar expressions can be written for the other faces. Thus the total pressure force on the +x face is now

$$\left(p + \frac{\partial p}{\partial x} \frac{dx}{2} \right) \, dy \, dz \qquad (6)$$

The difference in pressure forces on any two opposing faces is the resultant pressure force for the direction normal to those faces. Thus

$$F_{p_x} = \left(p - \frac{\partial p}{\partial x} \frac{dx}{2} \right) dydz - \left(p + \frac{\partial p}{\partial x} \frac{dx}{2} \right) dydz = - \frac{\partial p}{\partial x} \, dxdydz \qquad (7)$$

and again similar expressions can be written for other faces.

The only body force of any consequence in the current formulation of our problem is that due to gravity. By choosing our coordinate system such that the -z axis is in line with gravitational acceleration, we can immediately write

$$F_{B_x} = F_{B_y} = 0 \, . \qquad (8)$$

There are two body force components in the z directions. The first is due to the weight of fluid itself and the second is due to the solid particles. The total body force of the soil mixture shown in Figure 1 is the sum of its components' weights and is given by

$$\left[n\gamma_w + (1-n)\gamma_s \right] dxdydz \qquad (9)$$

where γ_w is the unit weight of the fluid and γ_s is the unit weight of the solids. A portion of this force is carried by the solid particles through interpartical contacts and is equal to the weight of the solids minus the weight of the displaced water or

$$\left[(1-n)\gamma_s - (1-n)\gamma_w \right] dxdydz \qquad (10)$$

The remainder of the body force is carried by the water and is equal to the difference in Equations 9 and 10.

$$F_{B_z} = \left[n\gamma_w + (1-n)\gamma_s \right] dxdydz - \left[(1-n)\gamma_s - (1-n)\gamma_w \right] dxdydz$$

$$= \gamma_w \, dxdydz \qquad (11)$$

It now remains to express the drag forces previously mentioned in some form before a dynamic balance equation can be written. To obtain such an expression, we argue from the point of view of the earlier statement that drag forces are the reaction to seepage forces. That is, they are equal in magnitude and opposite in direction by Newton's third law. The derivation of seepage forces can be found in any book on soil mechanics and can be written as

$$F_s = -i \cdot \gamma_w \cdot dxdydz \qquad (12)$$

where i is the hydraulic gradient decreasing in the direction of flow. The direction of F_s is in the direction of flow.

Even though we have opted to write such a simple relation for seepage forces, it should be remembered that they actually depend

on such things as fluid velocity, density, and viscosity and soil particle size and spacing. Acceptance of the expression implies acceptance of a direct relationship between such forces and fluid velocity and also implies acceptance of Darcy's law, which says there is a direct relationship between fluid velocity and hydraulic gradient. Ample experimental evidence exists to justify both assumptions for laminar flow, and since the flow of water through soil will nearly always be at very low velocities, we assume laminar flow always exists. Darcy's law can be written

$$v = - ki \tag{13}$$

where v is the apparent velocity of fluid flow and k is the coefficient of permeability and will be discussed in a later section. Then the seepage force can be written

$$F_s = \frac{v}{k} \cdot \gamma_w \cdot dxdydz \tag{14}$$

and drag on the fluid is

$$F_D = - F_s = - n \frac{v_s'}{k} \gamma_w \cdot dxdydz \tag{15}$$

where the minus sign indicates it is opposite in direction to the velocity, v_s' is the actual particle seepage velocity, and n is porosity.

Now we introduce the concept of total head. This is a well known quantity and the hydraulic gradient previously mentioned is always determined in terms of it. From basic fluid mechanics total head is

$$h = z + \frac{p}{\gamma_w} + \frac{v^2}{2g} \qquad (16)$$

The velocity head component is negligible compared to the other parts and thus dropped; leaving

$$h = z + \frac{p}{\gamma} \qquad (17)$$

as the definition of total head. From the above equation,

$$\frac{\partial h}{\partial x} = \frac{1}{\gamma_w} \frac{\partial p}{\partial x} \quad , \qquad (18)$$

$$\frac{\partial h}{\partial y} = \frac{1}{\gamma_w} \frac{\partial p}{\partial y} \quad , \qquad (19)$$

and

$$\frac{\partial h}{\partial z} = 1 + \frac{1}{\gamma_w} \frac{\partial p}{\partial z} \quad . \qquad (20)$$

The fluid balance equations in each orthogonal direction can now be written. For the x direction we have

$$ma_x = \Sigma F_{ix} \quad , \qquad (21)$$

or,

$$n\rho \frac{\partial v_x'}{\partial t} dxdydz = - \frac{\partial p}{\partial x} dxdydz - n \frac{v_x'}{k} \gamma_w dxdydz \quad . \qquad (22)$$

By writing pressure in terms of total head and reducing, the equation becomes

$$\frac{\partial v_x}{\partial t} = - \frac{\gamma_w}{\rho} \frac{\partial h}{\partial x} - \frac{\gamma_w}{\rho} \frac{v_x}{k} \qquad (23)$$

Since $\gamma = \rho g$, further reduction and rearranging gives

$$\frac{1}{g}\frac{\partial v_x}{\partial t} + \frac{\partial h}{\partial x} + \frac{v_x}{k} = 0 \qquad (24)$$

and a similar term can be written for the y direction.

In the z direction we have

$$n\rho \frac{\partial v_z'}{\partial t} dxdydz = -\frac{\partial p}{\partial z} dxdydz - \gamma_w dxdydz - n\frac{v_z'}{k}\gamma_w dxdydz \qquad (25)$$

and on reducing

$$\rho \frac{\partial v_z}{\partial t} = -\gamma_w \frac{\partial h}{\partial z} + \gamma_w - \gamma_w - \frac{v_z}{k}\gamma_w \qquad (26)$$

This equation assumes the same form as for the x and y directions.

The following system of equations results

$$\frac{1}{g}\frac{\partial v_x}{\partial t} + \frac{\partial h}{\partial x} + \frac{v_x}{k} = 0 \qquad (27)$$

$$\frac{1}{g}\frac{\partial v_y}{\partial t} + \frac{\partial h}{\partial y} + \frac{v_y}{k} = 0 \qquad (28)$$

$$\frac{1}{g}\frac{\partial v_z}{\partial t} + \frac{\partial h}{\partial z} + \frac{v_z}{k} = 0 \qquad (29)$$

which relates the forces acting on the fluid. If the inertial force is of no consequence, then changes in v with respect to t are negligible and the familiar expressions

$$v_x = -k\frac{\partial h}{\partial x} \qquad (30)$$

$$v_y = -k\frac{\partial h}{\partial y} \qquad (31)$$

$$v_z = -k\frac{\partial h}{\partial x} \qquad (32)$$

are evident. But before we can discard inertial forces, it must be shown that they are negligible.

In a one dimensional flow problem, the hydraulic gradient is

$$- \frac{\partial h}{\partial x} = \frac{H}{L} \tag{33}$$

where H is the difference in total heads between sample ends, L is the constant length of the sample, and the minus sign indicates h is decreasing in the positive x direction. For incompressible fluids it can be shown that this relationship is true for any instant in time which implies that any change in H leads to an instantaneous redistribution of head throughout the sample. Then the balance equation can be written

$$\frac{1}{g} \frac{\partial v}{\partial t} + \frac{v}{k} = \frac{H}{L} \tag{34}$$

Aravin and Numerov [1] give a solution for this differential equation as

$$v = e^{-\frac{g}{k}t} \left(v_0 + \frac{g}{L} \int_0^t e^{\frac{g}{k}\tau} H(\tau)\, d\tau \right) \tag{35}$$

where e is the base of natural logarithm, τ is a dummy time variable, and v_0 is the apparent velocity at t = 0. They further state that if H varies linearly with time (say H = t for simplicity), then an exact solution of the equation is

$$v_{ex} = \frac{kt}{L} \left(1 - \frac{k}{gt} \right) \tag{36}$$

The authors then illustrate the difference between this exact solution and an approximate solution derived from ignoring inertial effects and setting

$$v = \frac{kH}{L} \qquad (37)$$

Then

$$v_{approx} = \frac{kt}{L} \qquad (38)$$

and the relative error in these calculations is

$$\epsilon = \frac{v_{approx} - v_{ex}}{v_{ex}} = \frac{\frac{k}{gt}}{1 - \frac{k}{gt}} \qquad (39)$$

If k = 0.04 cm/sec, which characterizes a very porous soil, and t = 0.1 seconds, then ϵ < 0.05 percent. Thus the effect of considering inertial forces is seen to be negligible in calculations of the velocity, and therefore we may have good reason for solving transeint flow problems in the manner of successive steady-state solutions. But before even steady-state solutions can be accomplished, the continuity equation must be introduced.

The Continuity Equation

Before getting into the formulation of the continuity equation, it is appropriate to introduce a term defining the amount of water in a given soil volume. Such a term is the degree of saturation, S, or

$$S = \frac{V_w}{V_v} , \qquad (40)$$

which is the ratio of the volume of water to the volume of voids. The outcome of the preceding section would be the same even had we

not specified a completely saturated volume if we assume the air phase only affects the value of permeability k.

Consider now the same cubical soil volume as before. The mass of water flowing at a velocity v through the -x face in an increment of time dt is

$$\rho v_x'(S \cdot n \cdot dydz)dt \tag{41}$$

where again n·dydz is the total void area available for fluid flow and S·n·dydz is the area actually conducting water. Both S and n are properties of the volume and their use in defining areas is only an approximation though it should be a fairly good one if the soil is homogeneous. We will also consider S to be constant throughout the volume for any instant in time. The amount of water flowing through the +x face, which is a distance dx from the -x face is then

$$\rho v_x'(S \cdot n \cdot dydz)dt + \frac{\partial}{\partial x}(\rho v_x') \, dx \, (S \cdot n \cdot dydz)dt \tag{42}$$

and the difference between the mass flowing in and the mass flowing out is

$$-\frac{\partial}{\partial x}(\rho v_x') \, S \cdot n \cdot dxdydzdt \; . \tag{43}$$

Consideration of the other directions gives

$$-\frac{\partial}{\partial y}(\rho v_y') \, S \cdot n \cdot dxdydzdt \tag{44}$$

and

$$-\frac{\partial}{\partial z}(\rho v_z') \, S \cdot n \cdot dxdydzdt \; . \tag{45}$$

The amount of mass originally in the cube has now received an additional increment equal to

$$- \frac{\partial}{\partial t} (\rho S) \; n \cdot dxdydzdt \; . \tag{46}$$

The continuity equation can now be written by equating the sum of the individual mass flows to the total change in mass.

$$\left[\frac{\partial}{\partial x} (\rho v_x') + \frac{\partial}{\partial y} (\rho v_y') + \frac{\partial}{\partial z} (\rho v_z') \right] S \cdot n \cdot dxdydzdt$$

$$= \frac{\partial}{\partial t} (\rho S) \; n \cdot dxdydzdt \tag{47}$$

By considering incompressible fluid this becomes

$$\frac{\partial v_x'}{\partial x} + \frac{\partial v_y'}{\partial y} + \frac{\partial v_z'}{\partial z} = \frac{1}{S} \frac{\partial S}{\partial t} \tag{48}$$

which is the continuity equation of seepage flow in an unsaturated soil.

Recalling Darcy's equation and allowing for the possibility of directional permeabilities, the continuity equation can be written

$$k_x \frac{\partial^2 h}{\partial x^2} + k_y \frac{\partial^2 h}{\partial y^2} + k_z \frac{\partial^2 h}{\partial z^2} = \frac{n}{S} \frac{\partial S}{\partial t} \tag{49}$$

where the n comes about because we have converted from seepage velocities to apparent velocities.

If the soil is completely saturated, $\partial S/\partial t = 0$ and

$$k_x \frac{\partial^2 h}{\partial x^2} + k_y \frac{\partial^2 h}{\partial y^2} + k_z \frac{\partial^2 h}{\partial z^2} = 0 \; , \tag{50}$$

which is the continuity equation for both steady and unsteady seepage.

A Governing Equation

It is possible to develop a governing differential equation of transient flow only by making some very simplifying assumptions often attributed to Dupuit. Consider seepage to be essentially horizontal through a homogeneous and isotropic soil with an impermeable lower boundary. The flow has a phreatic surface and its slope is small so that equipotential lines are essentially vertical and velocities are constant along any vertical plane. Figure 2 shows the elemental volume for which a continuity equation will be written.

The total incremental volume of water entering thorugh the vertical sides in an increment of time is

$$\left[\frac{\partial(v_x'H)}{\partial x} + \frac{\partial(v_y'H)}{\partial y}\right] n \; dxdydt \qquad (51)$$

where H is the flow depth, considered to be nearly constant over the volume since the slope of the phreatic surface is small. It is now preferable to write this equation in terms of apparent velocities which we have previously described as the product of seepage velocity and porosity. Thus the incremental volume is

$$\left[\frac{\partial(v_xH)}{\partial x} + \frac{\partial(v_yH)}{\partial y}\right] dxdydt \qquad (52)$$

where v_x and v_y are now apparent or average velocities in their respective directions.
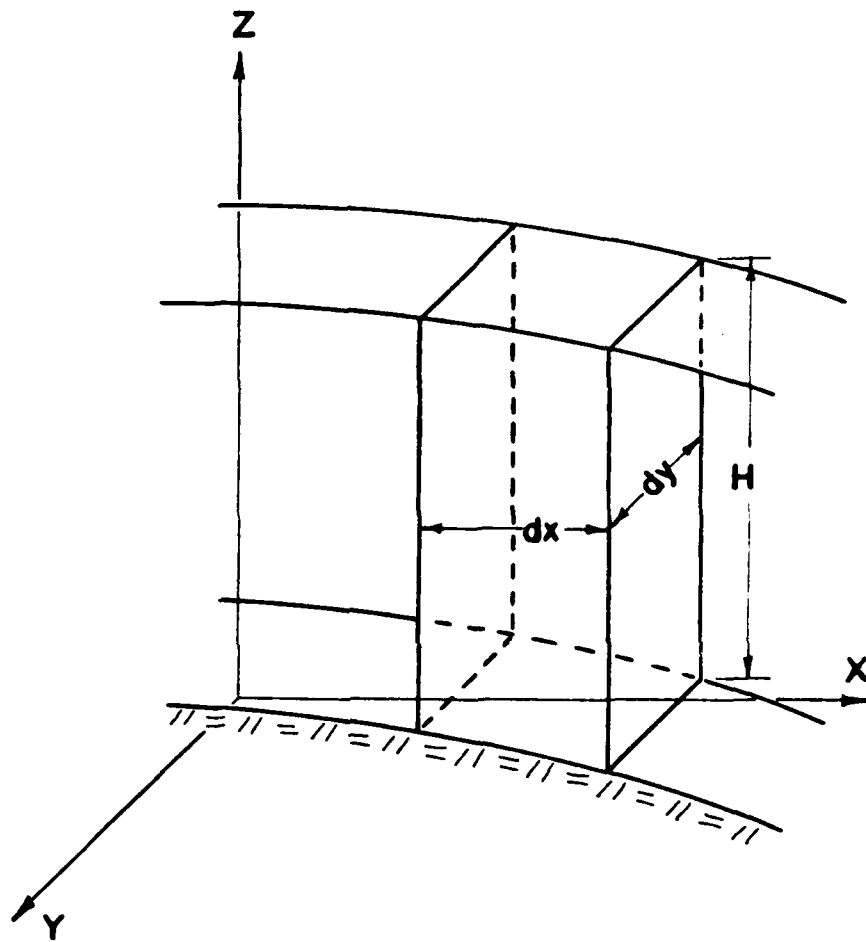
Figure 2. Elemental volume of soil on an
impermeable base and having a
free water surface.

The incremental fluid volume increase in the prism of soil can be expressed as

$$n \cdot \frac{\partial H}{\partial t} \, dxdydt \qquad (53)$$

and equating the two expressions yields

$$\frac{\partial(v_x H)}{\partial x} + \frac{\partial(v_y H)}{\partial y} = n \frac{\partial H}{\partial t} . \qquad (54)$$

Applying Darcy's law and substituting for the velocities results in

$$\frac{\partial}{\partial x}\left(H \frac{\partial H}{\partial x}\right) + \frac{\partial}{\partial y}\left(H \frac{\partial H}{\partial y}\right) = -\frac{n}{k}\frac{\partial H}{\partial t} \qquad (55)$$

which is the governing differential equation for the very simple flow pattern described.

When written with a term denoting infiltration from above, the equation is referred to as the Boussinesq Equation [1]. Dicker [5] calls it the Dupuit-Forchheimer formula and uses it to solve the rapid drawdown problem for an infinitely wide vertical embankment. Dicker [5] also has rederived the same equation without the restriction of constant velocities along any vertical plane by using flow quantities and a mean-value theorem.

Solutions

The rapid drawndown problem solved by Dicker is depicted in Figure 3. For this case the governing equation is written in the form

$$\frac{\partial}{\partial x}\left(h \frac{\partial h}{\partial x}\right) = -\frac{n}{k}\frac{\partial h}{\partial t} \qquad (56)$$
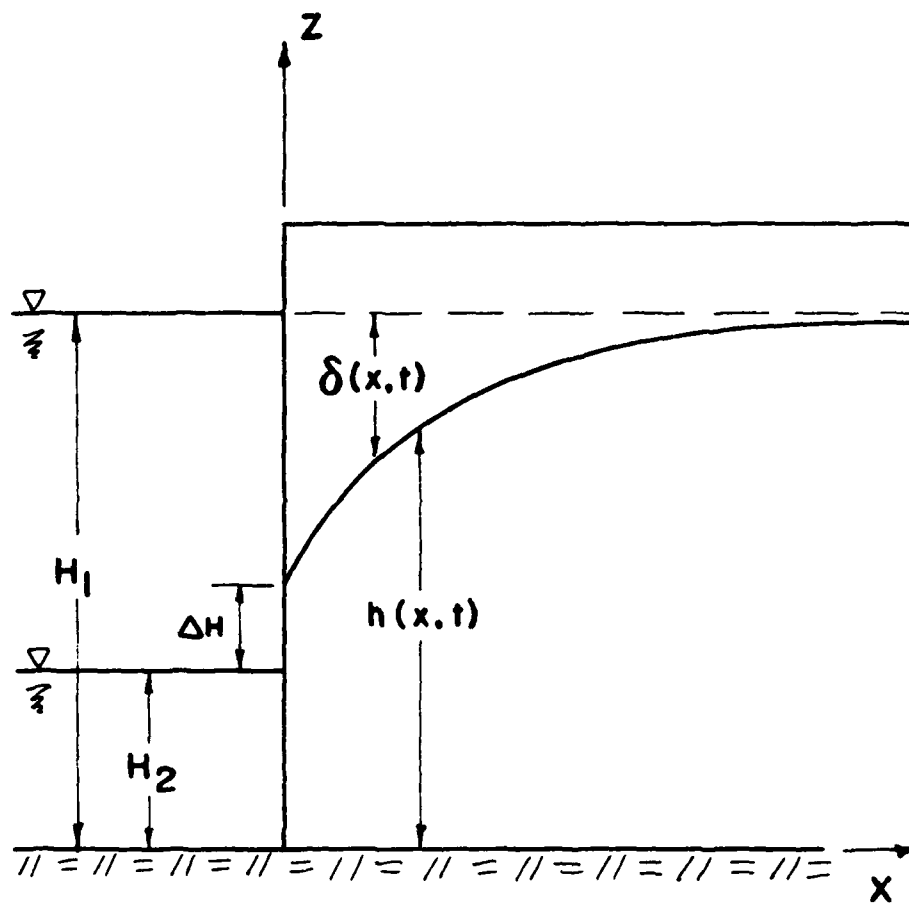
Figure 3. Two dimensional rapid drawdown problem.

with initial and boundary conditions

$$h(x,0) = H_1, \; x > 0 \tag{57}$$

$$k \frac{\partial h(0,t)}{\partial x} = \frac{2}{3} C n (2g)^{\frac{1}{2}} \left| H(0,t) \right|^{\frac{1}{2}} \tag{58}$$

where C is a discharge coefficient dependent upon exit conditions. The boundary condition for the face of the embankment is based on the relationship for a freely discharging orifice from fluid mechanics. The solution, written in terms of $\delta(x,t)$, is

$$\delta(x,t) = -\frac{\phi}{\alpha k} - \frac{2\phi}{(\pi k)^{\frac{1}{2}}} \left\{ \frac{\sqrt{\pi}}{2} \text{erf} \left(-\frac{x}{2(\beta t)^{\frac{1}{2}}} \right) \right.$$
$$\left. - \frac{e^{\alpha^2 \beta t + \alpha x}}{\alpha} \left[\frac{\sqrt{\pi}}{2} - \frac{\sqrt{\pi}}{2} \text{erf} \; \frac{x + 2\alpha\beta t}{2(\beta t)^{\frac{1}{2}}} \right] \right\} \tag{59}$$

where

$$\phi = \frac{2}{3} C n (2 g H_1)^{\frac{1}{2}} \tag{60}$$

$$\beta = \frac{kH}{n} \tag{61}$$

$$\alpha = \frac{C(2g)^{\frac{1}{2}}}{3k\sqrt{H_1}} \tag{62}$$

With the aid of a computer, this equation is easily solved, but once we have a solution it is not very useful since an embankment with a vertical face is not commonly built in practice.

Browzin [2] has offered a solution of the one dimensional Boussinesq equation which he applies to the more conventional trapezoidal embankment shape after rapid drawdown. However, his solution is based on a continuous succession of steady states where

the governing equation is

$$\frac{d^2h^2}{dx^2} + \frac{2\epsilon}{k} = 0 \qquad (63)$$

and ϵ is an infiltration rate. By integrating, defining $q = \epsilon x$, and applying Darcy's law, Browzin arrives at the ellipse equation

$$\frac{h^2}{H^2} + \frac{x^2}{a^2} = 1 \; , \qquad (64)$$

for the shape of the water surface at any time. Figure 4(a) gives the nomenclature for the problem. The crucial items in the solution are the factors n_2 and m_2 which describe the location of the ellipse apex. Browzin found them dependent on the dam shape and on the basis of experimental data from a Hele-Shaw flume related them to the upstream slope and the ratio H_1/L, see Figure 4(b).

The time at which the free surface passes a certain elevation, H, was determined to be

$$t = \frac{cn}{2k} L \left[C_1 \left(\frac{H_1}{H} - 1 \right) + C_2 \ln \left(\frac{H}{H_1} \right) + C_3 \left(1 - \frac{H}{H_1} \right) \right] \qquad (65)$$

by defining an incremental volume parallel to the free water surface, differentiating with respect to H, dividing by dt, equating to a flow rate derived from Darcy's law, and then integrating. The constants C_1, C_2, and C_3 are dependent on the embank-shape factors and are given in Figure 4(c). The c is a factor to correct for possible inaccuracies in the assumptions made and was experimentally found to vary between 0.9 and 1.4 depending on the embankment shape.
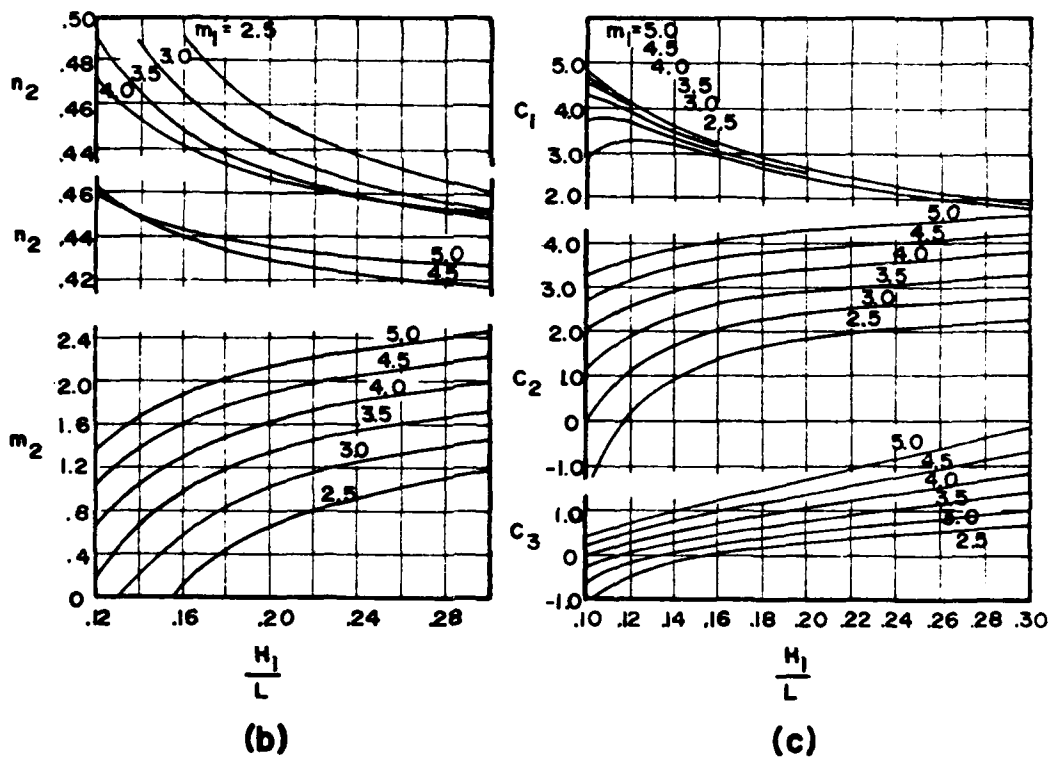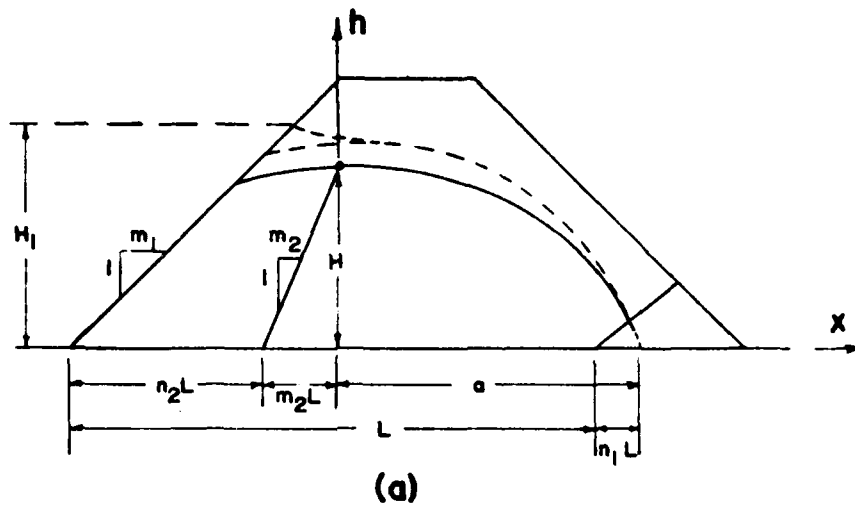
Figure 4. Charts for solution of rapid drawdown problem. (after Browzin)

A procedure for solving the rapid drawndown problem by Browzin's method can be summarized as follows:

1. Select H and compute time, t, from equation 65 using coefficients obtained from Figure 4(c). Using c = 1.0 will introduce an error which should not exceed 20 percent.

2. Obtain n_2 and m_2 from Figure 4(b) and plot H on an embankment cross section.

3. Construct the ellipse defined by equation 64.

If one wants the solution at a particular time, it would be necessary to make successive guesses at H until the desired t was obtained in equation 65.

The two preceding examples are representative of current state-of-the-art analytical solutions for transient flow problems. For completeness, we should also consider approximate solutions such as the numerical technique of finite differences, a version of which is presented by Rushton and Redshaw [10] in their recent book and the transient flow net technique described by Cedergren [3]. In the following section these two techniques are described.

Approximate Solutions

The solution of the transient flow problems by either of the two methods to be discussed next presupposes a knoweldge of steady state solutions by these methods. Both methods can be basically described as problems in determining new boundary conditions at some later time interval. Once the new boundary conditions are

described, a steady state solution is fitted to them. Using this new steady state solution, new boundary conditions are defined and another steady state solution if fitted. The process is repeated until the boundary conditions match the steady state boundary conditions at which time the transient flow becomes true steady state flow.

Transient Flow by Finite Differences

Recall that the governing equation previously derived (equation 55) was for essentially horizontal flow and vertical equipotential lines. As was pointed out, this is not a very realistic situation. There is very likely to be a vertical velocity component which may have a dominant effect on the problem and vertical equipotential lines will certainly seldom be encountered in common embankment shapes. It would be of great benefit to have a governing equation which considers such vertical flow.

Since solution of the problem depends on our ability to predict boundary conditions, and the only boundary we cannot already define is that of a free surface, let us focus our attention on a point on the free water surface and try to describe its vertical motion with respect to time. Consider the plane shown in Figure 5(a) to represent the water surface subject to translatory motions parallel to the three orthogonal directions. Since we are talking about approximations, we will approximate the motion of point A by the sum of three components. The only restrictions we make is that A remains on the free water surface and that its x and y coordinates
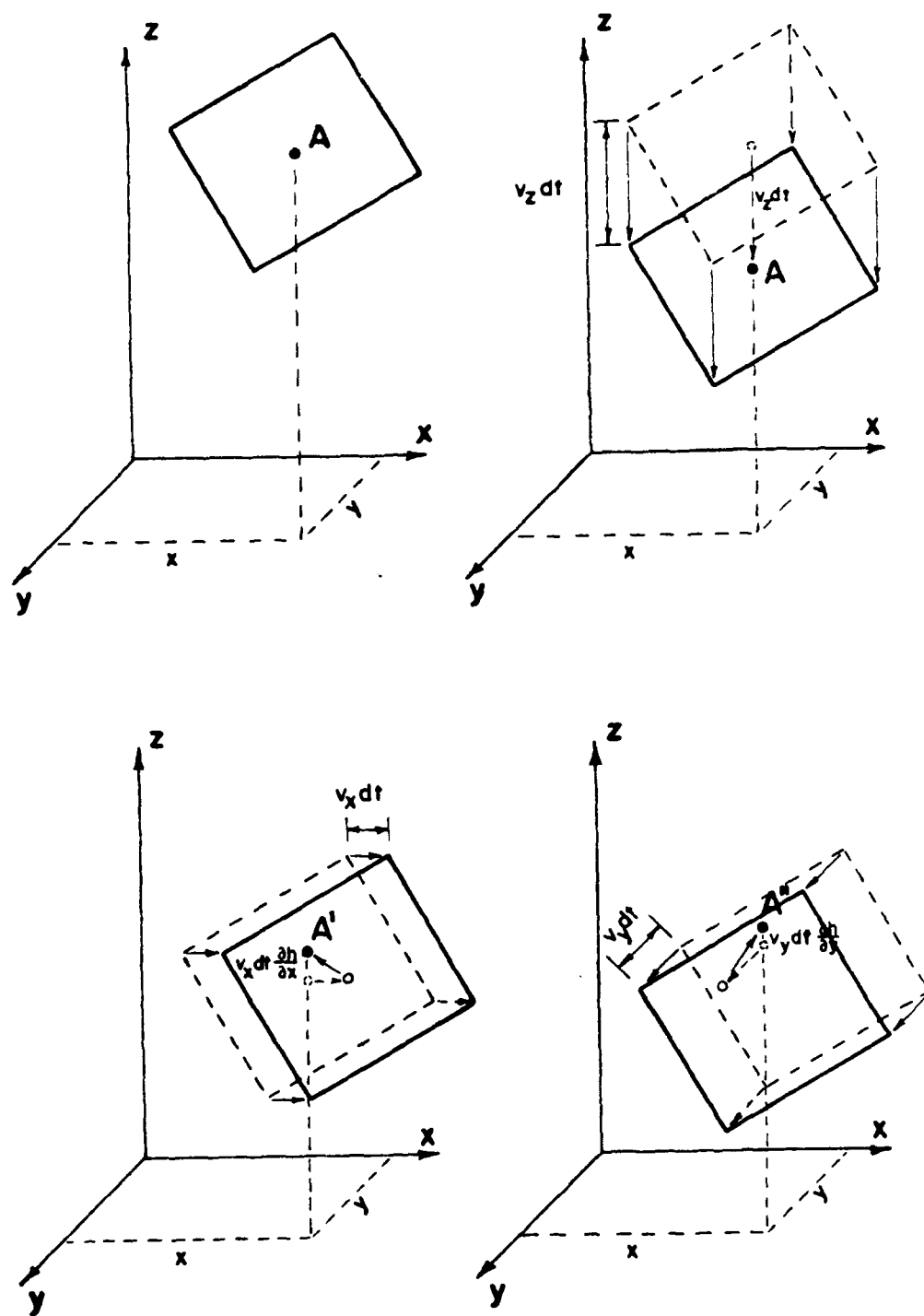
Figure 5. Movement of a free water surface.

are fixed. Thus the increment of vertical motion made by A can be called dH and is a function of x, y, and t. Figure 5(b) shows the water surface after being displaced in the z direction a distance $v_z \cdot dt$, and so for now, $dH = v_z \cdot dt$. Figure 5(c) shows the water surface after being displaced in the x direction a distance $v_x \cdot dt$. If we take the time interval sufficiently small, there will be no rotation of the plane. Since A must remain on the free water surface and its x,y coordinates are fixed, its new position will be A'. Now,

$$dH = v_z \cdot dt - v_x \cdot dt \left(- \frac{\partial h}{\partial x}\right) , \qquad (66)$$

where the minus sign indicates that a positive water slope direction is opposite to a positive velocity direction. Next we displace the water surface in the y direction a distance $v_y \cdot dt$ and point A' moves up the slope to A". The change in water surface elevation can thus be written

$$dH = v_z \cdot dt - v_x \cdot dt \left(- \frac{\partial h}{\partial x}\right) - v_y \cdot dt \left(- \frac{\partial h}{\partial y}\right) . \qquad (67)$$

Before applying Darcy's law, we should multiply through by the porosity to convert seepage velocities to apparent velocities. The equation can then be reduced to

$$\frac{dH}{dt} = - \frac{1}{n} \left[k_z \frac{\partial h}{\partial z} + k_x \left(\frac{\partial h}{\partial x}\right)^2 + k_y \left(\frac{\partial h}{\partial y}\right)^2 \right] \qquad (68)$$

which is the governing differential equation for our free water surface.

By the usual method of finite differences, an expression can now be written for the new water surface level based on existing total heads and some small increment of time. The accuracy of the calculations depend to a large degree on the size of time step chosen. Too large a time step will cause instability in the analysis and erroneous results. While there are no explicit formulas for calculating a time step which insures numerical stability, a probable maximum is that which produces a water surface movement of 5 percent to 10 percent of the ultimate steady state.

A procedure for solving the transient flow problem in an embankment by finite differences would be as follows:

1. Based on some instantaneous change in the headwater or tailwater levels, solve the problem as a steady state problem with the position of the phreatic surface the same as before the change. It must be kept in mind that the potential on seepage surfaces are the same as the elevation of the seepage surface since only atmospheric pressure is maintained there. This instantaneous change could be due to an instantaneous drawdown, instantaneous filling, or a series of partial drawdowns or fillings. Regardless of which is used, there is a unique steady state solution to the new conditions and calculations should proceed until this condition is reached or the real time represented by this instantaneous change is approached.

2. Using the solution obtained above, equation 68 is solved
   by finite differences to find the new water surface
   elevation on each vertical of the difference grid. The
   time interval used in this calculation should again be
   estimated to give a change in water surface no more than
   10 percent of the ultimate or partial change.

3. A steady state solution is again derived using the
   original changes in boundary conditions modified by the
   new water surface level.

4. The process of finding a new water surface and recalcu-
   lating the steady state solution is repeated until either
   this ultimate steady state is reached in the case of a
   complete drawdown or filling, or until the accumulated
   time steps equal the original time step represented by the
   instantaneous partial drawdown or filling. In the case of
   the latter, another instantaneous partial drawdown or
   filling must take place and boundary conditions on the
   faces of the embankment adjusted to account for this
   change. At some point the instantaneous partial changes
   will equal the total change. The process of calculating
   a new water surface and steady state solution is then
   repeated until the ultimate steady state is reached.

The Flow Net Method

Conceptually, the solution of transient flow problems by the
flow net method is the same as for the finite difference method. A

series of steady state solutions are fit to known or assumed

boundary conditions and the position of the phreatic surface is

adjusted according to the steady state solution. However, this

is a graphical solution and only a very few simple calculations

are necessary to insure consistency and for time determinations.

The method may be explained using the same situation described

in the previous section by means of the following procedure:

1. Based on some instantaneous change in the headwater or
   tailwater elevations, guess at a new free water surface
   profile and graphically solve the problem with these new
   boundary conditions by drawing a complete flow net,
   including both equipotential and flow lines. Judgement
   must be used in deciding how far to take this first guess
   in relation to the ultimate steady state. For large
   changes such as complete instantaneous drawdown, 10 per-
   cent is probably a good figure. For smaller partial
   instantaneous changes, 50 percent may be justified.

2. Consistency of this flow net must now be checked. For
   several flow paths in the region, calculate the ratio,
   L/i, where L is the length of the flow path and i is the
   hydraulic gradient along the path. If these ratios are
   not approximately equal, then points along the free
   surface need to be adjusted until a nearly constant group
   of ratios is obtained.

3. After a consistent flow net is achieved, the concurrent
   time interval is estimated as,

$$\Delta t = \frac{n_e}{k} \frac{\Delta \ell}{i} \tag{69}$$

where n_e is the effective porosity, k is the soil per-
meability, $\Delta \ell$ is the incremental distance along any flow
path (usually the longest one), and i is the hydraulic
gradient along this path.

4. Another free water surface position is now guessed and
    the process repeated. Guesses may be refined by considera-
    tion of the fact that the distance a point will move is
    related to the hydraulic gradient at that point. Converg-
    ing flow will also tend to cause greater movement while
    diverging flow will cause lesser.

5. The procedure is continued until the ultimate steady state
    solution is reached. The total time taken to reach the
    steady state is the sum of incremental times determined
    in Step 3.

Modelling of Transient Flow in Embankments

It is evident from the preceding sections that solution of the
unsteady seepage problem is at best only an approximation. Even
the so-called analytical solutions involve so many simplifying
assumptions that when applied to a real situation, their solutions
are probably less accurate than truly approximating methods of
finite differences and flow net. Since we are dealing in uncer-
tainties for the most part, it is reasonable to assume that a well
designed and properly employed model would give just as good

results with the added advantage that the principal factors influencing the flow can be visually observed and modified where necessary to improve the solution. In this section, the current principal methods of modelling transient flow are mentioned and ideas for future modelling are discussed.

Electrical Models

The use of electrical models in representing seepage flow is based on the similarity between Darcy's law and Ohm's law. Electrical analogies have long been used to successfully obtain steady state solutions to seepage problems. The essential feature of this method is to represent the field of flow by some conducting medium such as specially coated conducting paper, a network of resistors, or an electrolytic solution. Details of the modelling process will not be given here.

The investigation of transient flow by an electrical model is based on the assumption that at any particular moment the seepage may be considered steady. Thus this method is probably the least desirable of the available methods since it uncouples the process from the time variable.

The Hele-Shaw Method

This method attempts to simulate viscous flow with viscous flow and is probably the best of currently used modelling procedures for transient flow through embankments. The procedure is based on the fact that fluid flow through porous media mainly depends on

the hydraulic gradient, the mass density of the fluid, fluid
viscosity, and an area parameter characteristic of the cracks and
crevices in the porous media. These properties are simulated by a
model geometrically similar to its prototype and consisting of two
flat plates spaced a certain distance, d, apart. One of the plates
is glass or plastic so that the flow may be observed and recorded.
The conductivity of fluid flow in the channel between the plates is
proportional to d^3.

The permeability of a soil can be generally defined as

$$k = \frac{\kappa \rho g}{\mu} \tag{70}$$

where κ is a characteristic area term of the porous media, ρ is the
mass density of the fluid, g is gravity, and μ is the fluid vis-
cosity. This is modelled in the Hele-Shaw flume through a proper
combination of fluid properties and distance between plates.

The principal advantage of this model is that it is a con-
tinuous process and not discretized into a series of steady state
solutions. Once a model is calibrated to its prototype an infinite
number of headwater and tailwater changes may be simulated for
study. The time aspect of a Hele-Shaw model is scaled as the
length scale divided by the velocity scale or the length scale
divided by the permeability scale since velocity is directly pro-
portional to permeability.

Same Material Models

Every solution to the unsteady seepage problem presented so
far contains the same basic failing, that of trying to model soil

permeability. Whether it be by a number, a resistor, or the distance between flat plates, the modelling of soil permeability is the most critical element in any solution. While it may be correctly argued that we can three-dimensionally simulate known conditions, the fact remains that nature is full of unknowns. The best model material has got to be the actual prototype material. Only then are we certain of getting the correct relationship between permeability in a saturated and unsaturated state, for instance. This relationship plays a dominant role in the problem of moving saturation lines.

Of course, if we are to fully realize the advantages of same material modelling, the sample used in model construction must be truly representative of prototype material. This may entail the careful shaving of an undisturbed sample, or for structures to be constructed from remolded material, a duplication of the actual construction procedure in constructing the model.

Same material modelling for the study of transient flow phenomenon is practically non-existent at this time, mainly because surface tension effects which are of very minor importance in the prototype are the predominant effect in small scale models. It is economically not feasible to construct a model of the size required to nullify the effects of surface tension. However, these effects can be put in the proper perspective if the model is centrifuged.

Geotechnical centrifugal modelling has come of age in recent years. Its principal use so far has been in slope stability studies but is seeing increased use in other areas of geotechnical problem

solving. Centrifugal modelling of transient flow in earth embank-
ment is an obvious solution to the problem of surface tension
effects while getting the benefits of having the actual materials
represent themselves.

CHAPTER III

SIMILITUDE IN GEOTECHNICAL MODELLING

Before model test results can be extrapolated to prototype
performance, applicable scaling factors must be established and
verified. The establishment of these factors requires an under-
standing of similitude laws governing the problem. It is the
purpose of this chapter to examine those similitude laws and to
develop scaling relations necessary for proper modelling of
transient flow in soils.

Similarity

Geometric Similarity

The first and generally easiest to satisfy of the similitude
laws is that of geometric similarity. Very simply stated, it
requires that the general shape of a model is unchanged from that
of the prototype and that there be a constant ratio relating length
dimensions, L. Thus if we wish to represent a 100-foot high dam by
a 1-foot model, we have established a model ratio $\lambda = L_p/L_m = 100$,
where subscripts p and m denote prototype and model, respectively.
If lengths in any three orthogonal directions are all scaled by the
same ratio, λ, then cross-sectional areas and volumes are respec-
tively scaled by λ^2 and λ^3. In this case angular measurements,

being the dimensionless quotient of two identically scaled lengths, are not scaled but correspond exactly between prototype and model.

It is possible and maybe prudent in certain studies to use different model ratios for horizontal and vertical length dimensions. For instance, let λ_x and λ_y be the scaling factors in any two-dimensional x,y plane, then an area in this plane is scaled by the product $\lambda_x \cdot \lambda_y$. The tangent of angular measurements is changed by a quotient of λ_x and λ_y. If the angle in question subtends a deflection in the x-direction, then its tangent is scaled by λ_x/λ_y and if in the y-direction, then by λ_y/λ_x.

Kinematic Similarity

To produce kinematic similarity, it is necessary to add to those previously stated for geometric similarity the requirement that the velocities at corresponding points in prototype and model are proportional by the same constant ratio. Denoting this ratio by β, then

$$\beta = \frac{v_p}{v_m},$$ (71)

where v is velocity. A relationship between β and λ will be established in a later section.

Using the scale ratios defined up to this point, a time scale, τ, may be deduced as

$$\tau = \frac{T_p}{T_m}$$ (72a)

$$= \frac{L_p/v_p}{L_m/v_m} \qquad \text{(72b)}$$

$$= \frac{\lambda}{\beta} \qquad \text{(72c)}$$

since dimensionally, $v = LT^{-1}$.

Carrying this reasoning another step, we may also denote an acceleration ratio by n and state that

$$n = \frac{a_m}{a_p} = \frac{\tau^2}{\lambda} \qquad \text{(73)}$$

since again in dimensional terms, $a = LT^{-2}$. Here we have purposely written the acceleration ratio as model over prototype so that we may work in whole numbers when we discuss centrifugal modelling.

It should be noted that the relationship for the time scale implied in the last equation is strictly for kinematic effects. If a length ratio, λ, equal to the acceleration ratio, n, is chosen, then time would scale in the same proportion as length, i.e. $\tau = \lambda$. However, it may be shown that time scales as the square of the length ratio for problems in consolidation of clays modelled centrifugally.

Dynamic Similarity

For there to be dynamic similarity between a prototype and its model, corresponding forces must be in the same ratio. Some of the forces which may be of interest in this study are those due to weight (F_W), pressure (F_p), viscosity (F_V), surface tension (F_T), inertial (F_I), and seepage (F_S). Dynamic similarity requires

that those forces which have significant bearing on the problem should have constant ratios between model and prototype such that

$$\alpha = \frac{F_{Wp}}{F_{Wm}} = \frac{F_{Pp}}{F_{Pm}} = \frac{F_{Vp}}{F_{Vm}} = \frac{F_{Tp}}{F_{Tm}} = \frac{F_{Ip}}{F_{Im}} = \frac{F_{Sp}}{F_{Sm}} \qquad (74)$$

It is important to remember that only those forces having impact upon the problem need be modelled with dynamic similarity in mind.

A technique in fluid mechanics is to express the significant forces as dimensionless ratios such as

$$\left(\frac{F_I}{F_V}\right)_p = \left(\frac{F_I}{F_V}\right)_m \quad , \qquad (75)$$

the familiar Reynolds number, or

$$\left(\frac{F_I}{F_W}\right)_p = \left(\frac{F_I}{F_W}\right)_m \qquad (76)$$

which is the Froude number. Then, if it is determined that only inertial and weight forces make a significant contribution in a particular problem, one need only match the Froude number of the prototype to achieve dynamic similarity in the model.

To illustrate the application of this technique to soil mechanics, imagine we have a problem which involves weight and seepage forces as the only significant forces. To achieve dynamic similarity between a prototype and model we then need only require that

$$N = \left(\frac{F_W}{F_S}\right)_p = \left(\frac{F_W}{F_S}\right)_m = \text{constant} . \qquad (77)$$

Restricting our consideration to any unit volume of material, the weight force, which in this situation is a buoyant weight, is

$$F_W \text{ (per unit volume)} = (\rho_s - \rho_f)g \qquad (78)$$

where ρ_s is the mass density of solid particles, ρ_f is the mass density of the seeping fluid, and g is acceleration due to gravity. The seepage force per unit volume can be represented as

$$F_S \text{ (per unit volume)} = i\gamma_f = i\rho_f g \qquad (79)$$

where i is hydraulic gradient under which the fluid is flowing. Then

$$\frac{F_W}{F_S} = \frac{1}{i}\left(\frac{\rho_s}{\rho_f} - 1\right) . \qquad (80)$$

This ratio may be made constant in both prototype and model by simply choosing to use exactly the same materials in each system and setting the hydraulic gradient to be the same. If the hydraulic gradient, for some reason, must be changed, then the ratio of $\rho_s : \rho_f$ *must also be adjusted so that* $N_m = N_p$ *for dynamic similarity* to be maintained.

Centrifugal Modelling

As pointed out earlier for the time scale there may be a discrepancy between scaling ratios for centrifuged models and

those calculated by a strict scaling of the system dimensions of mass, length, and time. This discrepancy comes about because centrifugal modelling mainly involves simulating only macroscopic properties and dimensions of a prototype. It is convenient to not try to model the microscopic properties and dimensions for reasons which will become clear later.

How then do we determine scaling ratios for such "partial" modelling? The answer lies in a full understanding of the relationship each property and dimension plays in the particular phenomenon being modelled. A brute force method of determining such relationships would be trial and error, but many of the errors can be eliminated if we systematically analyze the problem through a technique long used in modelling hydraulic problems called dimensional analysis.

Model Ratios by Dimensional Analysis

To use this technique, one must be able to identify the basic parameters that influence the solution. Although a complete solution cannot usually be achieved, the proper relationship between parameters can be established. Once this relationship is made the effects of scale can then be deduced.

The Scaling Relationship for Flow Rate

To illustrate the method, let us consider the one-dimensional vertical flow of water through a column of soil. Experience with this type problem would lead one to guess that the total quantity

of flow through the soil is affected by the mass density of the fluid, ρ, the difference in potentials (measured in heads) at the top and bottom of the column, ΔH, the length of the column, ℓ, the area of the column, A, the viscosity of the fluid, μ, gravitational acceleration, g, and κ, the physical permeability of the soil which is independent of the fluid and has the dimension of length squared.

$$q = f(\ell, A, \Delta H, g, \kappa, \rho, \mu) \tag{81}$$

The above equation simply states that flow rate, q, is a function of the independent variables mentioned.

Buckingham's π theorem [8] states that if an equation is dimensionally homogeneous or does not depend on a particular system of units, then it can be reduced to a relationship among a complete set of dimensionless groupings or π terms. There is then an equation of the form

$$f'(q, \ell, A, \Delta H, g, \kappa, \rho, \mu) = 0 \tag{82}$$

and the task now is to determine a complete set of those dimensionless groupings.

An aid to determining the π terms is application of another theorem which states that the number of independent, dimensionless products in a complete set of variables is equal to the number of such variables minus the rank of their dimensional matrix. A dimensional matrix for our set would appear as

		q	ℓ	A	ΔH	g	κ	ρ	μ
(mass)	M	0	0	0	0	0	0	1	1
(length)	L	3	1	2	1	1	2	-3	-1
(time)	T	-1	0	0	0	-2	0	0	-1

$$\hspace{6cm} (83)$$

The rank of such a matrix is the order of its largest nonzero determinant. Taking the last three columns, we see that

$$\begin{vmatrix} 0 & 1 & 1 \\ 2 & -3 & -1 \\ 0 & 0 & -1 \end{vmatrix} = 2 \hspace{4cm} (84)$$

which is nonzero, and so the rank is 3. There are then $8 - 3 = 5$ independent π terms in a complete set.

There are a vast number of complete sets of dimensionless products that can be formed from any set of variables. However, Langhaar [8] describes a technique whereby the most advantageous set may be chosen with relative ease. Employing his method and "guessing" that $\Delta H/\ell$ is probably a significant grouping, one arrives at the following:

$$\pi_1 = \frac{q\rho}{\kappa^{\frac{1}{2}}\mu} \hspace{4cm} (85)$$

$$\pi_2 = \frac{\Delta H}{\ell} \hspace{4cm} (86)$$

$$\pi_3 = \frac{A}{\kappa} \hspace{4cm} (87)$$

$$\pi_4 = \frac{\Delta H}{\kappa^{\frac{1}{2}}} \hspace{4cm} (88)$$

$$\pi_5 = \frac{g\kappa^{3/2}\rho^2}{\mu^2} \hspace{4cm} (89)$$

For there to be complete similarity between any model and its prototype, the correspoinding π terms must be equal.

$$(\pi_i)_p = (\pi_i)_m \tag{90}$$

If it is decided that a certain variable originally included in the dimensional matrix has a negligible effect on the phenomenon under study and that variable appears in only one π term, that term may be discarded. If the variable appears in more than one term, a transformation of groupings to another complete set where it does appear in only one term must be made before that term can be eliminated.

Let us now inquire into the particular effect each variable grouping has on q, the flow rate, by combining π_1 with each of the remaining π's in turn. Thus in effect we are forming another complete set which will remain independent dimensionless products.

Then

$$\pi_1' = \frac{\pi_1}{\pi_2}$$

$$= \frac{q\rho\ell}{\kappa^{\frac{1}{2}}\mu\Delta H} \tag{91}$$

and

$$\left(\frac{q\rho\ell}{\kappa^{\frac{1}{2}}\mu\Delta H}\right)_p = \left(\frac{\rho\ell}{\kappa^{\frac{1}{2}}\mu\Delta H}\right)_m \tag{92}$$

for similarity. Therefore

$$q_p = \frac{\rho_m\ell_m\kappa_p^{\frac{1}{2}}\mu_p\Delta H_p}{\rho_p\ell_p\kappa_m^{\frac{1}{2}}\mu_m\Delta H_m} \cdot q_m \tag{93}$$

The coefficient on q_m, following the previously established definition, is the inverse of the model or scale ratio for flow rate. Since the thesis of this paper is centrifugal modelling with materials identical to the prototype, we will employ those restrictions here by stating that

$$\rho_m = \rho_p ,$$

$$\mu_m = \mu_p ,$$

$$\kappa_m = \kappa_p .$$

The equation then reduces to

$$q_p = \frac{\ell_m}{\ell_p} \cdot \frac{\Delta H_p}{\Delta H_m} \cdot q_m = \frac{1}{\lambda} \cdot \lambda \cdot q_m = q_m \tag{94}$$

which says that if flow rate is mainly dependent on the ratio $\Delta H/\ell$, then flow rate in the model is the same as flow rate in the prototype when this ratio is constant.

The same type analysis applied to

$$\pi_2' = \frac{\pi_1}{\pi_3}$$

$$= \frac{q \, \rho \, \kappa^{\frac{1}{2}}}{A \, \mu} \tag{95}$$

results in

$$q_p = \frac{A_p}{A_m} \cdot q_m = \lambda^2 \, q_m \tag{96}$$

and if, as is customary in centrifuge testing, $\lambda = n$ (n being the ratio of acceleration to gravity)

$$q_p = n^2 q_m \qquad (97)$$

This tells us that if the flow rate is mainly dependent on the cross-sectional area of the soil column, the flow rate in the prototype will be n^2 times that measured in the model.

Similarly, looking at π_1/π_4 one would find that

$$q_p = n q_m \qquad (98)$$

and by looking at π_1/π_5, we find

$$q_p = \frac{\kappa_p^2 g_p \rho_p \mu_m}{\kappa_m^2 g_m \rho_m \mu_p} \cdot q_m \approx \frac{g_p}{g_m} \cdot q_m = \frac{1}{n} q_m \qquad (99)$$

So it appears now that the scale ratio for flow rate can be anywhere between $1/n$ and n depending on what variable or combination of variables exerts the major influence. Laut [9] has hypothesized that the principal factors are contained in the dimensionless term

$$\pi = \frac{q\mu}{\rho g \kappa A} \qquad (100)$$

which is seen to be

$$\pi = \frac{\pi_1}{\pi_5 \cdot \pi_3}$$

in terms of the original groupings. This can be reduced to the relationship

$$q_p = \frac{\rho_p g_p \kappa_p A_p \mu_m}{\rho_m g_m \kappa_m A_m \mu_p} \cdot q_m = \frac{g_p A_p}{g_m A_m} \cdot q_m$$

$$= \frac{1}{n} \cdot \lambda^2 \cdot q_m = n \, q_m \tag{101}$$

for a centrifuged model using the same material.

The "correct" scaling relationship must be determined from actual model tests. It may turn out that the ratio is some uneven power of n because the effects of one parameter are dominant but the effects of another are not totally obscurred.

Steady State Flow in Soils

Using the method illustrated in the previous section, possible scaling relations will be developed for the parameters appearing in any consideration of steady state flow in soils. Since a part of the ultimate objective is to model such flow through an embankment, any particular influence a free water surface or phreatic line, has on such relationships will also be considered. It should be obvious that although the problem of the previous section was labeled one-dimensional, making it three-dimensional would not have involved any additional basic variables but only more length parameters which would not have affected the ultimate outcome.

Every treatise on flow in soils will reference the work of Darcy in some form. The relationships he experimentally derived are universally accepted and need not be expounded upon here. It is sufficient to state that due to his work, the importance of a term which has come to be called the permeability coefficient is

recognized for any problem of flow in soils. A knowledge then is required of how the coefficient of permeability, k, is related between model and prototype. In the most general case, k can be said to be dependent upon first the physical permeability of the soil, κ, described earlier as having dimensions of L^2 because it is indicative of interpartical flow channels. Permeability may also be influenced by the velocity of fluid flow and shearing stresses in the fluid, but shearing stresses will be omitted since they are dependent on the velocity gradient and the other independent variables of mass density of fluid, ρ, viscosity, μ, and gravity, g. Then it may be stated

$$k = f_1(v, g, \kappa, \mu, \rho) \tag{102}$$

or

$$f_1'(k, v, g, \kappa, \mu, \rho) = 0 . \tag{103}$$

By employing the previous technique of dimensional analysis and applying Buckingham's π theorem, one can arrive at the following dimensionless groupings:

$$\pi_1 = \frac{\rho V \kappa^{\frac{1}{2}}}{\mu} \tag{104}$$

$$\pi_2 = \frac{k\mu}{g \kappa \rho} \tag{105}$$

$$\pi_3 = \frac{\kappa^{3/2} \rho^2}{\mu^2} \tag{106}$$

The first term is the familiar Reynolds number often used to distinguish between laminar and turbulent flow regimes. Since

Darcy's relationships presupposes laminar flow, we conclude that this number must be small and consequently velocities must be small. It may then be permissible to discount the effects of velocity on permeability.

Through manipulation of the π_2 term we see that

$$k_p = \frac{g_p \kappa_p \rho_p \mu_m}{g_m \kappa_m \rho_m \mu_p} \cdot k_m \tag{107}$$

For centrifuge testing of the same materials (i.e. $\kappa_p/\kappa_m = \rho_p/\rho_m = \mu_p/\mu_m = 1$) this then states that

$$k_p = \frac{1}{n} k_m \tag{108}$$

or that the model is effectively n times more permeable than the prototype when identical materials are used. If some method could be conceived to also model the basic soil grain structure in the same ratio as other lengths so that $\kappa_p/\kappa_m = n^2$, then

$$k_p = n k_m \tag{109}$$

or the model would be n times less permeable than the prototype.

Let us now assert that the velocity of flow in soils is dependent on permeability, k, the hydraulic gradient, $\Delta H/\ell$, and the remainder of the independent variables used above.

$$v = f(k, \frac{\Delta H}{\ell}, g, \kappa, \mu, \rho) \tag{110}$$

Since k has just been shown to be dependent on the last four of these variables, it will be omitted. Since $\Delta H/\ell$ is itself a

dimensionless grouping, in the dimensional analysis we are left with

$$f'(v, g, \kappa, \mu, \rho) = 0 \tag{111}$$

and by an analysis analogous to that for k,

$$v_p = \frac{1}{n} v_m \tag{112}$$

So the velocity ratio is now seen to be related to the inverse of the length scale.

$$\frac{v_p}{v_m} = \beta = \frac{1}{n} = \frac{1}{\lambda} \tag{113}$$

The velocity scale ratio might have been guessed from the equation $v = ki$, but this is a risky practice when materials of the prototype are used in the model. Had we tried to guess at the scale relation for q from $q = kiA$, we may have been led astray.

The next item of interest in the flow through soils problem is that of pore pressures. It is customary in soil mechanics, when discussing this phenomenon, to use the term head. Since head has dimensions of length, there is a temptation to automatically assume that it will scale as other lengths, but it is worth the effort to prove this on the outside chance that one may have guessed wrongly.

Total head is correctly composed of three parts. The first is elevation, and since it is totally dependent on a length measurement, it will scale as length. The second part is that due to pressure. In nearly all problems of steady state flow through

soils, pore pressure is dependent upon the weight of the fluid and depth, d, below the free water surface.

$$p = f(d, g, \rho) \qquad (114)$$

A dimensional analysis will show that

$$p_p = \frac{\rho_p g_p d_p}{\rho_m g_m d_m} \cdot p_m = \frac{1}{n} \cdot \lambda \, p_m = p_m \qquad (115)$$

or that pressures in the prototype and model are the same if length is scaled inversely to acceleration. If we define pressure head as

$$h_\gamma = \frac{p}{\rho g} \qquad (116)$$

then it is obvious that since pressures are the same, pressure heads will scale as the inverse of the gravity scale or as length, i.e. $h_{\gamma p} = \lambda h_{\gamma m}$.

Velocity head is the final part of total head. It is normally considered small and neglected, but its effect should be investigated. The velocity head is usually written

$$h_v = \frac{v^2}{2g} \, . \qquad (117)$$

The velocity head scale is

$$\frac{h_{vm}}{h_{vp}} = \frac{v_m^2 g_p}{v_p^2 g_m} = \lambda^2 \cdot \frac{1}{n} = \lambda \, , \qquad (118)$$

or

$$h_{vm} = \lambda \, h_{vp} \qquad (119)$$

It then remains to be determined if this quantity may be neglected. Water flowing in a very permeable soil having k = 1 ft/sec under a very steep gradient $\Delta H/\ell$ = 1 would have an apparent velocity of 1 ft/sec. Velocity head in the prototype would then be about .015 feet. For most circumstances this is an insignificant quantity even at high acceleration ratios.

Now it can be stated that by neglecting velocity head total head does in fact scale as length between prototype and model.

$$(h_\rho + h_\gamma)_p = \lambda(h_\rho + h_\gamma)_m \tag{120}$$

Until now we have implicitly assumed that flow has been through saturated soils. If the soil is not saturated or the flow has a free surface, surface tension in the fluid will affect the flow. Surface tension manifests itself in the establishment of a capillary zone in the soil. It should therefore be sufficient in determining the effects of surface tension to determine the relationship between capillary zones in the prototype and model. The height, D, of capillarity is determined by surface tension, s, density of the fluid, ρ, gravity, g, and the effective diameter of interparticle voids, d.

$$D = f(d, g, s, \rho) \tag{121}$$

A dimensional analysis results in the following grouping necessary for similarity:

$$\left(\frac{s}{\rho g d D}\right)_p = \left(\frac{s}{\rho g d D}\right)_m \tag{122}$$

or

$$D_p = \frac{s_p \rho_m g_m d_m}{s_m \rho_p g_p d_p} \cdot D_m \qquad (123)$$

Assuming the same material is used in prototype and model,

$$D_p = n \cdot D_m \qquad (124)$$

or the effect of capillarity is exactly reproduced in the model, a condition very beneficial since we do not know exactly what these effects are. It is interesting to note that if the effective diameter of interparticle voids had been scaled as other lengths, D_p would equal D_m. This is a strong argument against using substitute materials in flow problems where capillary action is significant.

Similarity in Transient Phenomenon

All scaling relations needed for a study of steady state seepage have now been developed. Before these relations can be used in the modelling of transient flow, a relationship for the time scale must be established. The governing equation for unsteady one-dimensional flow for an elemental unit volume is

$$\frac{\Delta q_x}{V} = k_x \frac{d^2 h}{dx^2} \quad , \qquad (125)$$

where Δq_x is the change in flow rate in the x-direction, V is a unit volume, k_x is the coefficient of permeability in the x-direction, h is the total head of the volume, and x is the direction of flow. If elemental volumes are considered, the left side

of the equation can be reduced to

$$\frac{\Delta q_x}{V} = \frac{1}{\Delta t} \qquad (126)$$

Combining these terms into a dimensionless grouping and applying the rule that such terms must be equal for both model and prototype results in

$$\left(\Delta t \, k_x \frac{d^2h}{dx^2}\right)_p = \left(\Delta t \, k_x \frac{d^2h}{dx^2}\right)_m \qquad (127)$$

which dimensionally states

$$\Delta t_p = \frac{k_{x_m} \left(\frac{d^2h}{dx^2}\right)_m}{k_{x_p} \left(\frac{d^2h}{dx^2}\right)_p} \cdot \Delta t_m \; . \qquad (128)$$

Since d^2h/dx^2 is dimensionally $1/L$, the derivative terms will scale as L_p/L_m or λ, and since $k_m/k_p = n$

$$\Delta t_p = n^2 \Delta t_m \qquad (129)$$

This relationship is contrary to what was stated in a previous section (see equation 73) and is entirely due to the fact that we use the same material in both model and prototype. This relationship can also be shown on an intuitive basis. Consider the basic factors which affect the time it takes water to move from one point to another in a soil mass. Such factors would be the physical permeability, κ, the hydraulic gradient, $\Delta H/\ell$, the fluid density, ρ, viscosity, μ, the gravity, g, since we are only concerned with gravity flow, and x, the distance between points.

$$t = f(x, \frac{\Delta H}{\ell}, g, \kappa, \rho, \mu) \tag{130}$$

and the same dimensional analysis as before can be performed. A pertinent dimensionless grouping is

$$\left(\frac{\rho\kappa g t}{\mu x}\right)_p = \left(\frac{\rho\kappa g t}{\mu x}\right)_m . \tag{131}$$

Then

$$t_p = \frac{\rho_m \kappa_m g_m \mu_p x_p}{\rho_p \kappa_p g_p \mu_m x_m} \cdot t_m = n \cdot \lambda \cdot t_m = n^2 t_m , \tag{132}$$

which is the same as equation 129.

In summary, the pertinent scaling relations for the flow of water through soils have now been theoretically developed. Table 1 lists these relationships in terms of the acceleration factor n.

Table 1

Summary of Theoretical Scaling Relations
for Water Flow Through Soils

Property	Scale
Flow quantity	$q_p/q_m = n$
Permeability	$k_p/k_m = 1/n$
Velocity	$v_p/v_m = 1/n$
Pressure	$p_p/p_m = 1$
Head	$h_p/h_m = n$
Capillary rise	$D_p/D_m = n$
Time	$t_p/t_m = n^2$

CHAPTER IV

DESCRIPTION OF TESTING HARDWARE

All testing was conducted in the geotechnical laboratory of
the University of Colorado at Boulder utilizing the 10 g-ton geo-
technical centrifuge located there. Most periphery equipment was
specifically constructed for this particular test series. Moni-
toring and data recording were accomplished by standard manufactured
items. The purpose of this chapter is to detail each component's
function and, for specially constructed items, the details of
their construction.

The Centrifuge

Specifications and principal dimensions for the Genisco model
1230 centrifuge are given in Table 2. A principal advantage of
this centrifuge for soil modelling is its swinging baskets which
were specially made by modifying the original machine. This
enables samples to be placed and tested with resultant gravity
and acceleration forces always correctly oriented with respect to
the model. Therefore, a sample can be placed with an initial free
water surface if desired.

A vertical shaft on the rotation axis contains the electrical
and hydraulic slip rings. Of the 56 electrical slip rings, two are
committed to a video signal and three to power for the camera and

Table 2

Centrifuge Specifications

Manufacturer   Genisco

Model   1230-5

G-Range   Variable 1 to 262 G at
                            42 inch nominal radius

Driving System   25 H.P. hydraulic

Working Radii   42.0 inches – center to
                                    basket hinge
                            11.5 inches – hinge to basket
                                    floor

RPM Range   0-470 rpm

Payload Capacity   20,000 G-lbs (200 lb at
                            100 g)

Test Package Size   18-inch cube maximum

Electrical Pick-ups   56 slip rings

Fluid Transfer   2 hydraulic slip rings

Test Recording   Closed circuit TV

lighting. The remainder are available for test control and
monitoring. The shaft also contains two hydraulic slip rings
suitable for water or light oil to 3000 psi. On switching from
oil to water, a thorough flushing with warm soapy water followed
by clear water has proved to effectively remove all oil residue.
Before again using oil, the rings and lines are flushed with air
to evaporate the water.

Counterbalancing of the rotating arm was accomplished with a
watertight aluminum box partially filled with water. One of the
hydraulic slip rings was dedicated to the counterweight so that as
water was supplied to sample container, an appropriate amount could
also be fed into the counterweight during a test. This was neces-
sary to maintain a dynamic balance of the rotating system and
proved very effective. Figure 6 is a schematic of the rotating
arm and vertical shaft with baskets swung up as they are in a test.

Since testing also involved a release of water, a gutter was
installed on the interior of the centrifuge's protective enclosure
to collect the water released from the test package. A 2 inch
stiff plastic pipe was split along its length to form this gutter.
It was then braced and glued along one edge with silicone caulking
to the inside wall of the centrifuge.

The centrifuge controls are mounted on a separate panel.
Besides the basic on-off switch there is a solenoid valve switch
for emergency shutdown and a hand wheel for regulating centrifuge
rpm's. RPM is monitored by an optical cog-counting device and
displayed on a needle gauge. This system is considered accurate
to ±2 rpm.

60
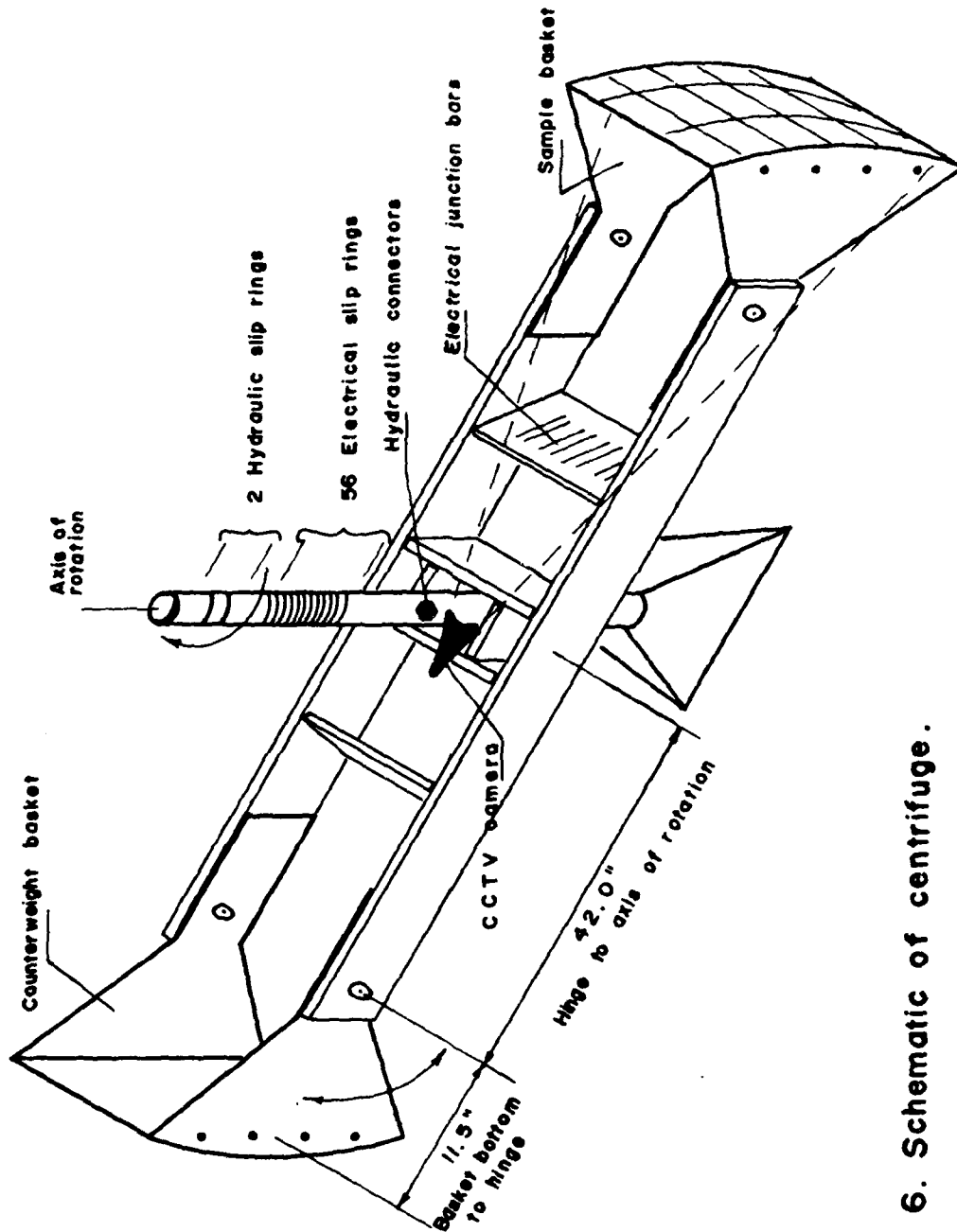
Figure 6. Schematic of centrifuge.

Testing is monitored by a video camera mounted near the axis of rotation and rotating with the centrifuge. Pictures are displayed on a black and white television and a video cassette recorder is used to record each test. This system proved to be a very valuable tool. Headwater rise and fall measurements were taken from the video record and all time measurements were made with voice notes on the cassette.

Normally only a top view of the sample would be available during a test, but a mirror mounted on the sample basket enables one to have a full side view also. While some of the machine capacity is tied up in this indirect viewing system, the benefit of being able to observe each test in progress is well worth the sacrifice. Details of the sample container and mirror mountings are shown in Figure 7. In this figure, the basket is swung down as it is when the centrifuge is not rotating.

Sample Container

The sample container was specifically constructed for this test series but is suitable for other applications also. Figure 8 shows an exploded view of the box. The principal construction material is aluminum because of its strength to weight characteristics. A plexiglass wall is used to allow a full side view of the sample during testing. Since plexiglass scratches very easily, a thin inner sheet is used for replacement purposes. The inner sheet is cross-hatched to aid in length measurements during a test. Before assembly, the container joints are coated with silicone caulking to make it watertight.
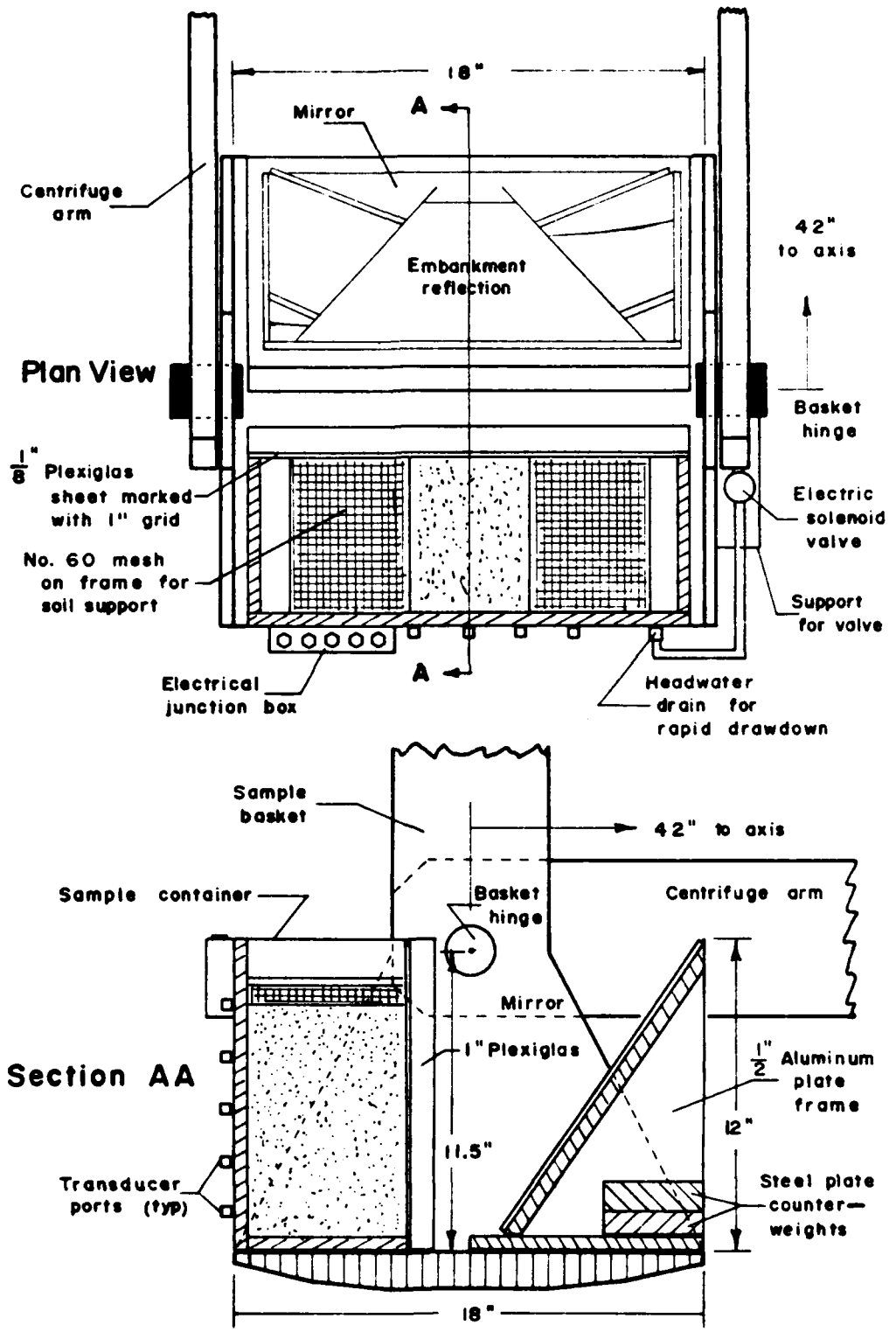
Figure 7. Detail of mounted sample container.
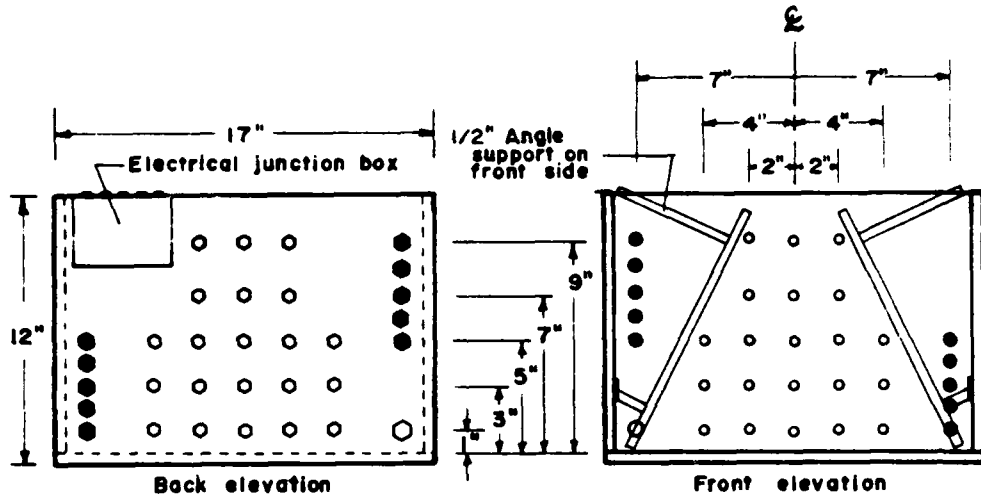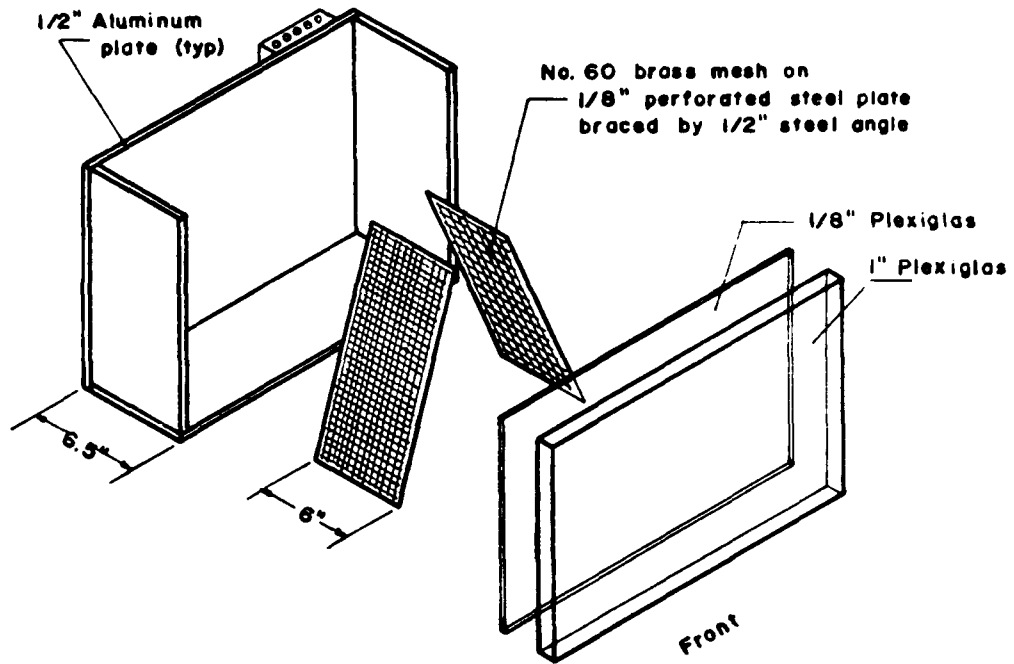
63

Figure 8. Details of sample container.

Because of the sandy nature of the soils to be used in the testing program, some support for the embankment was required. This support had to be as permeable as possible yet rigid enough to maintain its shape during sample placement and compaction. To accomplish this a 1/2 inch angle steel frame was constructed for each side. Onto this frame is bolted a 1/16 inch thick perforated steel plate which has been covered by a number 60 mesh brass screening. The system worked very well in allowing free water passage while acting as a filter to prevent erosion of the embankment.

Holes spaced one inch center to center on upstream and downstream ends of the box allow positive control of headwater and tailwater levels. A larger hole near the bottom of the headwater side is used for releasing water in a rapid drawdown simulation.

Standard brass fittings were modified for use as pressure transducer holders. Details of the transducer port and transducer (to be described later) are shown in Figure 9. Specifications of the ceramic filter are given in Table 3. These porous ceramic stones were specifically chosen for their high air entry value. Once saturated, the stones held that moisture during initial phases of each test until the sample itself was saturated. The ceramic filters were cored from a 6 mm thick by 6 inch diameter disk with a miniature diamond coring bit. They were mounted flush to the inside wall of the sample box with epoxy cement.

65
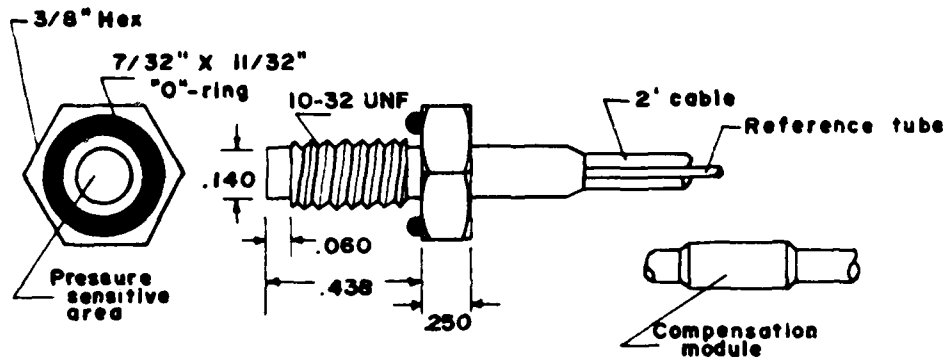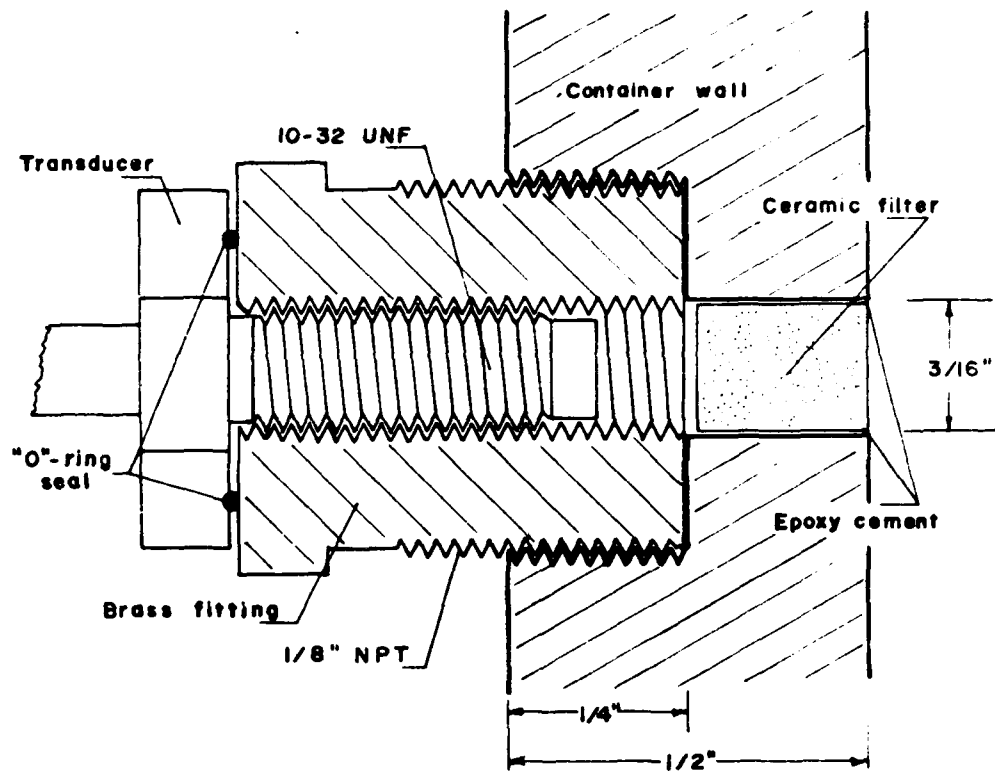
Figure 9. Details of transducer port and transducer.

Table 3

Properties of Porous Ceramic*

Manufacturer	Coors Porcelain Company
Designation	P-3-C
Bubble Pressure	19-28 psi
Pore Diameter	1.5 - 2.2 microns
Apparent Porosity	42.1%
Absorption	22.8%
Specific Gravity	1.83
Flow Rate	0.2 - 0.7 ml H_2O/sec/in^2 at 20 psi head
Permeability	23-40 x 10^{-3} Darcies at 20 psi head

*Reference ASTM 128-61

Pressure Transducers

Four miniature pressure transducers, Entran model EPS-1032, were used for pore pressure measurement during the tests. Specifications of the transducers are given in Table 4. These devices proved extremely reliable and to have a constant calibration ratio. In preliminary checks it was determined that the transducers in conjunction with power and data recording equipment used during tests required a warm-up period of about 2 hours which was faithfully observed during actual testing. Figure 10 shows transducer output as a function of time for a constant pressure. Maximum drift was determined to be about 0.1 psi/hr. The effects of drift were minimized by calibration of the transducers immediately prior to each test as will be explained in a later chapter.

The operating principle of the transducers is basically that of a wheatstone bridge resistor circuit on a diaphragm exposed to the fluid. They were mounted in the sample container such that the diaphragm was oriented parallel to the acceleration forces to minimize any effects centrifugal testing might have on the transducer itself. A series of tests proved their in-flight calibration ratio to be the same as under 1-g conditions. The back of the transducer diaphragm is referenced to atmospheric pressure through a small tube. A jet of air flowing past this tube, simulating eddie air currents during centrifuge operating, was shown to have no effect on transducer output.

Table 4

Transducer Specifications

Manufacturer	Entran Devices, Inc.
Designation	EPS-1032
Range	#'s 1 & 2, 250 psi #'s 3 & 4, 100 psi
Sensitivity	#1 0.43 mV/psi #2 0.47 mV/psi #3 0.91 mV/psi #4 0.97 mV/psi
Impedance	Input 500 ohms (nom.) Output 250 ohms (nom.)
Excitation	6.0 V D.C.
Combined Non-Linearity and Hysteresis	±0.5% F.S.
Repeatability	0.25%
Thermal Zero Shift	±1.5% F.S./100°F
Thermal Sensitivity Shift	±2%
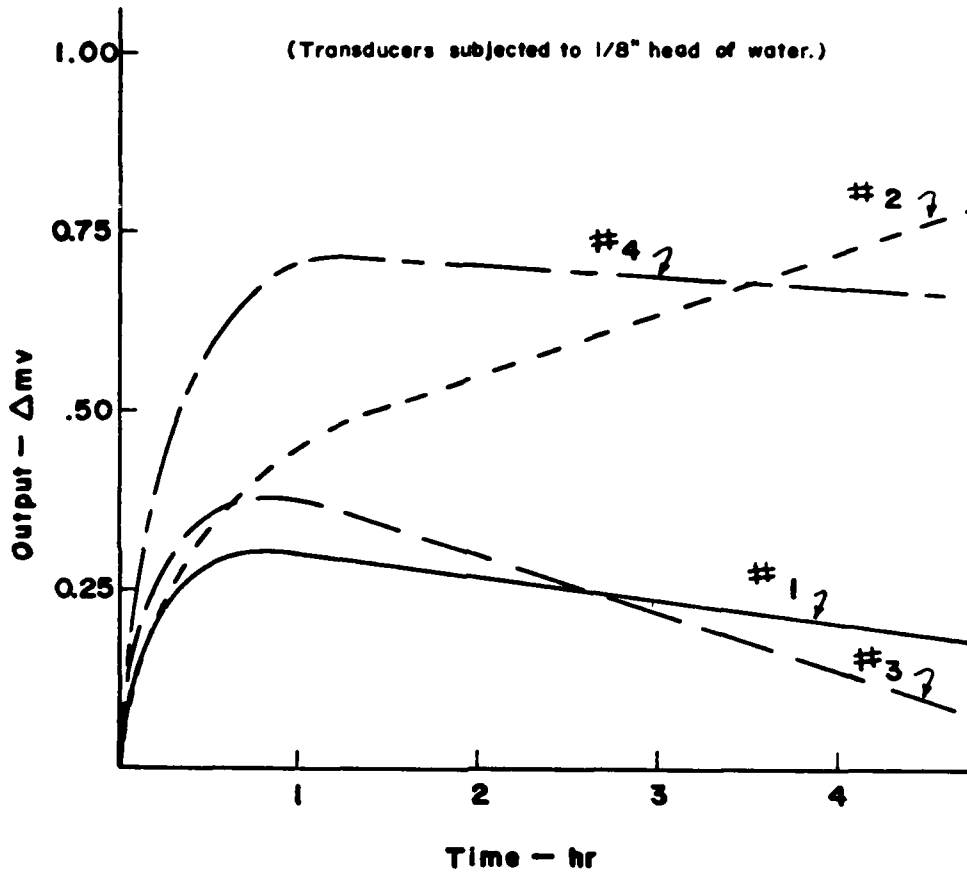
Figure 10. Transducer drift as a function of time.
(For transducer calibration, see Table 4.)

Water Supply and Control

The conduct of the tests involved the filling, maintaining a flow, and the draining of water. Water supply for the first two phases was contained in two 7½ gallon stiff plastic containers. A 5 psi air pressure was maintained on the containers to assist in the movement of the water. Flow rate was regulated by valves installed in the supply lines. To maintain dynamic balance in the centrifuge, one container is dedicated to the counterweight while the other supplies the sample container.

Simulation of rapid drawdown requires a method of rapidly releasing water from the headwater side of the sample. This was accomplished by piping an electrical solenoid valve into the head-water drain. The valve was mounted such that its induction core was in line with acceleration forces. At 75 g the valve operation was impaired due to its own self-weight, but at the maximum test of 50 g its operation was normal. Mounting the valve with its core perpendicular to acceleration forces may be the solution to higher g-testing but then the valve housing may be put in jeopardy since it is a standard off-the-shelf item not specifically designed for centrifuge testing. Another solenoid valve was installed on the counterweight to insure dynamic balance during drawdown. The controls for the two solenoids were separate on-off switches outside the centrifuge.

As previously mentioned, headwater and tailwater levels were maintained in the sample container by simply removing a plug at the levels desired. Excess water was then continuously released.

Most of this was collected in the gutter but some splashes off the wall onto the centrifuge floor.

Data Collection

The heart of the data acquisition and recording system is a Hewlett-Packard model 3485A scanning unit. It is coupled to a model 3480A digital voltmeter and a model 5055A printer. The scanning unit reads the four transducer outputs in less than one-half second and the printer produces a paper tape of the readings for later reduction. As each reading was taken, an audio mark was made on the video cassette recorder so that a positive correlation could be made between transducer output, time, and head-water level.

A three channel x-y-y' plotter was also used to record the output of two of the transducers on a time scale. This provided an immediate visual record which was invaluable in determining when steady state had been reached and when pressures had completely dissipated.

Figure 11 is a line drawing of the testing hardware arrangement showing the relative position of major items during a typical test.
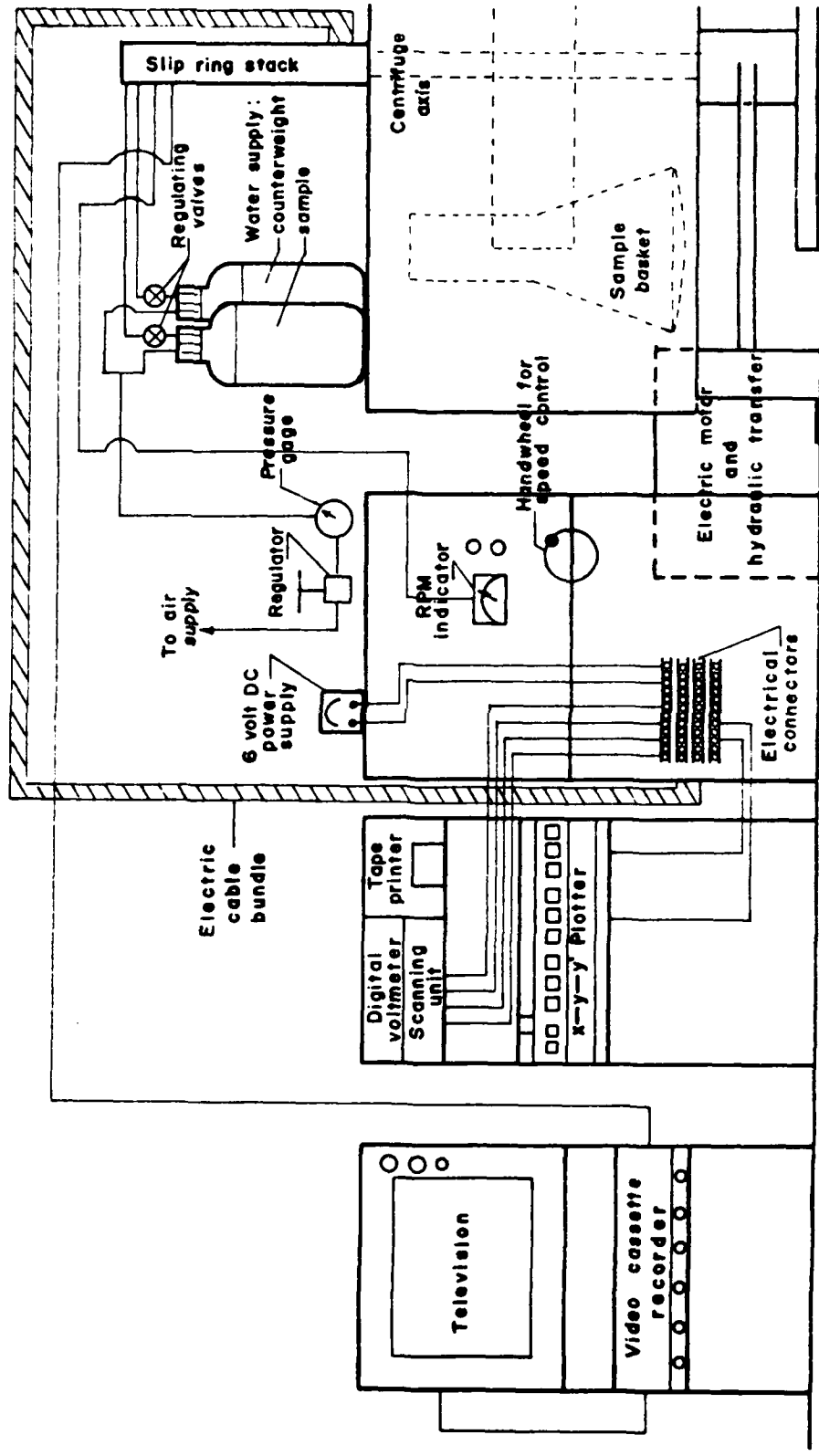
Figure 11. Schematic of centrifuge, controls, and monitoring equipment.

CHAPTER V

TEST PROCEDURE

The objectives of the experimental phase of this research
are threefold: first, to develop an apparatus suitable for model-
ling the transient flow problem in a geotechnical centrifuge;
second, to establish a procedure for the conduct of transient flow
modelling; and third, to verify the scaling relationships applicable
to fluid flow modelling. The purpose of this chapter is to focus
on the second objective by describing how the tests were carried
out. The procedure adopted, devised somewhat by trial and error,
appears successful. The first objective was covered in the pre-
ceding chapter and the third will be covered later.

Preparation for the Tests

Modelling Materials

Any discussion of testing procedure must necessarily begin
with a description of materials used in the testing. For the
procedure to be described, a radical change in the materials would
mean changes in some phases of the testing but the basic approach
should remain unaltered. However, there may be abnormalities in
the results which can only be explained through a knowledge of the
properties of the materials involved.

Four different soils were used in this study. They are all specially proportioned mixtures of mainly sand and silt grains. Specifications for each mixture are given in Table 5. These soils were selected because they have been the subject of extensive investigation at the University of Colorado and much is known of their properties. Some typical properties and their values are listed in Table 6.

Soils were prepared by dry sieving the parent material into the required fractions and then recombining these fractions in the specified proportions. So the nomenclature Original soil does not indicate an in-situ soil but a reconstituted one. It is called original because specifications for the remainder of the soils are based on it. The Coarse Removed soil is the same as Original with all materials retained on a number 20 sieve removed. The Same D-10 soil is designed also without the coarse grains and to have the same percentage of D_{10} sizes as Original. The CU soil is also the same finer grains proportioned to have the same uniformity coefficient as Original. Grain size distribution curves are shown in Figure 12. The dashed curves indicate results of dry sieve analysis after a series of flow tests. As can be seen, there was a minor loss in the finest grain sizes.

The modelling fluid was distilled water. Since headwater levels were recorded by visual observation, the water was dyed with food coloring to give a better visual record. The addition of the coloring was considered to have no influence on the properties of either the water or the soil.

Table 5

Sample Grain Size Specifications

Sieve Number	Percentage Passing			
	Original	Coarse Removed	Same D-10	Same CU
4	100	—	—	—
10	88	—	—	—
20	60	100	100	100
40	24	40	35	79
60	16	27	21	60
120	10	17	10	26
200	8	13	8	16
400	5	8	5	10

Table 6

Engineering Properties of Sample Soils

	Original	Coarse Removed	Same D-10	Same CU
Max. Rel. Density (dry) (pcf)	120.9	113.0	116.0	119.75
Min. Rel. Density (dry) (pcf)	99.5	97.0	93.5	91.0
Specific Gravity	2.67	2.67	2.67	2.69
Angle of Internal Friction	50°	46°	50°	48°
Cohesion Intercept (psi)	0	0	0	0
Permeability (ft/sec)	4×10^{-7}	8×10^{-7}	3×10^{-7}	4.5×10^{-7}
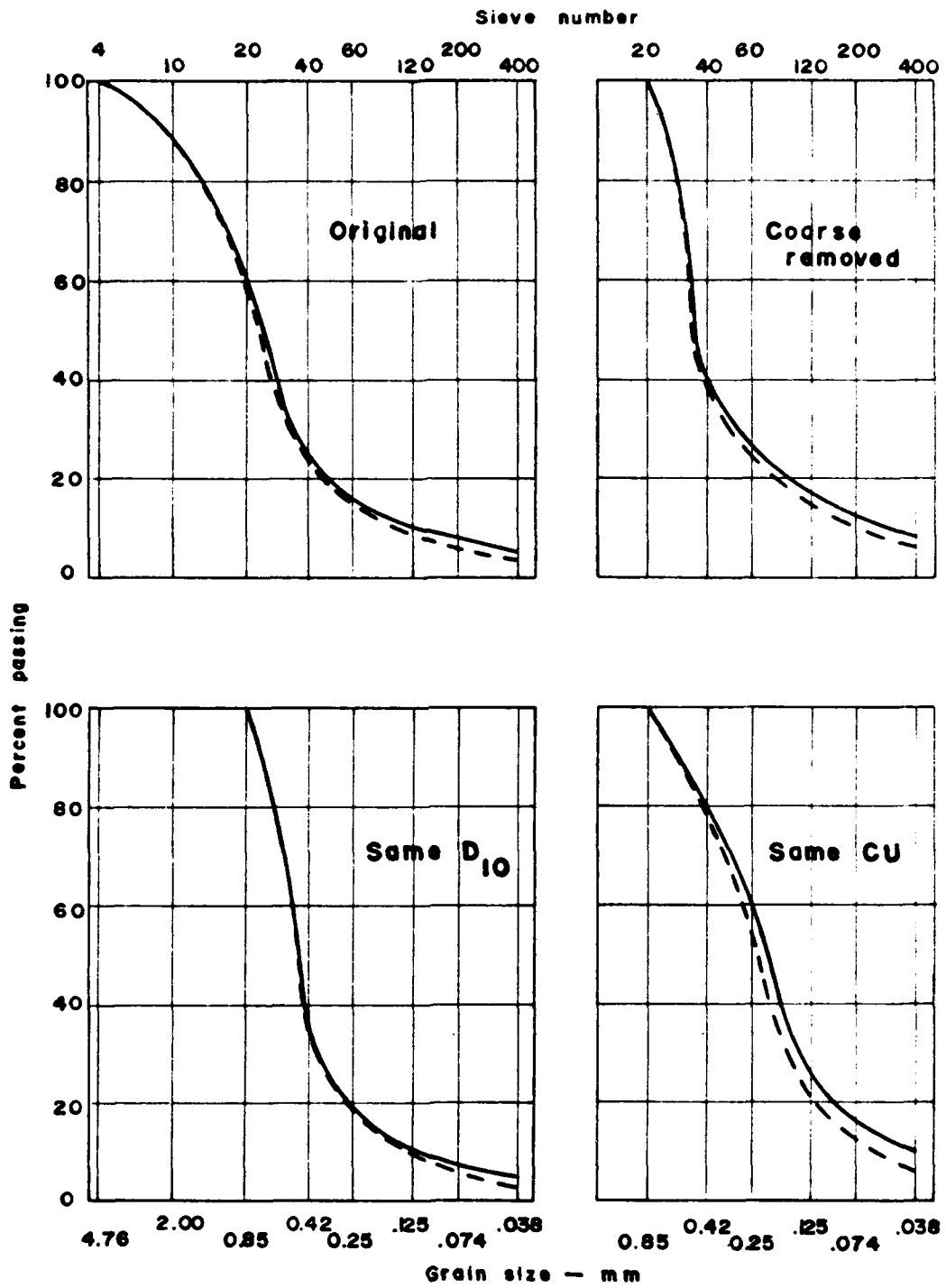
Figure 12. Grain size distribution curves.

Sample Preparation

All soil samples were prepared in an identical manner. After dry batching to the correct specificaitons, water was added to obtain a moisture content of 10 percent. This moisture content was selected to insure that there was sufficient water in the soil to prevent any drying of the ceramic filters. Assuming typical moisture density curves for these sandy materials, this moisture content should also be on a fairly flat portion of the curve, thus making reproduction of densities easier.

Material was then compacted in layers into a fully assembled sample container from the top. Each lift had a compacted thickness of about one-half inch. The top of each lift was scarified transverse to the cross section before the next lift was placed. Each lift was thoroughly compacted with a tool specially designed for use in constructing a model section with sloping sides. After compaction to the required height, the density of each sample was determined. Table 7 gives in place densities of the four samples tested. Although every sample was placed at a uniform moisture content, centrifugal acceleration will cause a redistribution of water held in the soil. Figure 13 shows the results of moisture content determinations at various levels in the sample after testing at 50 g. Note that during the test there was a free water surface near the base of the embankment and some of this water may have been drawn by capillarity up into higher levels during deceleration and subsequent sampling for moisture determination.

Table 7

In-Place Sample Densities

|	Wet Density pcf	Dry Density pcf	Moisture Content %	Porosity	Void Ratio
Original	136.8	124.3	10	.24	.34
Coarse Removed	131.7	119.7	10	.28	.39
Same D-10	128.9	117.2	10	.30	.42
Same CU	123.0	111.8	10	.33	.50
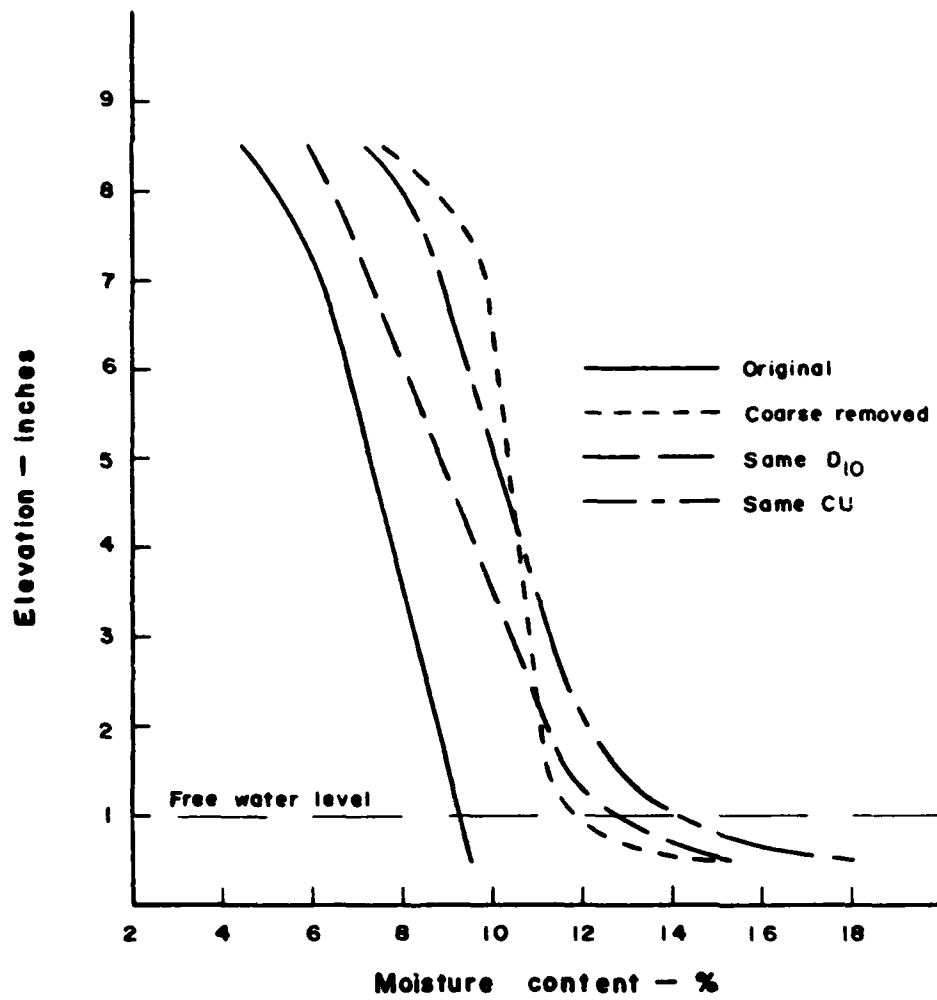
Figure 13. Moisture content as a function of depth after centrifuging at 50 g.

Before the soil was deposited in the sample container, all ceramic filters were saturated by filling the container with distilled and de-aired water, and allowing the water to percolate through them at least overnight. After the sample was placed and density determined, the transducer ports to be immediately used were again flushed from outside with distilled and de-aired water under 10 psi pressure. This also served to saturate a volume of soil in contact with the filter and further retard any possible drying before the container could be installed in the centrifuge.

Conduct of the Tests

Transducer Calibration

In a preliminary series of tests it was determined that although transducer sensitivity remains constant, there is a shift in the zero reading over a period of time. This shift was also evident whenever a transducer was moved from one port to another and when going from one g-level to another. To account for this shift, a calibration to determine the zero reading was done immediately before every test. This calibration consisted of putting a known level of water in the sample and centrifuging at the appropriate g-level until the readings became constant. Using the readings at this static pressure, the zero position of each transducer could be calculated.

Transient Flow Simulation

Once the transducers were calibrated, the centrifuge was stopped and the sample was drained, headwater and tailwater plugs were removed at the eight inch and one inch levels respectively, and the test package was accelerated in the centrifuge to the test g-level. When a stable centrifuge speed was reached, audio-video recording and two channel plotting were initiated. The time of each set of transducer output readings was referenced to an audio mark on the video record as were other major events such as the start of reservoir filling or the beginning of rapid drawdown.

Reservoir filling was begun by simply opening the valve from the water supply bottles. Output readings were taken every 10-15 seconds as the headwater level increased to its maximum. Once the headwater reached the previously opened drain plug, filling was complete and excess water was released through the drain. A flow greater than what was seeping through the embankment model was maintained so that there was always some excess being released. This insured a constant headwater level. Transducer output readings were taken about every 30 seconds until a steady state condition existed. During this process and that which followed, the tail-water elevation was kept constant by an open drain.

Drawdown simulation was accomplished by simultaneously closing the headwater supply valve and opening the solenoid drain valve near the upstream base. As the water was released, output readings were taken every 5 seconds until a steady state condition again existed.

A Test Series

Each of the four soil samples was used in nine separate transient flow tests. There were only four pressure transducers available for use, and so to get a sufficient distribution it was necessary to duplicate tests with the transducers at three different levels. To ascertain any differences due to the centrifugal acceleration, each sample was also tested at three different g levels. Figure 14 shows the locations where transducers were installed for the three test groupings.

The sequence of tests for each soil is as follows:

1. Install four transducers at 1 inch level and conduct three tests at 50 g, 37.5 g, and 25 g respectively.

2. Install transducers at 3 inch level and conduct three tests at 50 g, 37.5 g, and 25 g respectively.

3. Install transducers at 5 inch level and repeat.

It should be noted that each test was conducted only after the sample was fully drained and a transducer calibration had been accomplished. Before moving a transducer, the ceramic filter at the new location was flushed with distilled and de-aired water under pressure to insure saturation and the exclusion of air from the port.

As stated above, each sample was tested at three different g levels. In centrifuge testing, the radial acceleration experienced by a soil particle is calculated by the formula

$$a = \omega^2 r \qquad (133)$$
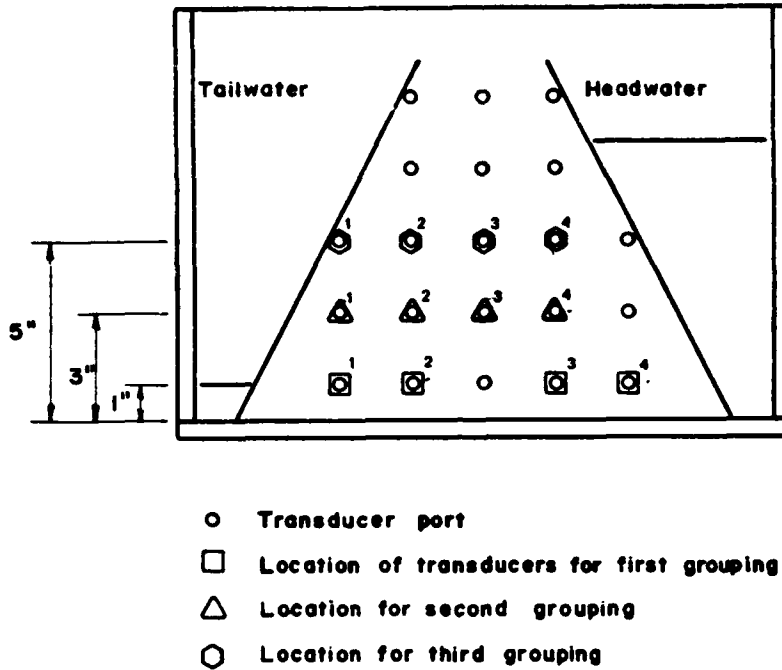
Figure 14. Transducer locations for each test grouping in a series.

where ω is the rotational speed measured in radians per time unit and r is the radial distance from the axis of rotation to the particle. It is therefore impossible for a soil sample having a finite height to experience the same acceleration over its full height during any one test. The larger the distance from the rotational axis, the less will be the variation in acceleration experienced by the upper and lower most particles in a sample. Acceleration levels stated in these test series are based on a radial distance from axis of rotation to the center of gravity of the embankment section equal to 49.25 inches. Since the same section was used throughout, this distance remains constant. To produce 25 g, 37.5 g and 50 g at the center of gravity, a rotational speed of 134 rpm, 164 rpm, and 189 rpm, respectively, is required.

Steady Flow Tests

In addition to transient flow tests, a steady flow test was also conducted with each sample at the three different g levels. The objective of these tests was to get a steady state flow rate from which scale factors for flow rate and sample permeability could be estimated. The tests were performed by maintaining a reservoir level beneath the overflow drain by manipulation of the inflow valve. Since there was no overflow, the amount of water going through the sample could be measured as the amount used from the supply bottle.

The testing procedure for each soil type was as follows:

1. Accelerate the sample to 25 g and fill the headwater reservoir to the 7 inch level on the embankment.

2. Manipulate the water supply valve to maintain a constant water level on the embankment without overflow.

3. Once equilibrium is reached, measure the time it takes a specified volume of water to leave the supply bottle.

4. On conclusion of the test at 25 g, accelerate the sample to 37.5 g without drainage or deceleration. Repeat steps 2 and 3.

5. After the 37.5 g test, accelerate to 50 g without drainage or deceleration and repeat steps 2 and 3.

CHAPTER VI

EXPERIMENTAL RESULTS

The raw data from each transient flow test consist of an audio-
video cassette recording and a paper tape containing transducer
voltage output. In this chapter, the manner of reducing these
data and resulting plots are given.

Each test is identified by a three part label, for example
CU-37-3. The first part indicates the type soil, the second indi-
cates the g level, and the third is the elevation head of the
transducers. In the example, the test was with Same CU soil at
37.5 g and with transducers 3 inches above the base of the sample.

Data from steady state tests to estimate permeability are
also presented.

Total Head versus Time

Figures A-1 through A-12 in the Appendix are graphs of total
head at the particular transducer location plotted as a function
of time. Figure 14 of the previous chapter shows the transducer
location in relation to the embankment cross section. Thus each
curve gives a history of the total head experienced by a particular
point in the embankment. Also shown in the figures is the headwater
level as a function of time. This curve was entirely generated

from the video record of each test. Tailwater elevation was always at the 1 inch level and is not shown.

The ordinate of each figure is total head. One should recall from previous chapters that total head is equal to the sum of pressure head and elevation head. For ease in referencing total head to the sample embankment, values shown are in inches of water at a particular rotational speed. These heads are calculated by adding the elevation of the transducer measured from the base of the sample to the pressure head recorded by that transducer. Transducer readings are reduced to a pressure head by the formula,

$$h_p = (A - B) \cdot C_i \qquad (134)$$

where A is the transducer voltage reading, B is the zero reference voltage determined during calibration, and C_i is a factor dependent upon transducer sensitivity and approximate water level. In determining B, account was taken of the fact that under centrifugal acceleration, a static water surface is curved as shown in Figure 15. Thus based on the observed water level on the sample container side, a circular arc with center at the axis of rotation is scribed on a scaled drawing and the actual head of water above each transducer is used to determine B for that transducer at a particular g-level and elevation.

The factor C_i has dimensions of inches/volt and is calculated by

$$C_i = \frac{1728\ g}{\gamma_w \omega^2 r}\ \frac{1}{c} \qquad (135)$$
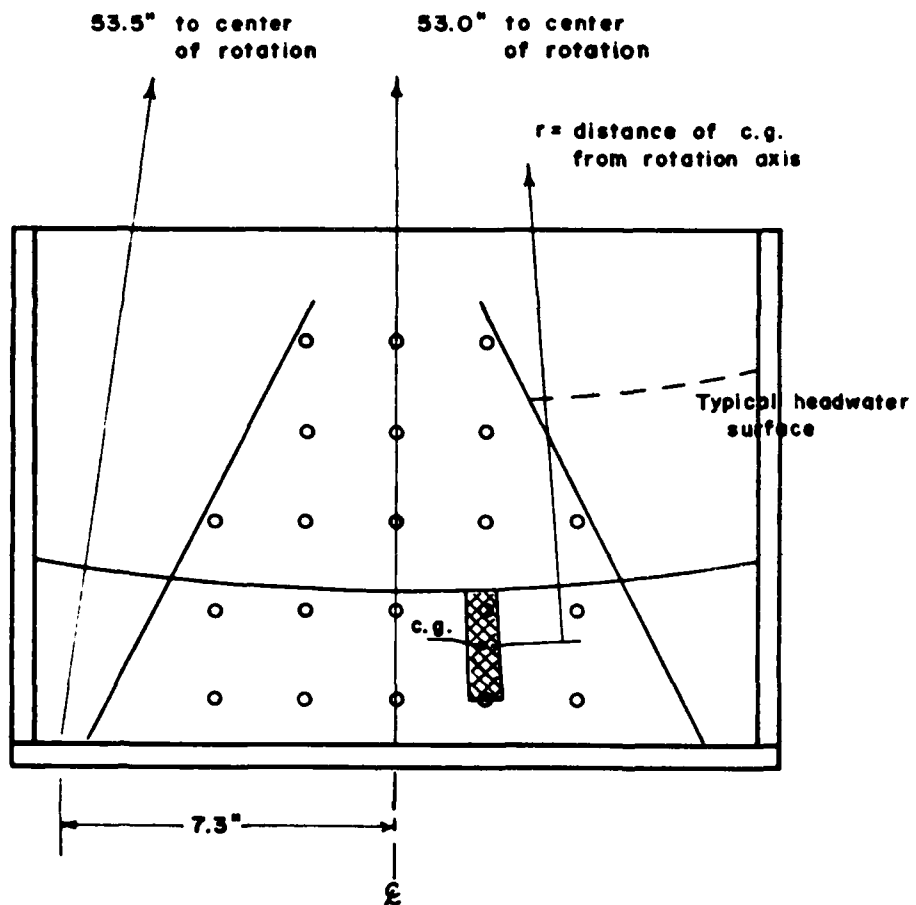
Figure 15. Curved water surface due to
centrifugal acceleration and
example of water column
exerting pressure head.

where g is the gravitational constant equal to 32.2 ft/sec^2, γ_w is the unit weight of water in pcf, ω is the rotational speed in radians/sec, r is radius in ft of the center of gravity of the water column causing the pressure, and c is the sensitivity factor for the transducer in question in volt/psi. Table 8 gives values of $C_i \cdot c$ for transducer levels and water heights encountered in the test series.

These factors are derived by considering the depth of the water column above the transducer since it is responsible for the pressure head measured. The factor is actually a continuous function of the radius of the center of gravity of this water column but has been lumped in one inch intervals for ease of calculations. So, for example, the factor for total head of 4.5 inches at 25 g and with transducers at 1 inch level is calculated by substituting into equation 135 above the proper ω for 134 rpm and r = 50/12. This distance is based on a 4 inch column of water above the transducer which puts the center of gravity of this column 3 inches above the bottom of the sample container which is 53 inches from the rotation axis as shown in Figure 15.

To illustrate the data reduction procedure, a typical example is as follows:

During a calibration run at 50 g with the transducers at the 1 inch level, the water level on the sample container side is observed at 4.1 inches. From Figure 15, it can be seen that this gives a water elevation of 3.5 inches over transducer number 3. This gives a 2.5 inch column of water

Table 8

Data Reduction Factors for Each Transducer Level
as a Function of the Total Head

$C_i \cdot c$ (in./psi)

Total Head	Transducers at 1" Level			Transducers at 3" Level			Transducers at 5" Level		
(in.)	25 g	37.5 g	50 g	25 g	37.5 g	50 g	25 g	37.5 g	50 g
1-2	1.0552	0.7044	0.5304	—	—	—	—	—	—
2-3	1.0655	0.7113	0.5356	—	—	—	—	—	—
3-4	1.0761	0.7184	0.5409	1.0978	0.7329	0.5518	—	—	—
4-5	1.0868	0.7256	0.5463	1.1090	0.7404	0.5575	—	—	—
5-6	1.0978	0.7329	0.5518	1.1204	0.7480	0.5632	1.1440	0.7638	0.5751
6-7	1.1090	0.7404	0.5575	1.1321	0.7558	0.5691	1.1562	0.7719	0.5812
7-8	1.1204	0.7480	0.5632	1.1440	0.7638	0.5751	1.1686	0.7802	0.5874

Values of c for each transducer used can be found in Table 4.

at 50 g acting on transducer number 3. From Table 8, the
reduction factor, $C_i \cdot c$, is found to be 0.5409 in/psi for
total heads between 3 and 4 inches. From Table 4, the sensi-
tivity for transducer number 3 in 0.91 mV/psi. Therefore,

$$C_i = \frac{C_i \cdot c}{c} = 0.5944 \text{ in/millivolt} \tag{136}$$

Suppose that the transducer reading was 15.25 mV for this
calibration, then B can be back-calculated from equation 134
since we know h_p = 2.5 inches, A = 15.25 mV, and C_i = 0.5944.

$$B = \frac{A \cdot C_i - h_p}{C_i} = 11.04 \text{ mV} \tag{137}$$

This value for B is then used for reduction of all data
from transducer number 3 in this particular test. Since
all tests involve a rising total head followed by a falling
total head, the top $C_i \cdot c$ value in the table for the proper
test conditions is used until the calculated total head
indicates the next $C_i \cdot c$ value should be used.

A typical trace of transducer output as recorded on the x-y-y'
plotter is shown in Figure 16. As can be seen, there are regions
at the beginning and end of the record when the transducer is
apparently registering negative pressure. The presence of these
negative pressures can be explained in terms of surface tension on
the face of the ceramic filters. In the early stages of a test,
the ceramic filter is above the saturation line in the embankment.
The decreasing slope of the transducer output is probably due to
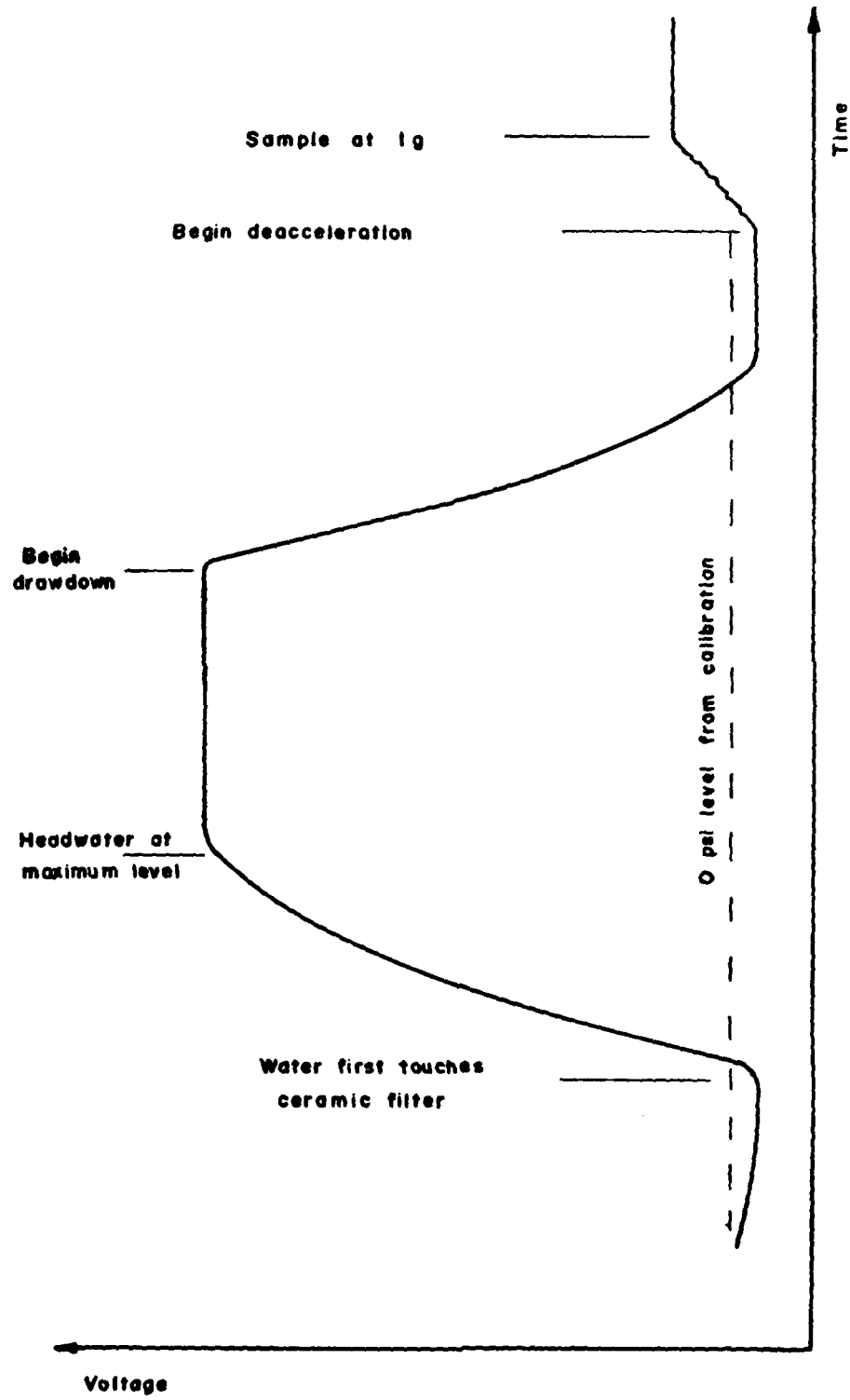
Figure 16. Typical trace of transducer output during a test.

drying of the filter face on a microscopic scale. As the top layer
of water is evaporated, the menisci have a decreasing radius leading
to increased tension which is transmitted through the saturated
filter to the transducer. Another possibility for the negative
pressure is that the centrifugal force tends to pull water from the
saturated filter when it is above the saturation line, but this
does not account for the decreasing slope. A case for the former
possibility was made by circulating air over a saturated but exposed
filter at 1 g. Before the air was caused to circulate, the trans-
ducer output was nearly constant. When the air was circulated, the
transducer output showed a marked downward trend. A case for the
latter possibility is made by the shape of the curve after drawdown
in Figure 16 which is typical of several tests. The distinctive
flattening of the curve can more realistically be explained in terms
of a centrifugal pull on the water in the saturated filter. The
correct explanation of the negative pressure is probably a combina-
tion of the above.

It was shown that these negative pressures are of no conse-
quence in the conduct of the transient flow tests. By varying the
water level in the sample container while being centrifuged without
a soil sample, it was shown that transducer calibration was
unaffected by prolonged exposure to air. After a reading at a
certain water level, the water was drained to fully expose the
ceramic filter face. Relatively high negative pressures were
allowed to develop, and then the water was brought back to the
original level. The transducer output showed a sharp increase as

the filter was covered and then increased as the water level increased. The final reading matched the initial reading.

The increase in transducer output during deceleration as shown on the right of Figure 16 also supports the theory that centrifugal pull is responsible for negative pressures, but the steadily decreasing pressure as shown on the left of Figure 16 is still best explained in terms of evaporation from the filter face. Figure 16 also shows a zero shift in the transducer between test g-level and 1 g. However, the method of calibration described earlier would take this shift into consideration.

Equipotential Distribution During Transient Rise

For each set of tests at a particular g level and soil type, equipotential lines are plotted for five headwater levels during the rise of the phreatic surface. These plots are shown in Figures A-13 through A-24 in the Appendix which also include the steady state situation for comparison. Since it was not possible to exactly duplicate the headwater rise in every test, an average rise was selected from the three under consideration. The head-water level to be plotted was then chosen from this average curve at the times 1 min, 2 min, 3 min, 4 min, and 6 min respectively. Total head was then read from each of the three tests at this head-water level and used to generate the curves depicted. Numbers under each embankment section indicate the values of total head at the corresponding transducer location at that time instant.

Equipotential Distribution During Rapid Drawdown

Using headwater levels during drawdown from the tests with transducers at the 1 inch level for each particular soil type and g-level, equipotential lines were again plotted and are shown in Figure A-25 through A-36 in the Appendix. These headwater levels correspond to the times 15 sec, 30 sec, 45 sec, 1 min, and 2 min after the start of drawdown. The steady state condition is again reproduced in the first section for reference.

Steady State Flow Tests

The results of these tests are quantities of water flowing during a particular time period. Measured quantities are plotted against time in Figure 17 through 20 for each soil type and g level. For the Original soil, the results of two separate groups of flow tests are plotted. The first group of these tests was conducted after the sample had been saturated and drained but before the series of transient flow tests. The second test group was conducted after the transient flow tests had been completed.

Figure 18 for the Coarse Removed soil shows three test groupings. The first two groupings were conducted under the same circumstances as for the Original soil. The third grouping was conducted immediately after the second with no drainage of the soil between the two tests. Flow tests on the other two soils were conducted after the transient flow tests.

Discussion of the test results and their interpretation will be given in the next chapter.
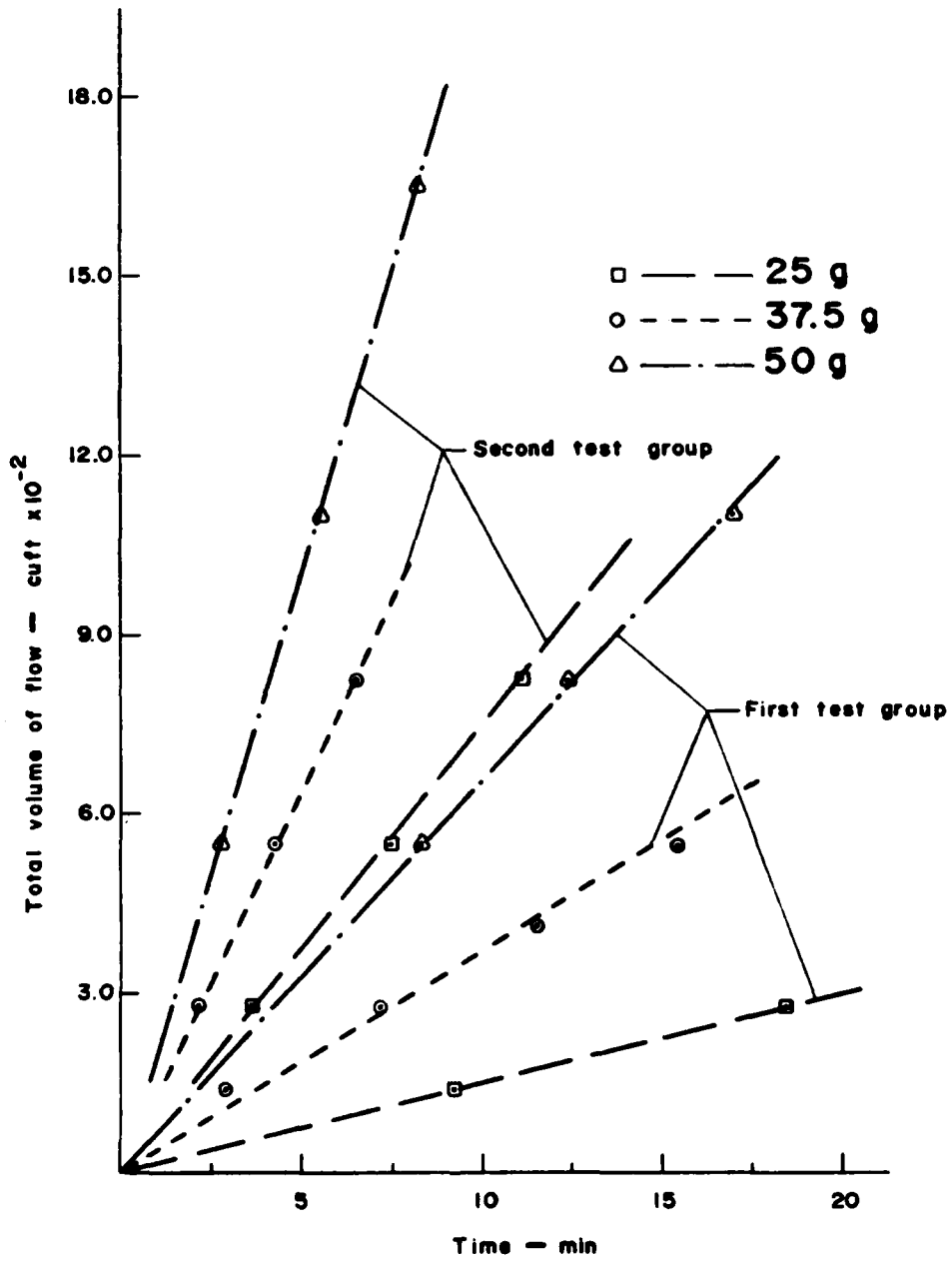
Figure 17. Volume of flow as a function of time for Original soil.

97
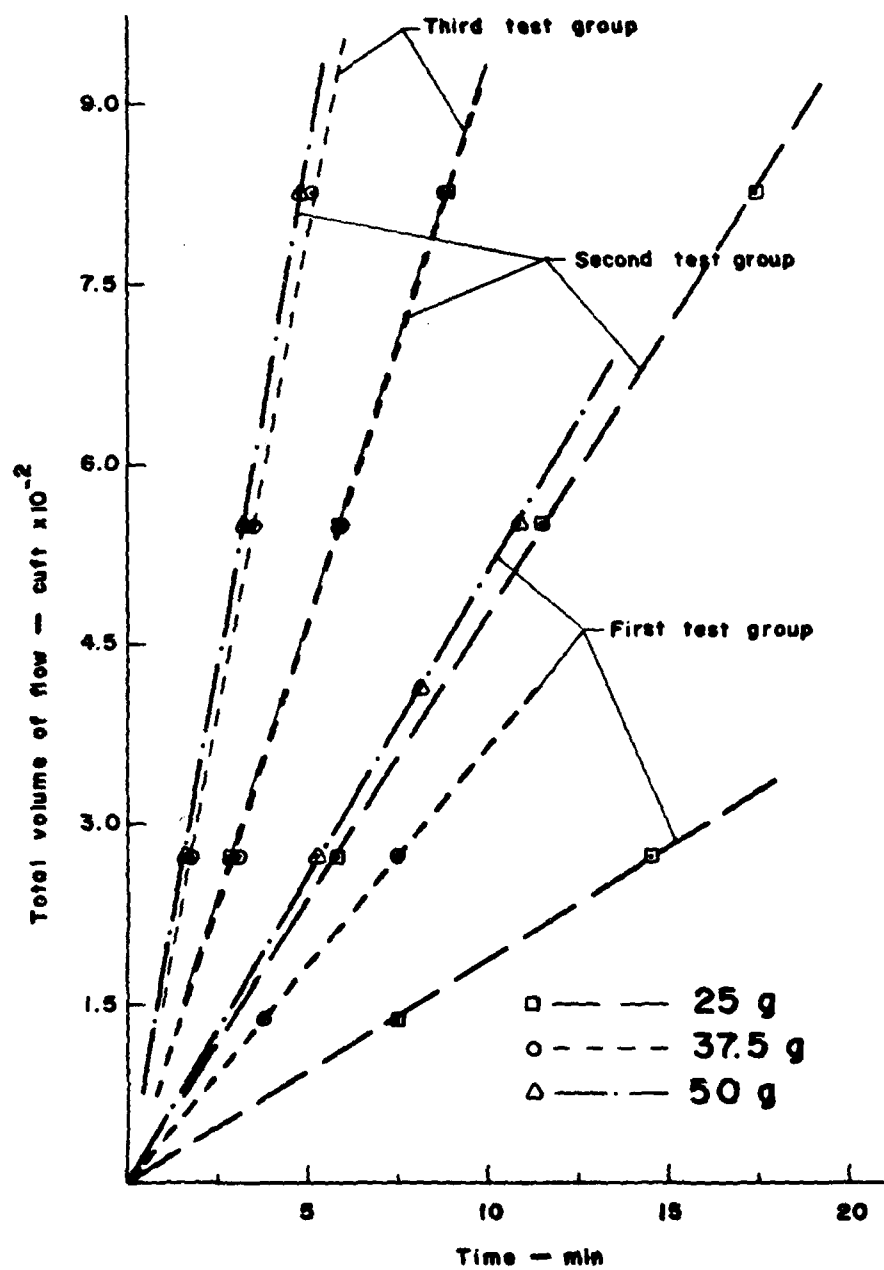
Figure 18. Volume of flow as a function of time
for Coarse Removed soil.
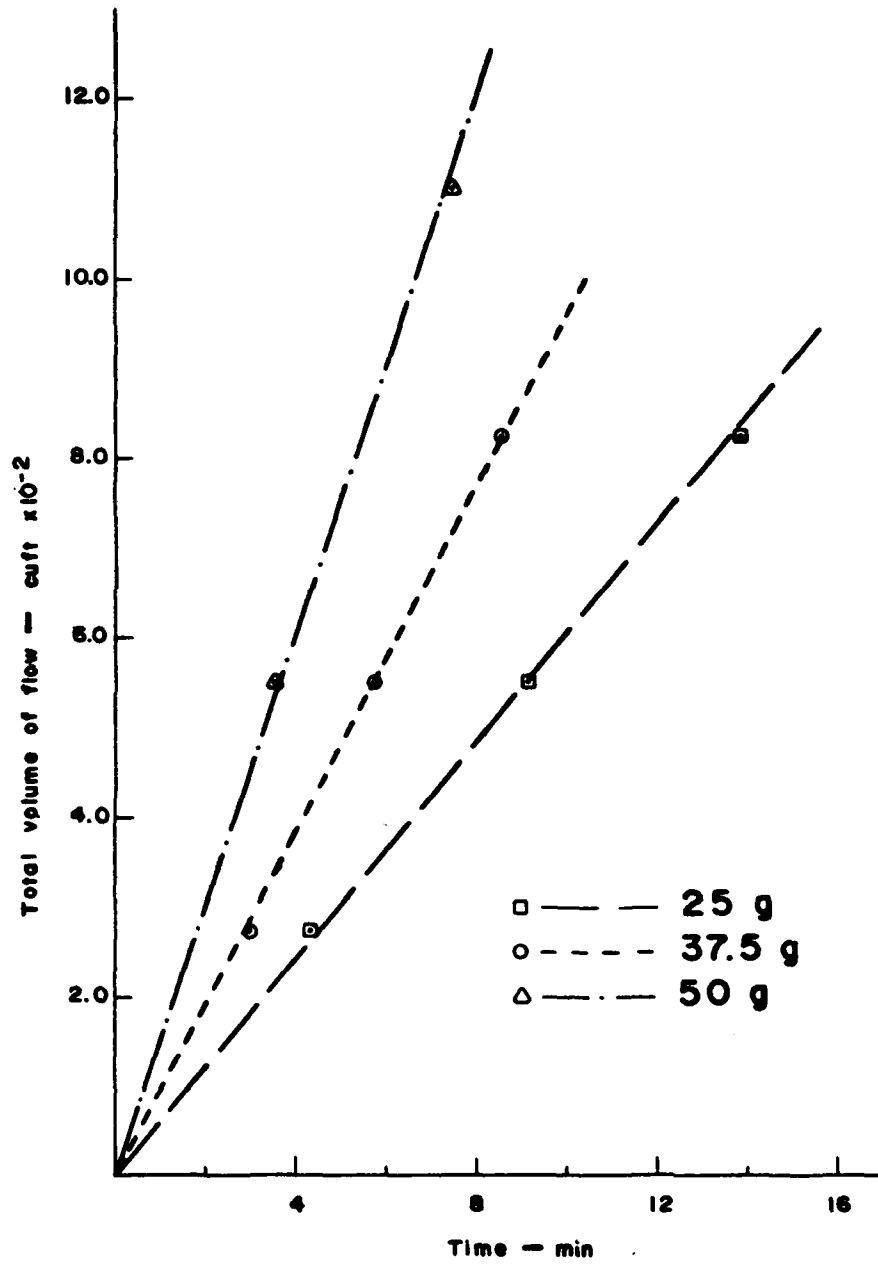
Figure 19. Volume of flow as a function of time for Same D_{10} soil.
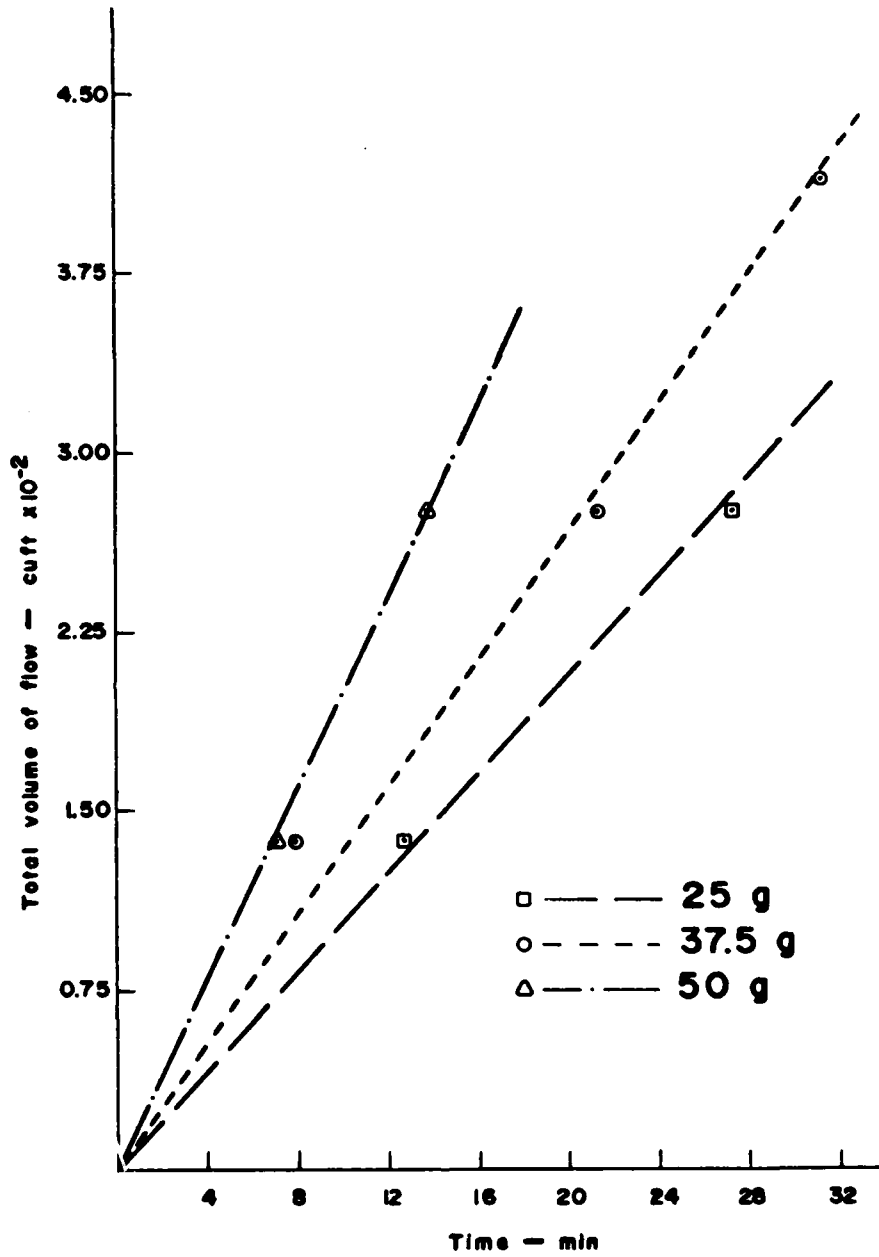
Figure 20. Volume of flow as a function of time for Same CU soil.

CHAPTER VII

DISCUSSION OF TEST RESULTS

The results of tests reported in the previous chapter will now
be examined in an attempt to verify previously theorized scaling
relationships and compared with known solutions where possible.

Steady State Flow

Since the majority of previous research has been concerned
with steady state flow conditions, there are several well-developed
methods available for rapidly solving such problems for widely
varying soil conditions and embankment shapes. Comparison of the
experimentally derived equipotential distribution to that derived
from a conventional calculation is the logical first step in
evaluating the experimental results. Since equipotential distri-
bution at steady state depends only on embankment shape, headwater
and tailwater levels, and relative permeabilities, many of the
experimental variables can be eliminated. Thus, the only variable
affecting the experimentally derived steady state solution for
equipotential distribution should be the relative maximum and
minimum permeabilities in each sample and their orientations.
Since each sample was compacted vertically in horizontal layers,
the principal permeability directions should be in the horizontal
and vertical directions. If the soil samples were truly isotropic,

permeability would have no effect on equipotential distribution.

The method of calculation chosen to be used here is a finite element program which calculates head at the nodal points of triangular elements and adjusts the position of nodes on the phreatic surface to comply with the requirement that pressure head is zero there. Known heads are specified for the upstream and downstream boundary conditions, and the bottom of the embankment is considered impermeable.

As indicated previously in Figure 15, the pressure head in a centrifuged sample is dependent on the distance from the center of gravity of the water column producing the pressure to the axis of rotation. For the embankment geometry and orientation used in these experiments, this means that there is a linearly varying head on the embankment faces. On the downstream face, this variation is insignificant. However, on the upstream face for a typical water elevation of 7.75 inches on the embankment, there is a head of 8.10 inches at the base. The effect of this varying head was analyzed by the finite element program and is shown in Figure 21. In this figure, the soil is assumed isotropic and conforms to actual sample dimensions. The dashed lines indicate the phreatic surface and equipotential distribution for a constant head of 7.75 inches on the upstream face. The solid lines are for a linearly varying head from 7.75 inches at the water surface to 8.10 inches at the base. As can be seen from the figure, the effect of this head variation is to shift equipotential lines downstream and to raise the phreatic line. Although shown only for the isotropic
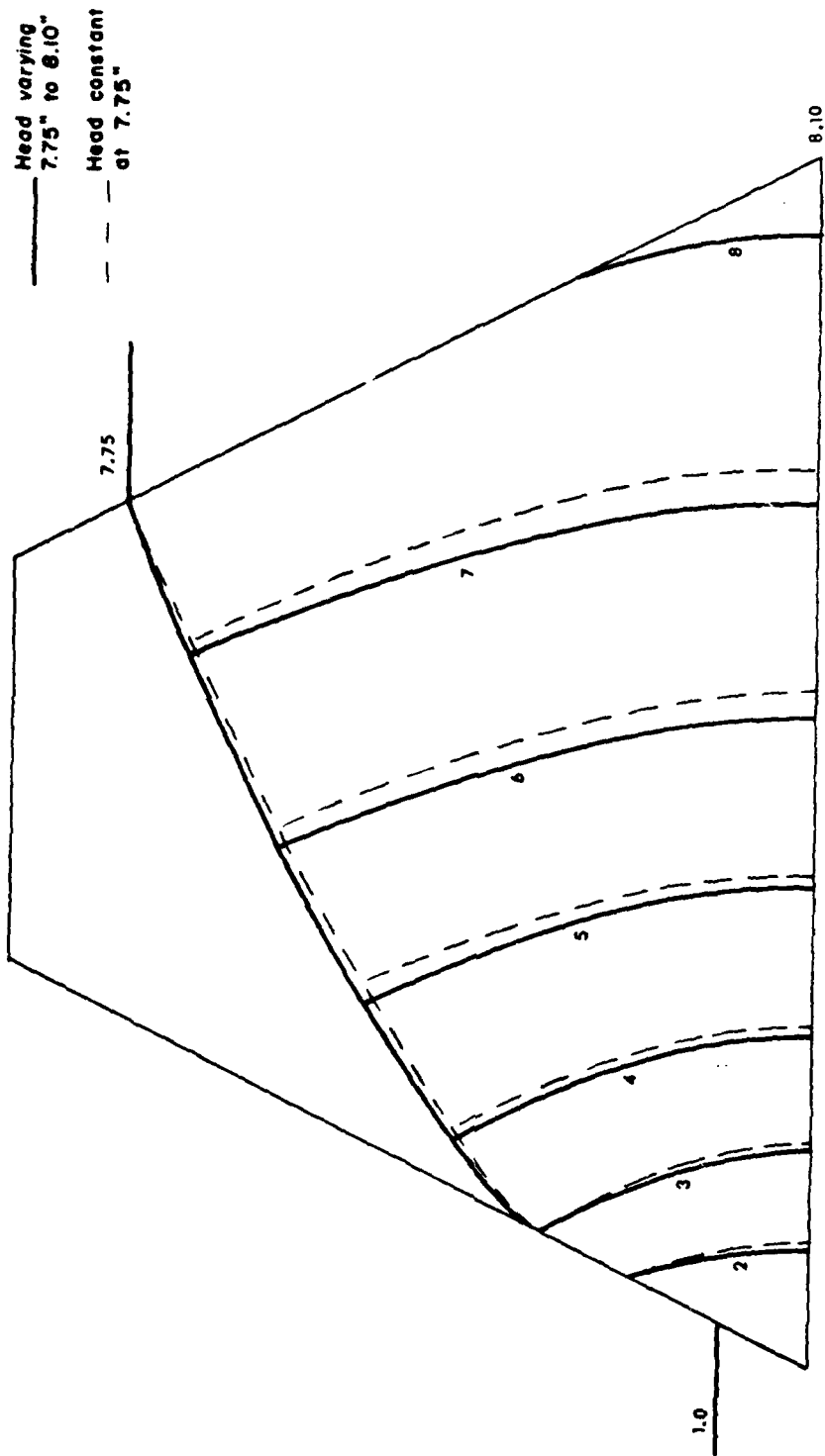
Figure 21. Effect of varying upstream head for isotropic case.

case, the same type shift was found in all combinations of relative horizontal and vertical permeabilities which were computed.

Since none of the experimentally derived steady state equipotential distributions is a very good match to the isotropic computed solution, the possibility that the soil samples are anisotropic due to the method of placement arises. As stated before, the principal directions of any anisotropy should be horizontal and vertical. In an attempt to get a better match between computed and experimental results, finite element solutions were obtained for varying degrees of anisotropy. Figure 22 shows the results of computations for vertical to horizontal permeability ratios of 1:2, 1:3, and 1:5 and how they compare to the isotropic case. The figure shows that as the horizontal permeability increases relative to the vertical permeability, the effect is a rise in the phreatic surface and a shift at the base of equipotential lines in an upstream direction proportional to the degree of anisotropy. This higher phreatic surface is more characteristic of the experimental results but the equipotential lines are not.

Figure 23 indicates the effect of vertical to horizontal permeability ratios of 2:1, 3:1, and 5:1 for the same embankment section. In this and the previous figure, the problems were solved with a linearly varying head on the supstream face. The figure shows that as vertical permeability increases with respect to horizontal permeability, the phreatic surface is lowered and equipotential lines become more vertical. These near vertical equipotential lines are somewhat characteristic of experimental results especially near the downstream face.

104
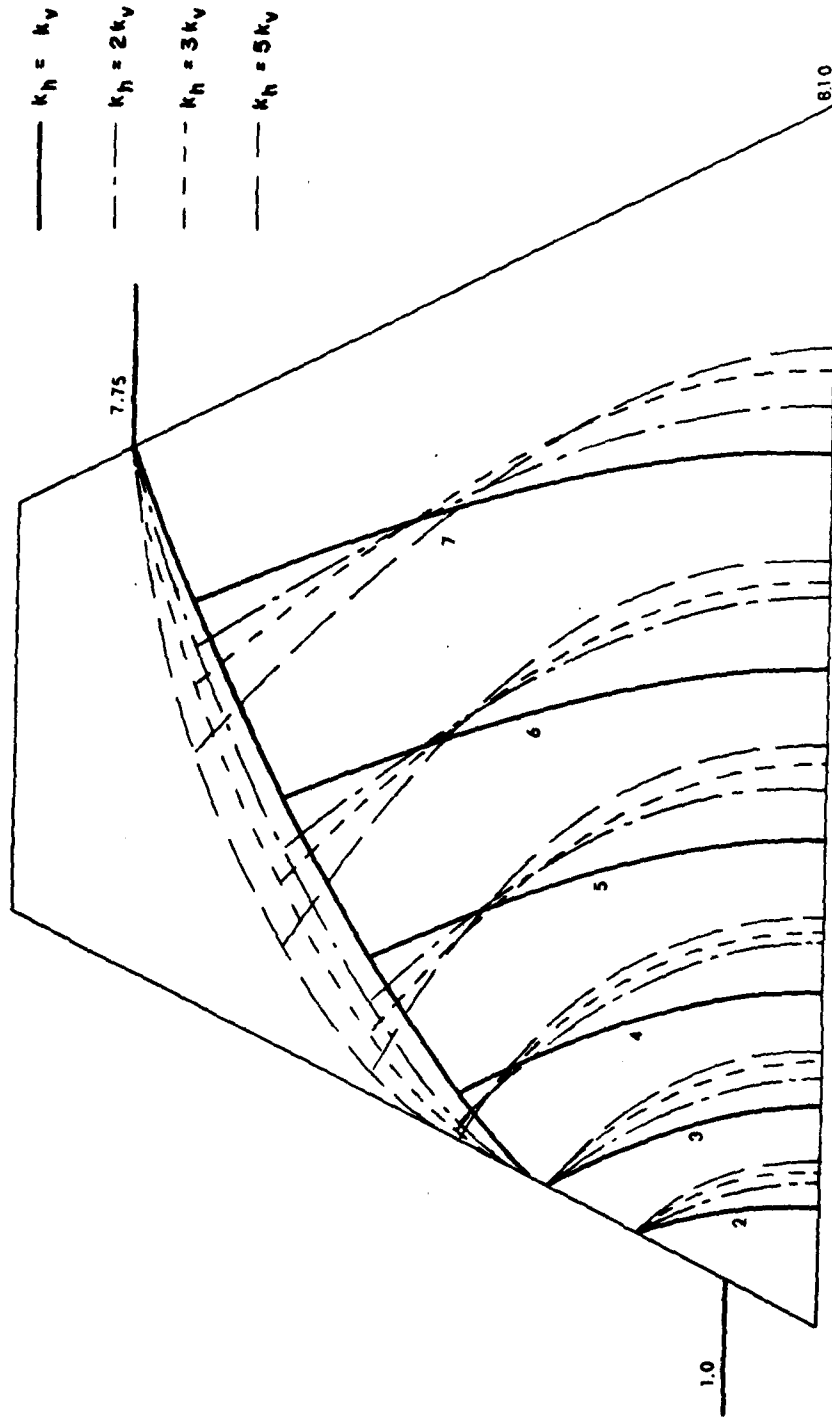
Figure 22. Effects of horizontal permeability greater than vertical.

$k_h = k_v$
$k_h = 2k_v$
$k_h = 3k_v$
$k_h = 5k_v$
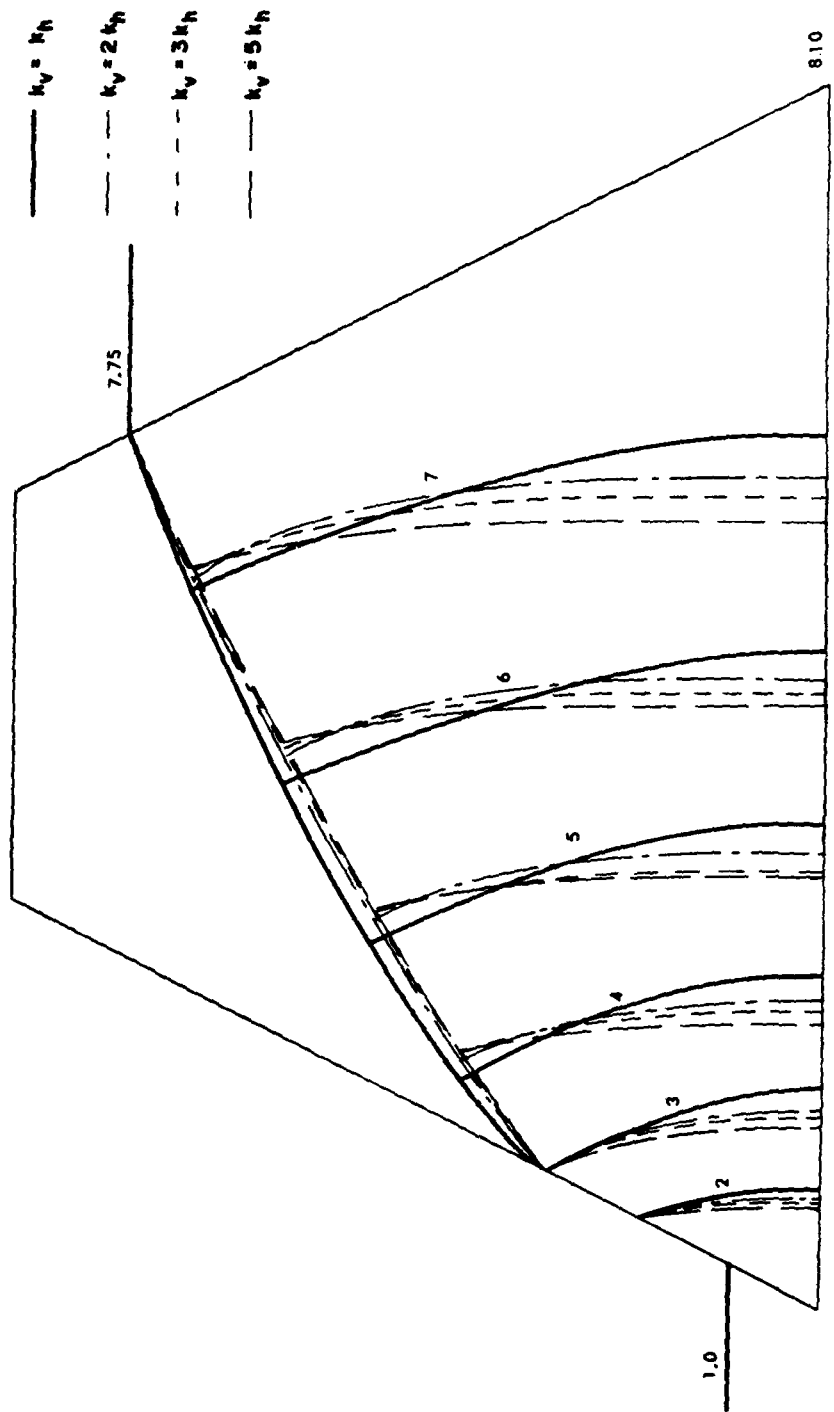
Figure 23. Effects of vertical permeability greater than horizontal.

The possibility that permeability may change between the lower and upper portions of the embankment because of varying stress levels was also investigated using the finite element method. The embankment was divided into four zones within the flow region nd isotropic permeabilities of 1.0, 1.7, 2.4, and 3.0 were assigned from lower to higher zones respectively. Figure 24 shows the results of this analysis in comparison with the completely iso-tropic case. As can be seen from the figure, the effect of the varying isotropic permeability is to raise the phreatic surface and to cause equipotential lines to be more vertical. This cer-tainly comes closer to the experimental results than the previous theoretical trials, but still does not adequately represent them.

Comparison of experimental results with these theoretical solutions reinforces the belief that better solutions to flow problems will come about only through improved techniques of modelling. It has been shown that no combination of permeabilities with conventional mathematical models can theoretically represent what was found in the experiments. For example, the high exit gradients as depicted by the closely spaced equipotential lines near the downstream face in the steady state conditions in Figures A-13 through A-24 are not indicated in the calculated solutions. This would lead to a gross overestimate of slope stability if calculated equipotentials were used.

Transient Flow

Plots of total head as a function of time in Figures A-1 through A-12 show a remarkable consistency between tests and

107

Homogeneous and isotropic.

Nonhomogeneous with permeability varying from 1.0 at bottom to 3.0 at top.
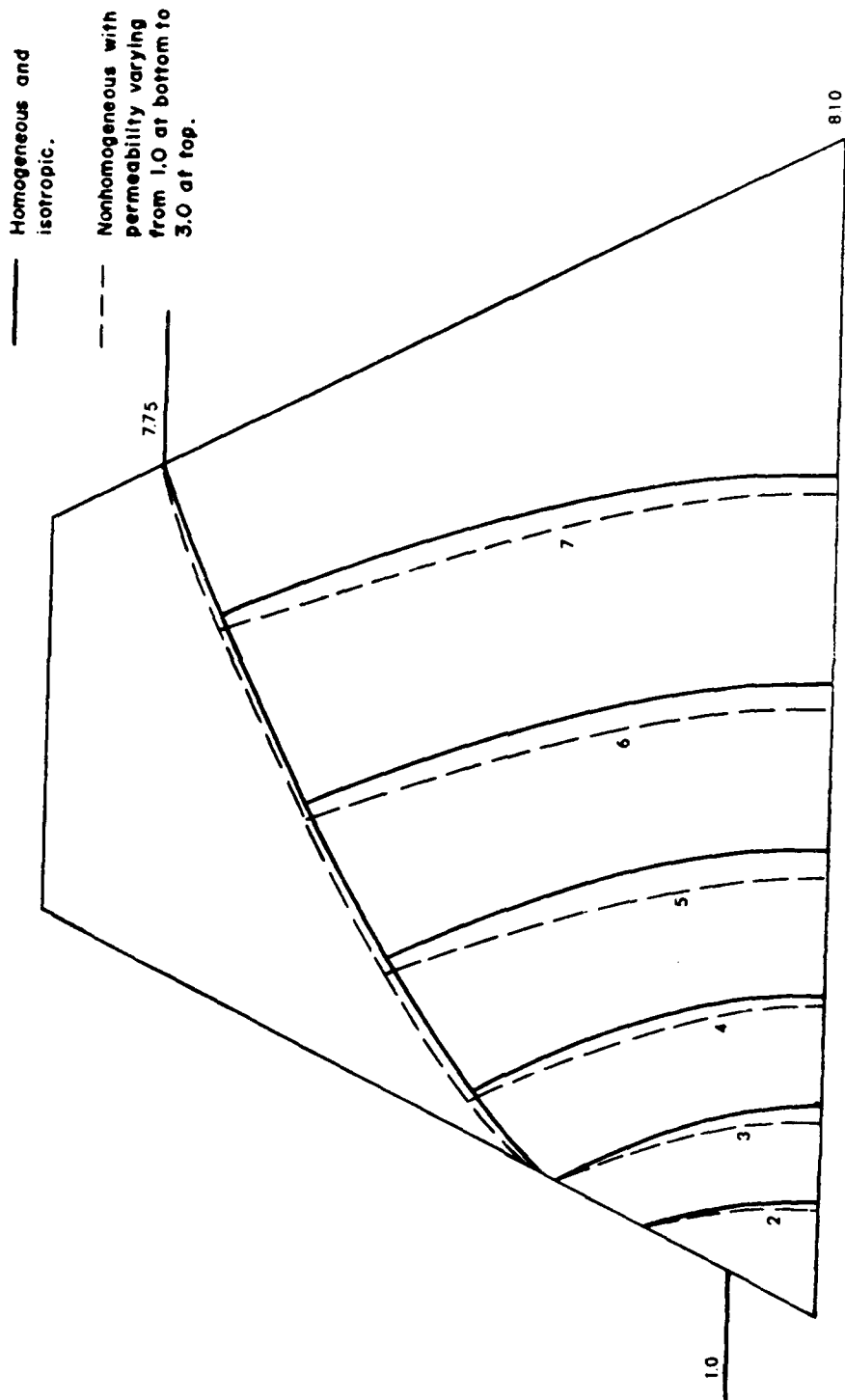
Figure 24. Effect of nonhomogeneous embankment.

therefore lead one to place confidence in them. If these results are in fact as accurate as expected, the equipotential plots for headwater rise shown in Figures A-13 through A-24 and for headwater drawdown shown in Figures A-25 through A-36 should also be fairly accurate representations.

All figures contained in the appendix involve soils which had been previously saturated. To see what effect this makes in the head development in a soil, the Coarse Removed sample was monitored during filling for the first flow test at 50 g. Results are shown in Figure 25. This figure should be compared with test CR-50-1 in Figure A-6. As expected, there is a marked lag in the development of heads because of the smaller permeability of the "virgin" soil.

The fact that total head inside the embankment falls at a rate faster than the headwater level during drawdown in many cases for the coarser soils indicates that it may not be entirely correct to neglect velocity heads in an analysis involving these sandy materials, especially near the upstream face. However, this aspect of the transient flow phenomenon will be left as a topic for future research.

Using the maximum flow rate in Figure 17 for Original soil at 50 g and the approximate area of the exit face shown in the steady state equipotential plot of Figure A-15, one can calculate a maximum apparent velocity of flow. This is converted to seepage velocity by dividing by .25, the porosity of Original soil as shown in Table 7. A maximum seepage velocity of 1.3×10^{-2} fps is thereby obtained. This confirms the earlier assumption that velocity heads
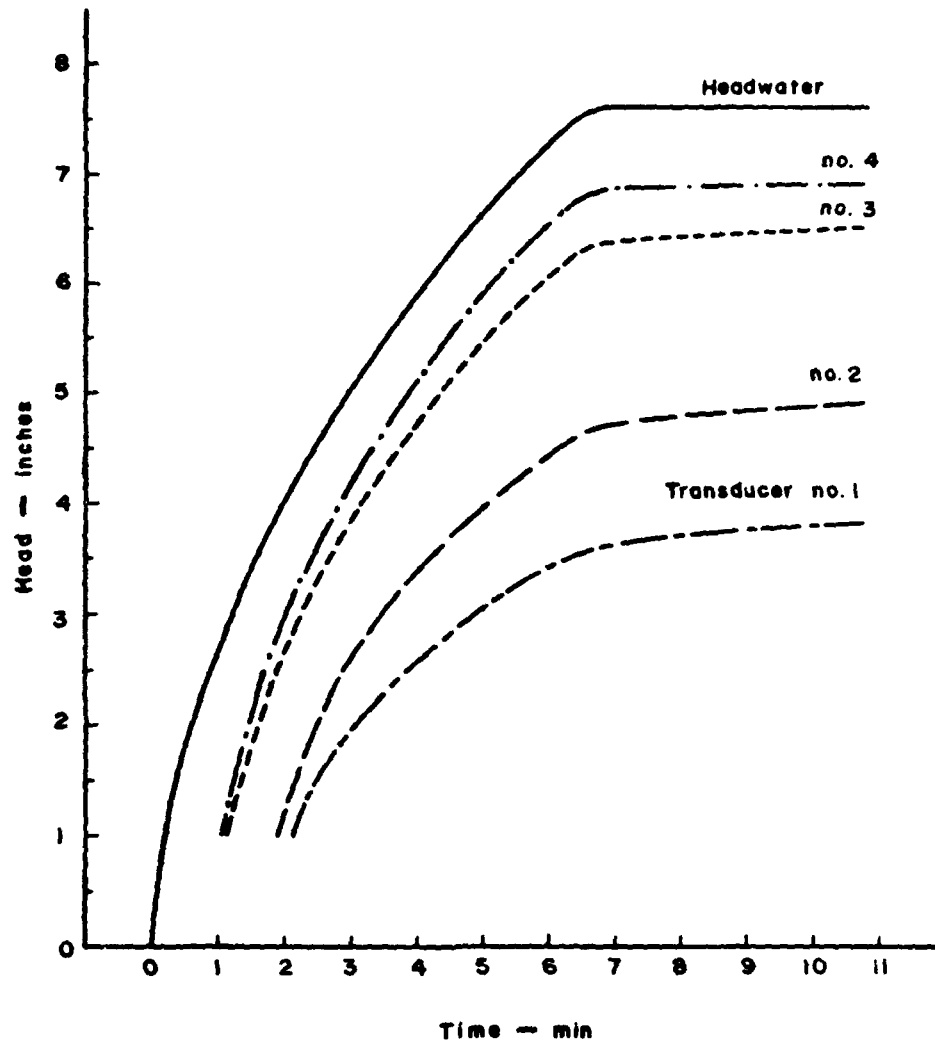
Figure 25. Head rise in sample not previously saturated.

are negligible and also can be used to verify that flow remains laminar. Aravin and Numerov [1] recommend that Darcy's law may be used for Reynold's number, R, less than 4 to 6, where

$$R = \frac{v_s d\rho}{\mu} \tag{138}$$

and d is the effective diameter of soil particles. Normally the effective diameter of soil particles is assumed to be the grain size at 10 percent passing from a grain size distribution curve. By conservatively assuming d = 0.05 mm for Original soil, a Reynold's number less than 2×10^{-2} is obtained. Thus, it is safe to assume that laminar flow occurred in the experiments described above.

Scaling Relations for Pressure and Head

In reducing the experimental data to obtain the plots contained in the appendix, it was assumed that both pressure and head quantities would scale as theorized. That is

$$\psi_p = \frac{P_p}{P_m} = \frac{1}{n} \cdot \lambda = 1 \tag{139}$$

and

$$\psi_h = \frac{h_p}{h_m} = \lambda . \tag{140}$$

These relationships are considered verified by the fact that using the factors produces consistent results.

Scaling Relations for Flow Rate and Permeability

From Figures 17 through 20 of the previous chapter, experimental flow rates can be determined. Table 9 lists these measured flow rates by soil type and g level and also a calculated flow rate for each soil model at 1 g. This calculated flow rate was determined for a unit embankment thickness from the equation

$$q = k \cdot \Delta h \cdot \frac{N_f}{N_d} \; . \tag{141}$$

In the above equation, the value used for k, permeability, is that contained in Table 6 which was extrapolated from laboratory tests for the particular void ratio in each sample. The total head loss, Δh, is 6.00 inches times the acceleration scale factor. The ratio of number of flow channels to number of potential drops, N_f/N_d, was estimated from a flow net constructed on the isotropic equipotential distribution shown in Figure 21. A value of 0.4 is used for all soil samples.

In Table 9, the rates listed for the models are those measured experimentally. A range is given where more than one steady state flow rate test was conducted on a sample. The rates listed for the prototypes were calculated for an embankment whose dimensions are scaled up by the acceleration scale factor of the model listed in the line above it. The flow rates listed in the table for both model and prototype are the values calculated for the actual dimensions. In other words, the rates listed for the models are for unit model thickness and the rates listed for the prototype are for unit prototype thickness.

Table 9

Experimental and Calculated Flow Rates

	Original $\left(\dfrac{\text{cfs/ft}}{\times 10^{-5}}\right)$	Coarse Removed $\left(\dfrac{\text{cfs/ft}}{\times 10^{-5}}\right)$	Same D_{10} $\left(\dfrac{\text{cfs/ft}}{\times 10^{-5}}\right)$	Same CU $\left(\dfrac{\text{cfs/ft}}{\times 10^{-5}}\right)$
Model at 25 g	4.9 – 25.0	6.2 – 31.1	20.2	3.4
Prototype*	0.20	0.40	0.15	0.22
Model at 37.5 g	12.3 – 42.6	11.9 – 52.6	32.1	4.4
Prototype	0.30	0.60	0.22	0.34
Model at 50 g	21.8 – 66.6	17.0 – 57.1	50.3	6.7
Prototype	0.40	0.80	0.30	0.45

*Values for prototype are calculated from the FEM solutions using isotropic k values obtained from permeability tests. Prototype dimensions are model dimensions scaled up by acceleration factor.

The scaling relationship for flow rate can now be calculated from these results. It was previously theorized that this factor could be anywhere between $1/n$ and n^2. If the total flow rate is called Q, where

$$Q = q \cdot w \qquad (142)$$

and q is defined by equation 141 and w is the embankment width, a flow rate scale is then

$$\psi_q = \frac{Q_p}{Q_m} = \frac{q_p w_p}{q_m w_m} \qquad (143)$$

Since flow rates have been listed for one foot actual widths, the ratio w_p/w_m is equal to unity and therefore

$$\psi_q = \frac{q_p}{q_m} \qquad (144)$$

A permeability scale factor ψ_k can also be calculated from the experimental results for a prototype embankment. Rewriting equation 141 in dimensionless form and setting these dimensionless prototype and model quantities equal to one another yields

$$\psi_k = \frac{k_p}{k_m} = \frac{q_p \, \Delta h_m \left(\dfrac{N_f}{N_d} \right)_m}{q_m \, \Delta h_p \left(\dfrac{N_f}{N_d} \right)_p} \qquad (145)$$

Since all embankments are geometrically similar, the ratios N_f/N_d are identical for model and prototype. The ratio of heads $\Delta h_m/\Delta h_p$ is equal to $1/n$ when a 1-g prototype is centrifugally modelled; but has a value of unity when both model and prototype have

identical heads. The latter is the case if one considers identical embankments tested at different g levels in which one of the models is arbitrarily called the prototype. Thus, for centrifuged models of a 1-g prototype

$$\psi_k = \frac{1}{n}\,\psi_q \qquad\qquad (146)$$

and for the same model tested at different g levels,

$$\psi_k = \psi_q \quad . \qquad\qquad (147)$$

Table 10 lists calculated scale factors for flow rate and permeability using q from Table 9 for ratios involving 1 g prototypes (category 1); and using flow rates from Figures 17 through 20 for ratios involving models and prototypes which are both centrifuged (category 2). In the table, some values have been reduced to factors containing the acceleration ratio n to facilitate comparison with theoretical results.

Equation 101 developed in Chapter 3 is restated as

$$\frac{Q_p}{Q_m} = \frac{g_p A_p}{g_m A_m} = \frac{g_p w_p d_p}{g_m w_m d_m} \qquad\qquad (148)$$

where w is width of the embankment and d is depth of flow. If unit widths are used for both model and prototype and $d_p/d_m = \lambda$, then

$$\psi_q = \frac{1}{n}\cdot\lambda = 1 \quad . \qquad\qquad (149)$$

This says that theoretically a value of unity should have been been obtained for ψ_q values for the models of category 1 shown in

Table 10

Flow Rate and Permeability Scale Factors

Category*	Acceleration Ratio n	Original Soil		Coarse Removed Soil		Same D_{10} Soil		Same CU Soil	
		ψ_q	ψ_k	ψ_q	ψ_k	ψ_q	ψ_k	ψ_q	ψ_k
(1)	$g_p = 1$ $g_m = 25$ $n = 25$	0.04 to 0.01	$\frac{.04}{n}$ to $\frac{.01}{n}$	0.06 to 0.01	$\frac{.06}{n}$ to $\frac{.01}{n}$	0.01	$\frac{.01}{n}$	0.06	$\frac{.06}{n}$
	$g_p = 1$ $g_m = 37.5$ $n = 37.5$	0.02 to 0.01	$\frac{.02}{n}$ to $\frac{.01}{n}$	0.05 to 0.01	$\frac{.05}{n}$ to $\frac{.01}{n}$	0.01	$\frac{.01}{n}$	0.08	$\frac{.08}{n}$
	$g_p = 1$ $g_m = 50$ $n = 50$	0.02 to 0.01	$\frac{.02}{n}$ to $\frac{.01}{n}$	0.05 to 0.01	$\frac{.05}{n}$ to $\frac{.01}{n}$	0.01	$\frac{.01}{n}$	0.07	$\frac{.07}{n}$
(2)	$g_p = 25$ $g_m = 37.5$ $n = 1.5$	$\frac{1}{1.7n}$ to $\frac{1}{1.1n}$	$\frac{1}{1.7n}$ to $\frac{1}{1.1n}$	$\frac{1}{1.3n}$ to $\frac{1}{1.1n}$	$\frac{1}{1.3n}$ to $\frac{1}{1.1n}$	$\frac{1}{1.1n}$	$\frac{1}{1.1n}$	$\frac{1}{.9n}$	$\frac{1}{.9n}$
	$g_p = 25$ $g_m = 50$ $n = 2.0$	$\frac{1}{2.2n}$ to $\frac{1}{1.3n}$	$\frac{1}{2.2n}$ to $\frac{1}{1.3n}$	$\frac{1}{1.3n}$ to $\frac{1}{1.8n}$	$\frac{1}{1.3n}$ to $\frac{1}{1.8n}$	$\frac{1}{1.2n}$	$\frac{1}{1.2n}$	$\frac{1}{n}$	$\frac{1}{n}$
	$g_p = 37.5$ $g_m = 50$ $n = 1.33$	$\frac{1}{1.3n}$ to $\frac{1}{1.2n}$	$\frac{1}{1.3n}$ to $\frac{1}{1.2n}$	$\frac{1}{1.1n}$ to $\frac{1}{1.4n}$	$\frac{1}{1.1n}$ to $\frac{1}{1.4n}$	$\frac{1}{1.2n}$	$\frac{1}{1.2n}$	$\frac{1}{1.1n}$	$\frac{1}{1.1n}$

the first three rows of Table 10. If unit widths and d_p/d_m ratios equal to unity are used as in the models of category 2, then

$$\psi_q = \frac{1}{n} .$$
(150)

This means that a result of 1/n for ψ_q values in the last three rows would be in complete agreement with theory. In all cases, to agree with the theoretical relationship of equation 108 in Chapter 3, ψ_k should equal 1/n.

The seemingly poor agreement between theory and experimental results for the cases where a 1 g prototype is used (category 1) is probably due to a drastic change in the permeability of the soil samples brought about by centrifugal testing. Figures 17 and 18 of the previous chapter do indicate changes of up to 5 times the permeability first measured. (See, for example, the range in flow rate for Original soil between the first and third test at 25 g). This change in permeability is no doubt the result of the loss in fines as shown by the grain size distribution curves of Figure 12 for sieve analysis before and after a test series, and due to incomplete saturation during the earlier tests.

Another probable reason for poor agreement is the fact that soil permeability at 1 g was extrapolated from laboratory tests at higher void ratios by a straight line on a semi-log plot of void ratio versus permeability. In all cases, this extrapolation was over about one order of magnitude which could lead to a large error if the permeability-void ratio curve did not continue on a straight line at the lower in-place void ratios.

There is relatively good agreement between theory and experimental results for the cases where both models and prototypes were centrifuged (category 2). Any disagreement can again be explained in terms of changing permeability. For example, a twofold change is shown in Figure 8 between the second test group and the third for consecutive tests, i.e. the same quantity flows in half the time. It is interesting to note that results for Same CU soil which more nearly approaches the well graded fine grain soil used in engineered embankments are practically identical with theory in this case and also come closest to theory in the case of a 1 g prototype. This suggests that a true embankment material of very fine grained silt–clays properly protected to prevent loss of fines might match theory exactly.

The better correlation for category 2 comparisons comes primarily from the fact that only centrifuged models are compared. This is a direct reflection of the internal consistency in centrifuge modelling, similar to the concept of verification of scaling laws through modelling of models. On the other hand, when centrifuged models of 1 g prototypes are compared to the ficticious prototypes which could only be analyzed by numerical methods, the poor comparison indicates that perhaps the physical phenomenon assumed in the numerical analysis may not be accurate.

Time Scaling Relations from Transient Flow Tests

A theoretical time scale relationship for transient flow was formerly given in equation 132 which is here rewritten in the form

$$\psi_t = \frac{t_p}{t_m} = \frac{g_m}{g_p} \frac{x_p}{x_m} \tag{151}$$

In this expression, ψ_t can be calculated if some characteristic length measurement representing a flow path or other identifiable length can be found for model and prototype. Equation 128 which also relates time in the prototype to time in the model suggests that this characteristic length might be total head which we choose to use here. If one considers the rise and fall of the phreatic surface to be represented by the change in total head at a certain point, then this is certainly a valid measurement on which we can base calculation of the time scale. Therefore,

$$\psi_t = \frac{g_m}{g_p} \frac{h_p}{h_m} \tag{152}$$

and if heads are scaled inversely to gravity, ψ_t is theoretically n^2. If both model and prototype are at the same length scales, as is the case when the same embankment is centrifuged at different g levels, then the ratio of heads is equal to unity and ψ_t has a theoretical value of n.

Determination of actual values of ψ_t would be routine if the motion of a particular water particle could be plotted and timed. Since this is not possible, other indicators of motion must be used. Total head would be a perfect indicator of vertical motion of the phreatic line if equipotential lines were exactly vertical. This condition seems to be most nearly satisfied in the test results during early stages of drawdown and near the tailwater side of the embankment. Therefore the total head as measured by transducer

no. 2 installed at the 5 inch level and transducer no. 1 installed
at the 3 inch level (see Figure 14 for exact locations) will be
used to indicate changes in the phreatic surface.

Due to the unavailability of reliable and expedient methods of
calculating transient flow solutions, and because of the large
discrepancies encountered in the previous section between experi-
mental and calculated solutions for steady state flow, only experi-
mental results will be used here. Also, since in equation 132, it
was assumed that the physical permeability of a soil was unchanged
between model and prototype, the first transient flow test where
changes are probably the greatest in each series will not be used.
By using only the latter test in each series, discrepancies due to
permeability change should be of a smaller magnitude but will still
not be eliminated totally.

Table 11 lists times form the start of drawdown for the total
head to drop equidistances at the same point in the same soil for
various g levels. Table 12 shows scale factors in terms of the
acceleration ratio n for the three combinations of acceleration
ratios. As previously stated, an exact factor of n would be in
perfect agreement with theory. As can be seen from the table there
is generally good agreement with theory and no one soil shows a
better agreement than others.

Table 11

Time of Phreatic Surface Drop

Acceleration Level	Original		Coarse Removed		Same D_{10}		Same CU	
	Trans #2	Trans #1	Trans #2	Trans #1	Trans #2	Trans #1	Trans #2	Trans #1
25 g	0.13 (.10")	1.00 (.55")	0.38 (.45")	0.83 (.85")	0.67 (.85")	0.92 (1.15")	3.00 (1.25")	2.46 (2.55")
37.5 g	0.08	0.71	0.29	0.58	0.46	0.67	2.46	2.17
50 g	0.05	0.58	0.25	0.46	0.33	0.58	1.75	1.92

121

Table 12

Time Scale Factors

Acceleration Ratio - n	Original		Coarse Removed		Same D_{10}		Same CU	
	Trans #2	Trans #1	Trans #2	Trans #1	Trans #2	Trans #1	Trans #2	Trans #1
1.5 $g_p = 25$ $g_m = 37.5$	1.1n	.9n	.9n	1.0n	1.0n	.9n	.8n	.8n
2.0 $g_p = 25$ $g_m = 50$	1.3n	.9n	.8n	.9n	1.0n	.9n	.9n	.8n
1.33 $g_p = 37.5$ $g_m = 50$	1.2n	.9n	.9n	.9n	1.0n	.9n	.9n	.9n

CHAPTER VIII

CONCLUSIONS AND RECOMMENDATIONS

This research has shown the practicality and validity of
modelling the transient flow phenomenon in the centrifuge. Scaling
relations pertinent to the flow problem have been shown to be
consistent with theory to a good degree of accuracy. It is sub-
mitted that inconsistencies encountered due to changing permea-
bility is not peculiar to just this method of testing but a common
occurrence typical of real embankment materials. These changes
seem to be less pronounced in the finer grain samples, but the
change brought about when going from a partially saturated to a
saturated state will always occur. These changes are unaccounted
for in any current mathematical model and can only be properly
modelled by testing of the material to be actually used in con-
struction. The benefit of this type testing in embankment
stability analysis is obvious. Even current mathematical steady
state solutions are incapable of predicting the very high exit
gradients found in the experiments.

The testing hardware proved suitable for its purpose. How-
ever, the testing procedure could be improved by obtaining more
pressure transducers so that from 12 to 15 points could be monitored
during each test. This would eliminate discrepancies caused by
permeability changes between tests and allow for a more accurate

representation of equipotential distribution as the flow developed. A better method of transducer calibration should be sought before very fine grained soils are tested. The method used here would probably not be feasible for clayey soils requiring considerable time for steady state pore pressures to develop.

Fugure research should focus on the modelling of embankment materials more commonly used in actual construction. Some work should be devoted to sample preparation to insure that this very important aspect duplicates field procedure as closely as possible and produces a sample truly representative of the prototype. There is also no reason why flatter embankment slopes and natural filter materials should not replace the artificial mesh filter and support used in these experiments. This may decrease the height of the sample which can be handled by current hardware, but testing at a higher g level should still permit modelling of prototypes up to 50-60 feet in height. In the case of smaller embankment samples, transducers should be closer spaced to obtain readings at sufficient points in the embankment for determination of equipotential distribution.

The process described in this paper could ultimately be used in embankment design, but before a specific procedure can be recommended more experience with centrifuge modelling of the phenomenon of transient water flow is needed.

BIBLIOGRAPHY

1. Aravin, V.I. and S.N. Numerov, <u>Theory of Fluid Flow in Unde-</u> <u>formable Porous Media</u>, Jerusalem, Isreal Program for Scientific Translations, 1965, 511 pp.

2. Browzin, B.S., 1961. "Nonstead-State Flow in Homogeneous Earth Dams after Rapid Drawdown." <u>Proceedings of the</u> <u>Fifth International Conference of Soil Mechanics and</u> <u>Foundation Engineering</u>, Paris, Vol. II, pp. 551-554.

3. Cedergren, H.R., <u>Seepage, Drainage, and Flow Nets</u>, 2nd Ed., New York, John Wiley & Sons, 1977, 534 pp.

4. Daugherty, R.L. and J.B. Franzini, <u>Fluid Mechanics with</u> <u>Engineering Applications</u>, Sixth Edition, New York, McGraw-Hill Book Company, 1965, 578 pp.

5. Dicker, D., "Transient Free-Surface Flow in Porous Media," <u>Flow Through Porous Media</u>, R.J.M. DeWiest, Editor, New York, Academic Press, 1969, pp. 298-330.

6. Fumagalli, E., <u>Statical and Geomechanical Models</u>, New York, Springer-Verlag, 1973, 182 pp.

7. Lambe, T.W. and R.V. Whitman, <u>Soil Mechanics</u>, New York, John Wiley & Sons, Inc., 1969, 553 pp.

8. Langhaar, H.L., <u>Dimensional Analysis and Theory of Models</u>, New York, John Wiley & Sons, Inc., 1962, 166 pp.

9. Laut, P., 1975. "Application of Centrifugal Model Tests in Connection with Studies of Flow Patterns of Contaminated Water in Soil Structures." <u>Geotechnique</u>, v. 25, pp. 401-406.

10. Rushton, K.R. and S.C. Redshaw, <u>Seepage and Groundwater Flow</u>, Chichester, U.K., John Wiley & Sons, Inc., 1979, 339 pp.

11. Skoglund, V.J., <u>Similitude, Theory and Applications</u>, Scranton, PA, International Textbook Company, 1967, 320 pp.

APPENDIX
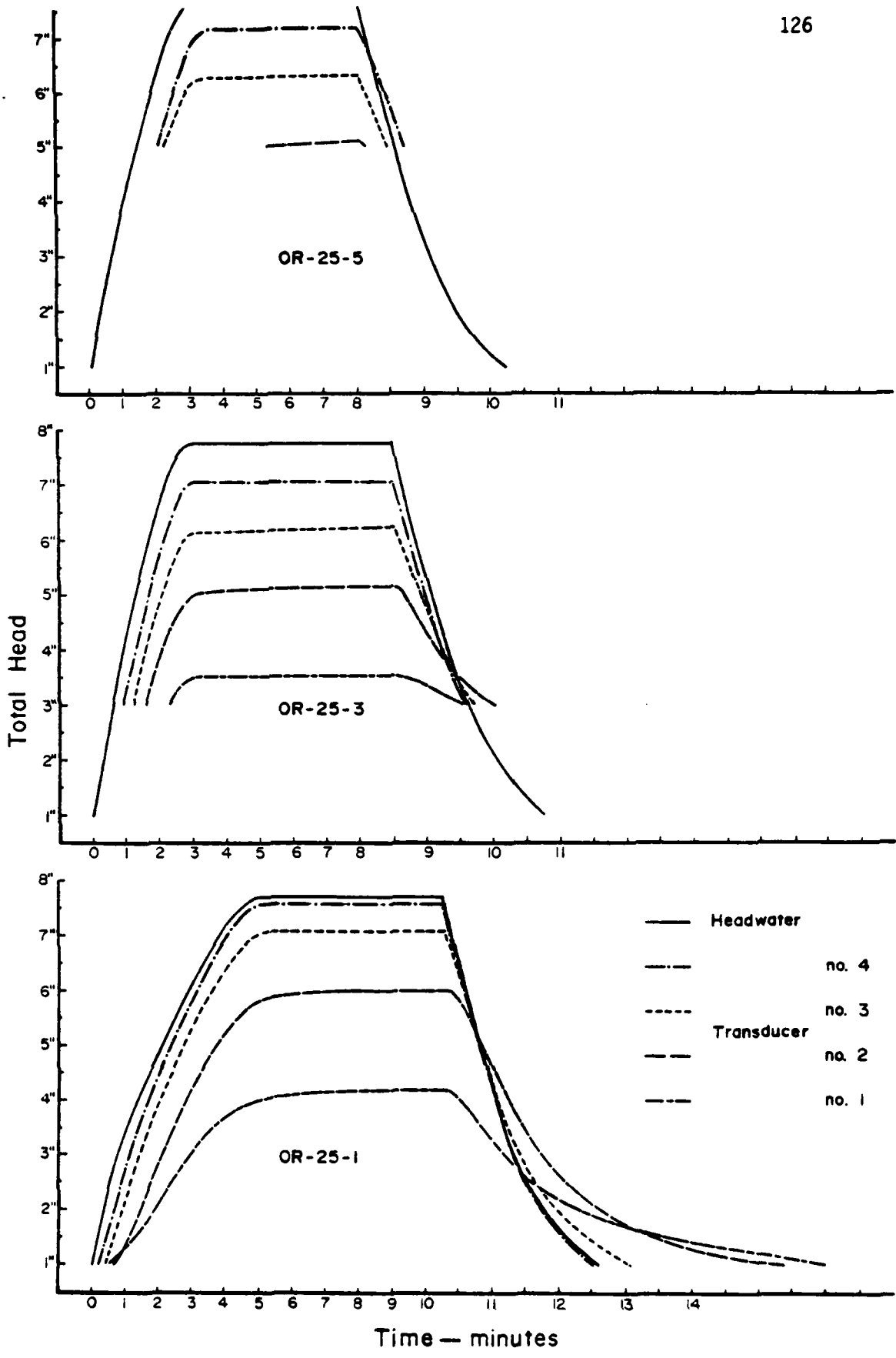
Figure A1. Total head versus time for Original soil at 25 g.
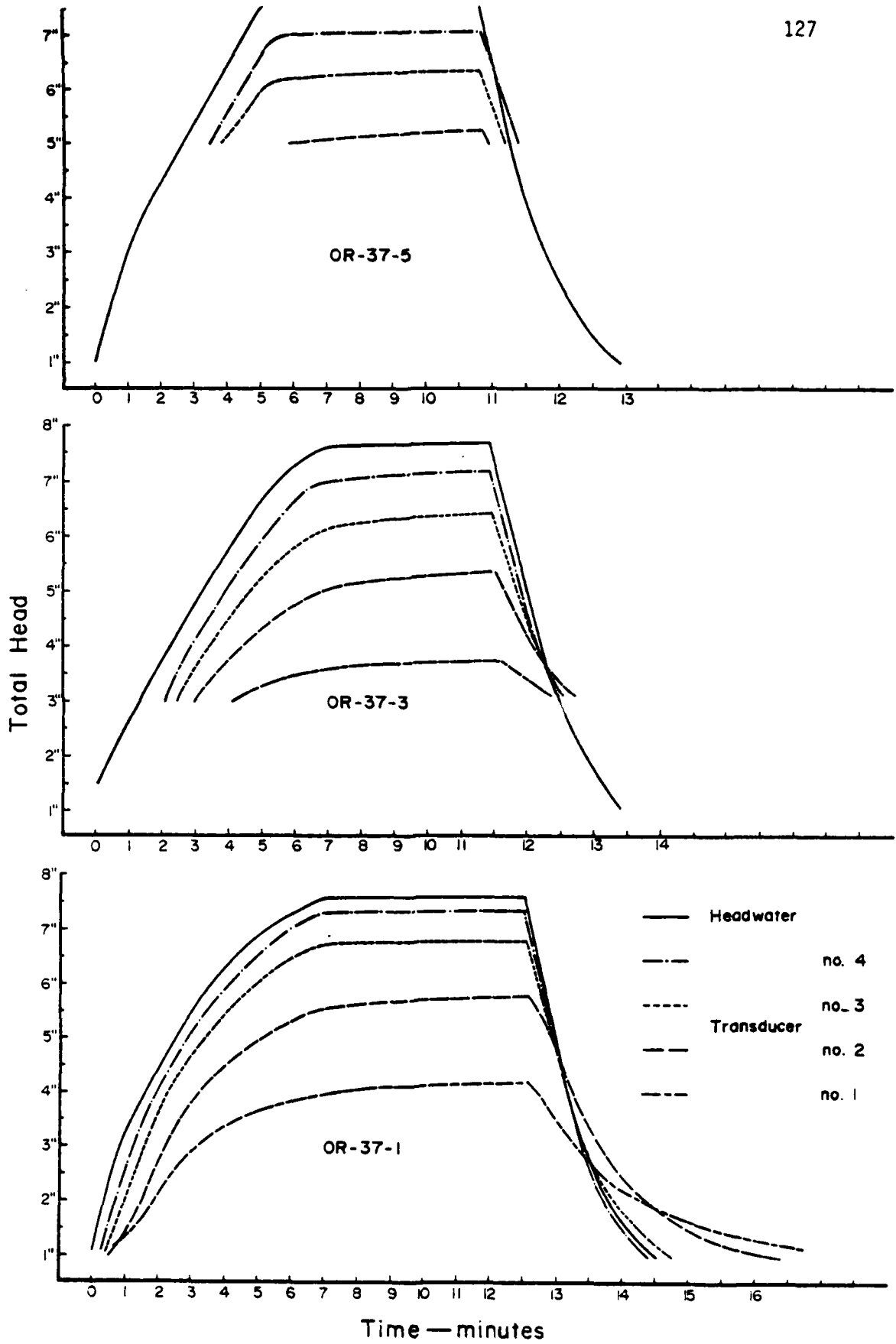
Figure A2.   Total head versus time for Original soil at 37.5 g.
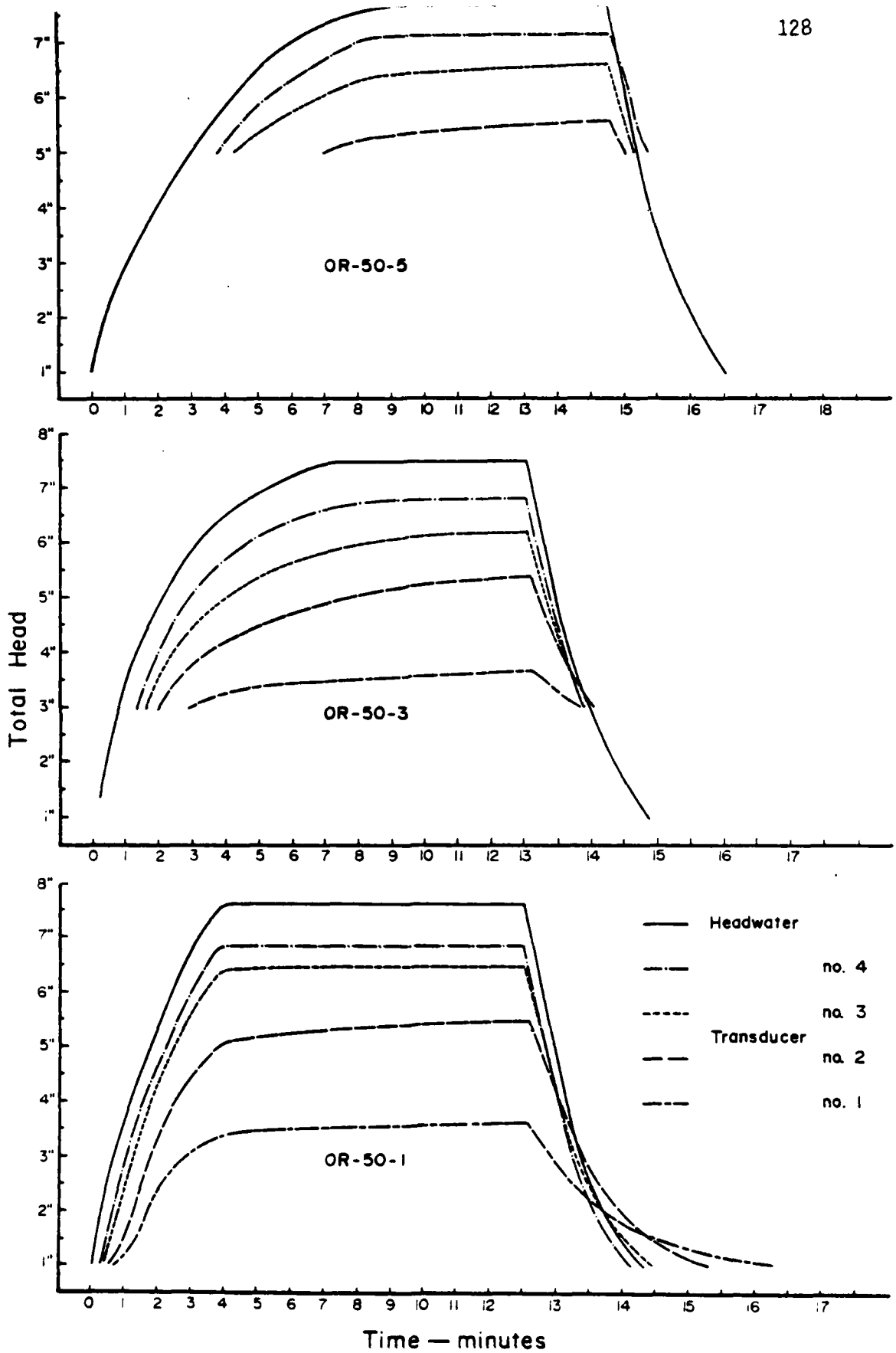
Figure A3.   Total head versus time for Original soil at 50 g.
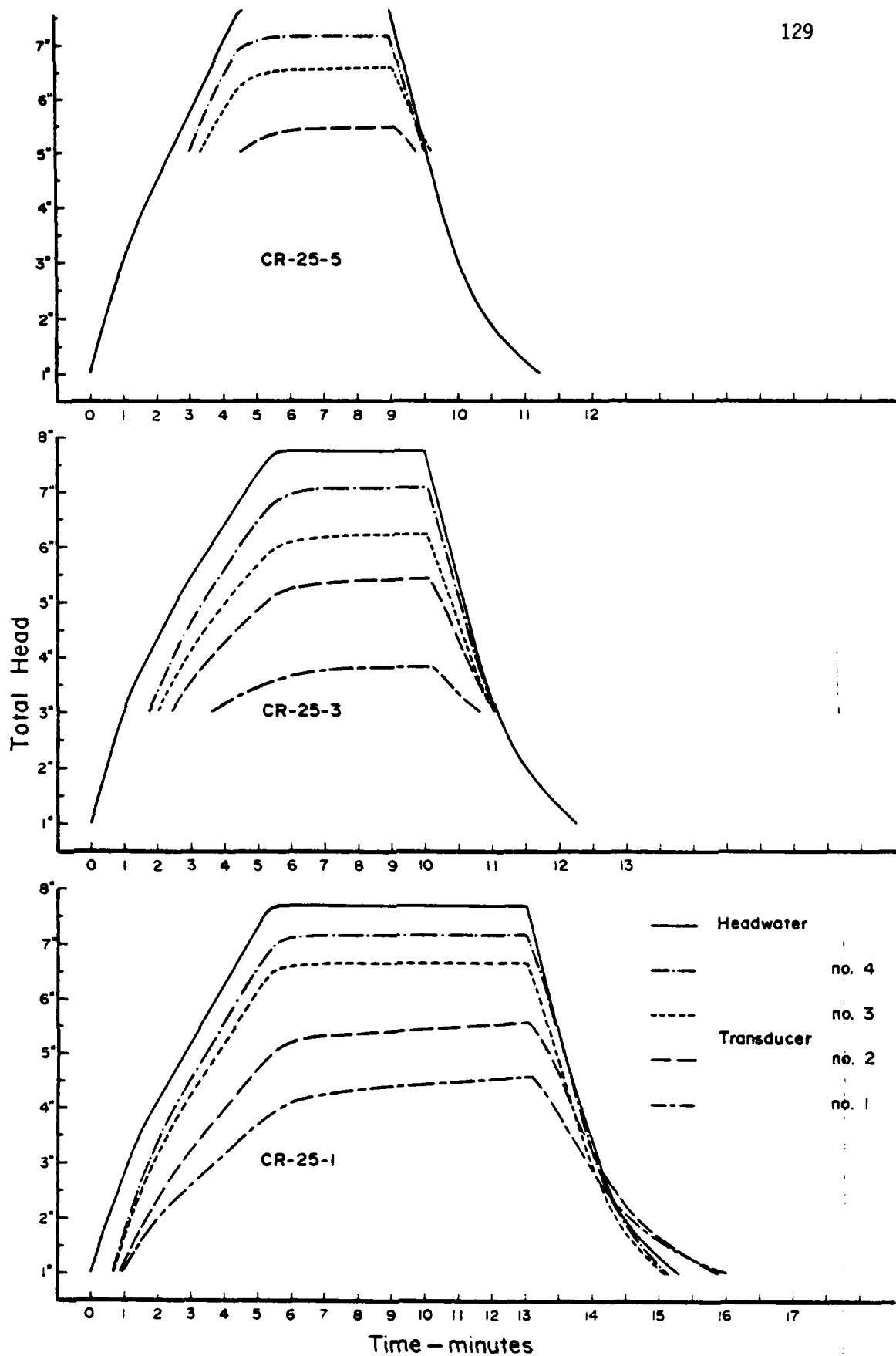
Figure A4.   Total head versus time for Coarse Removed soil at 25 g.
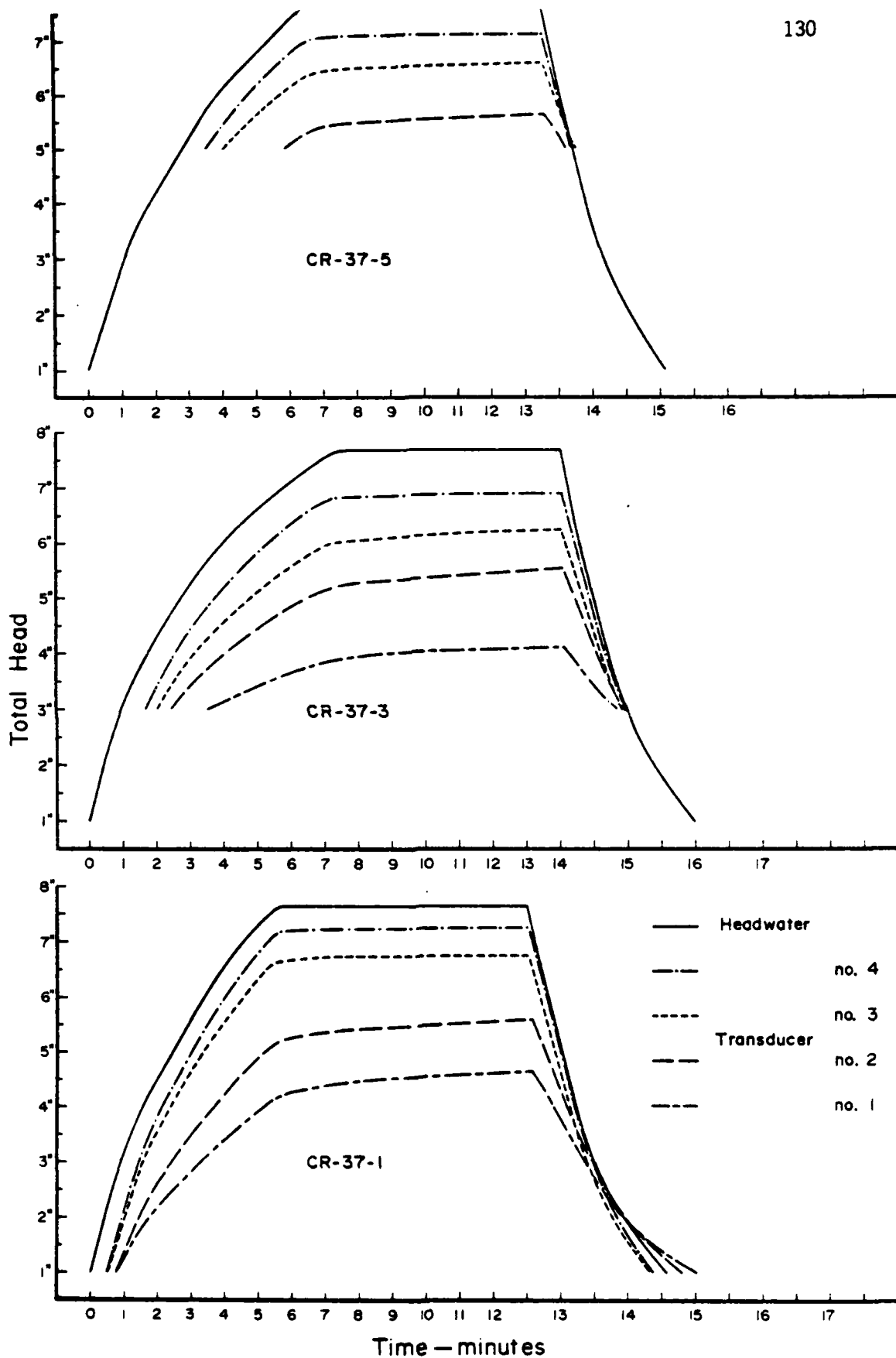
Figure A5. Total head versus time for Coarse Removed soil at 37.5 g.
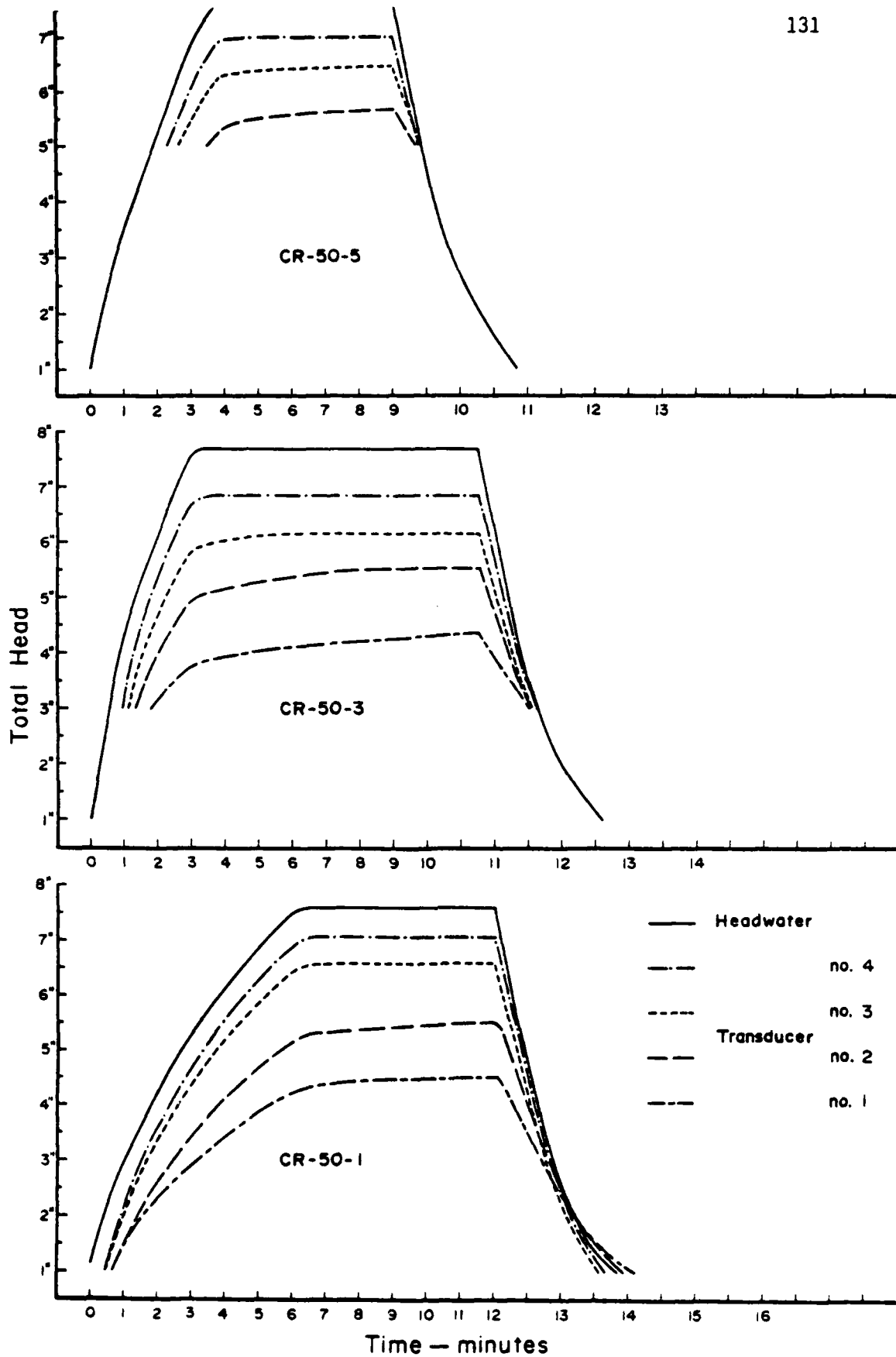
Figure A6. Total head versus time for Coarse Removed soil at 50 g.
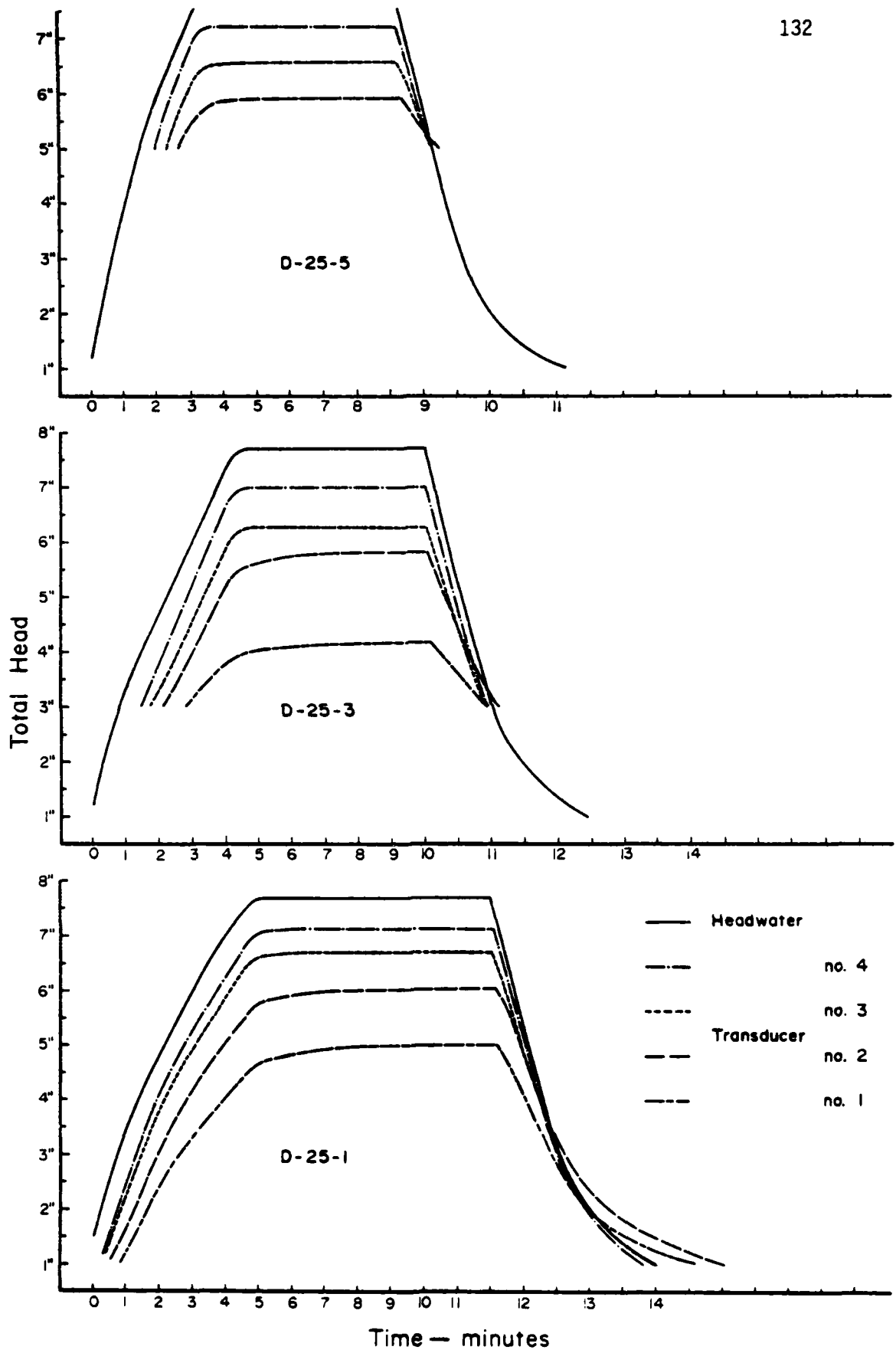
Figure A7. Total head versus time for D_{10} soil at 25 g.
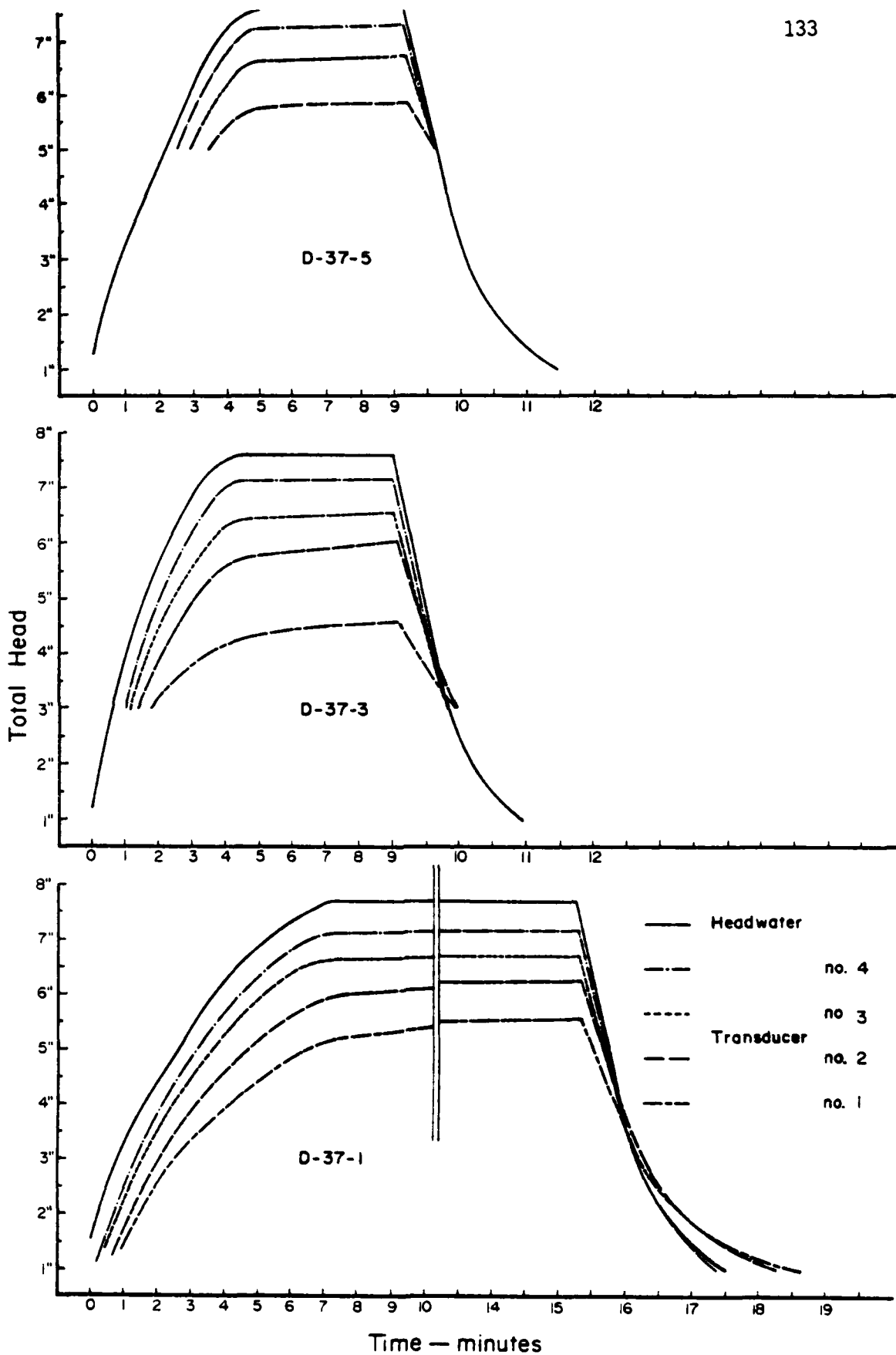
Figure A8. Total head versus time for D_{10} soil at 37.5 g.
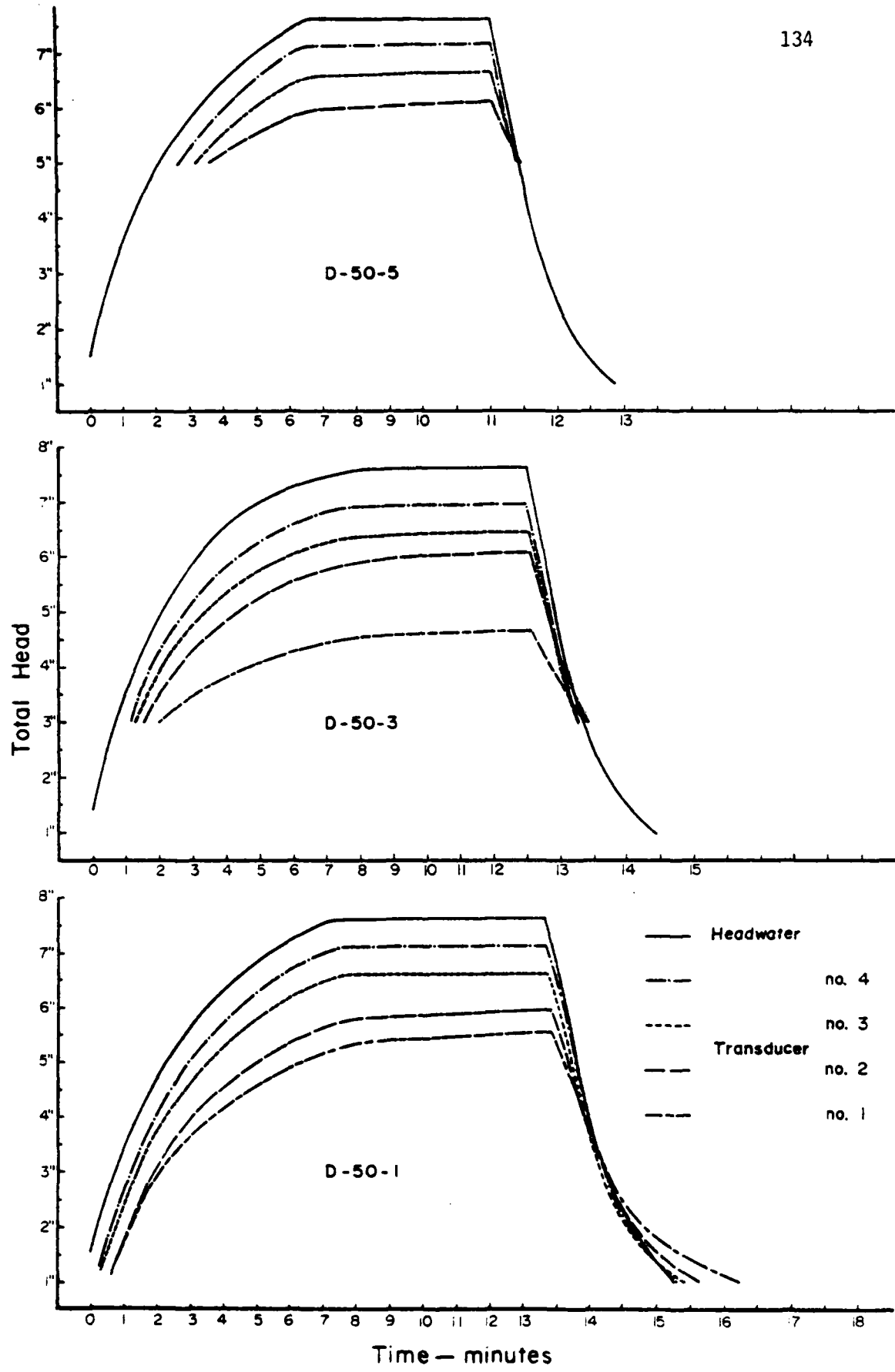
Figure A9. Total head versus time for D_{10} soil at 50 g.
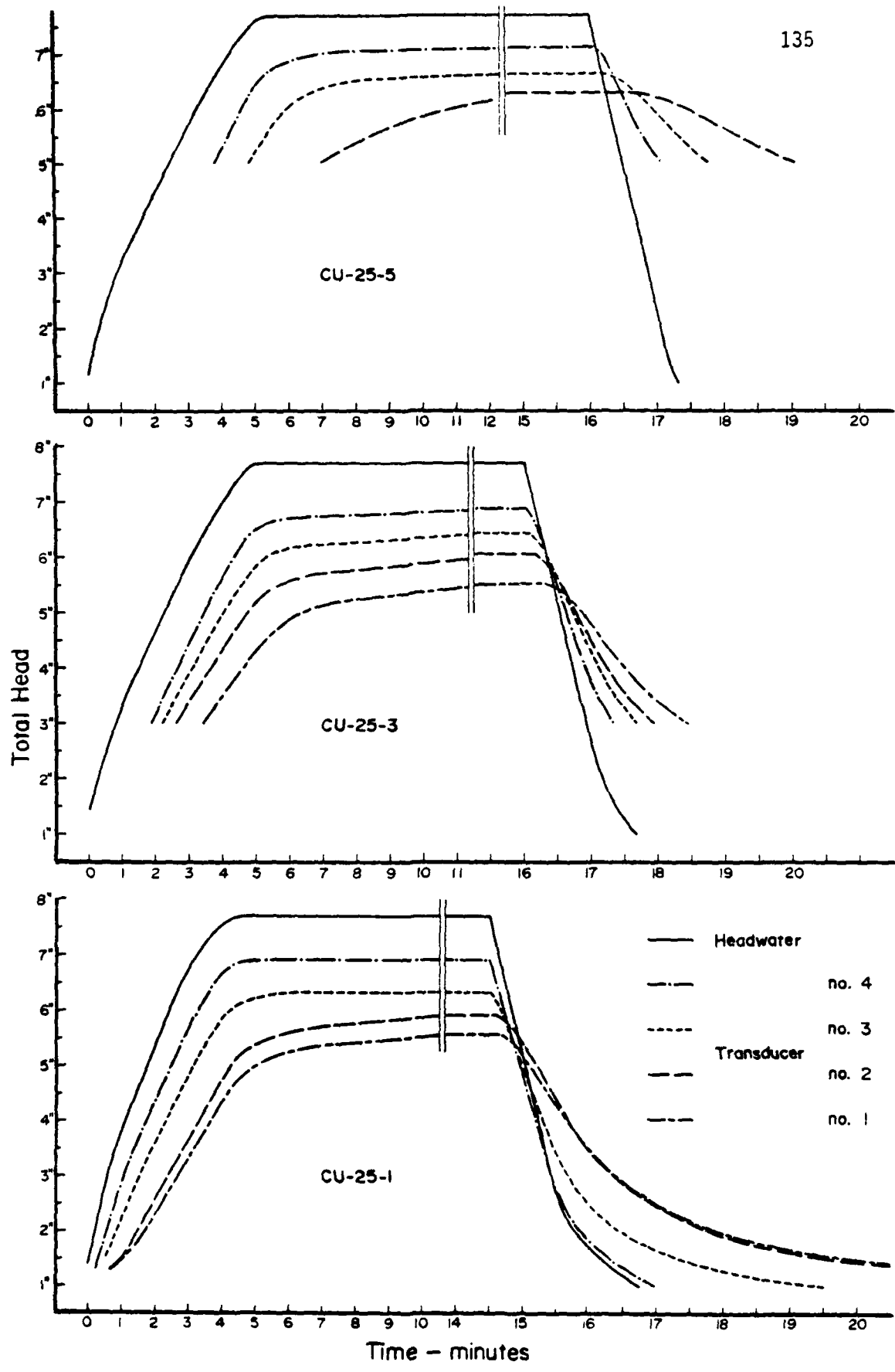
Figure A10. Total head versus time for CU soil at 25 g.
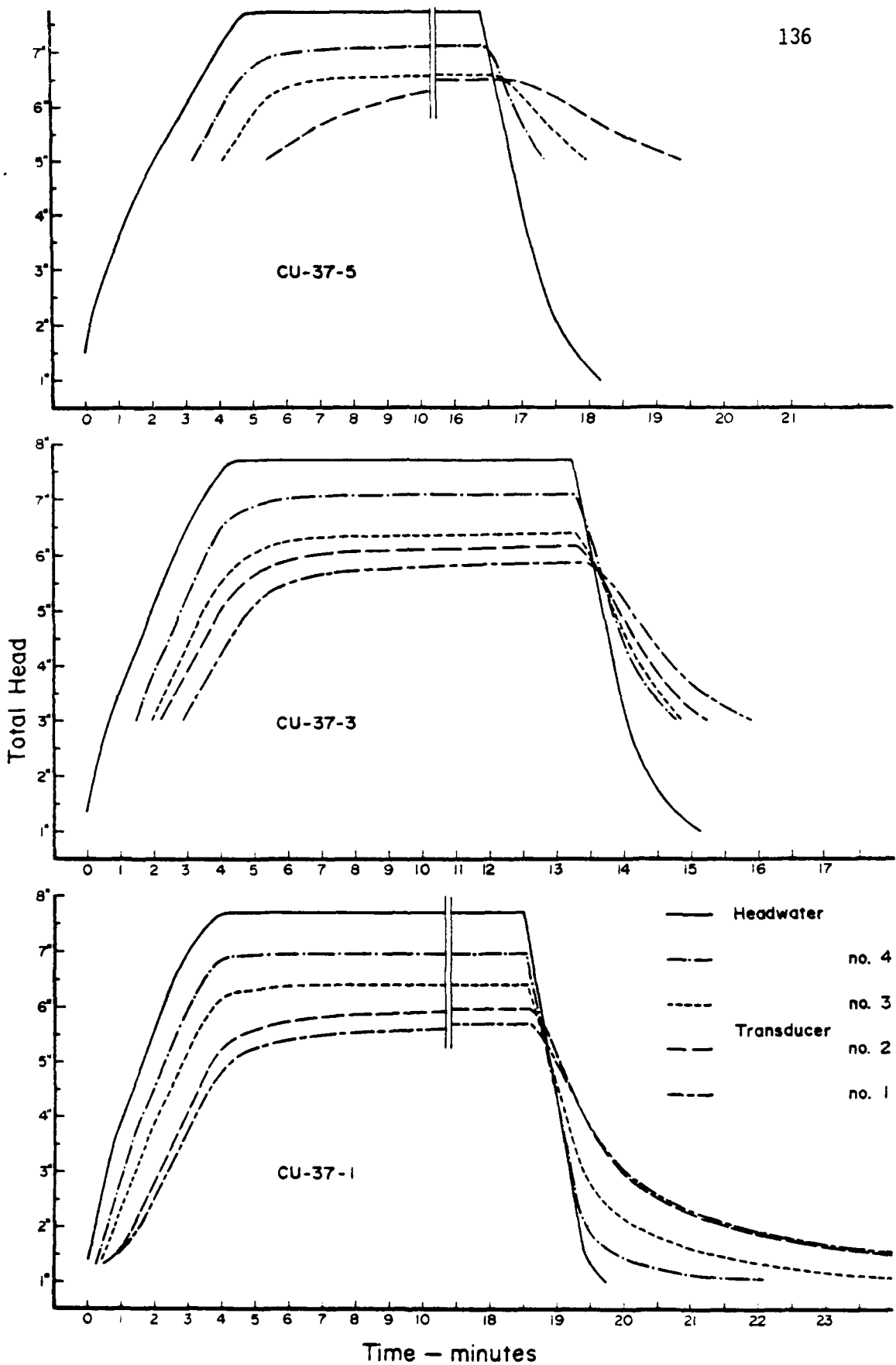
Figure A11. Total head versus time for CU soil at 37.5 g.
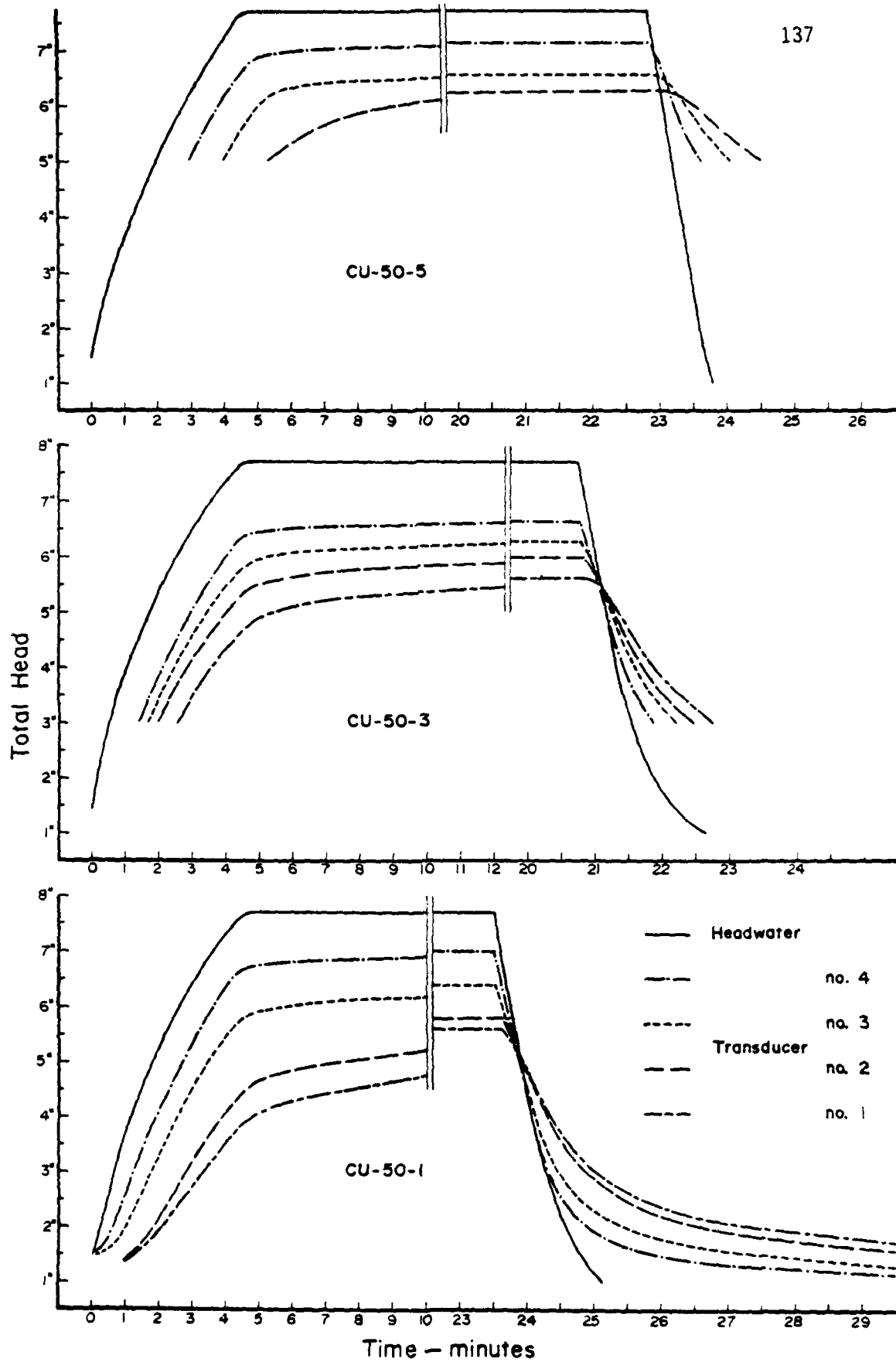
Figure A12.   Total head versus time for CU soil at 50 g.
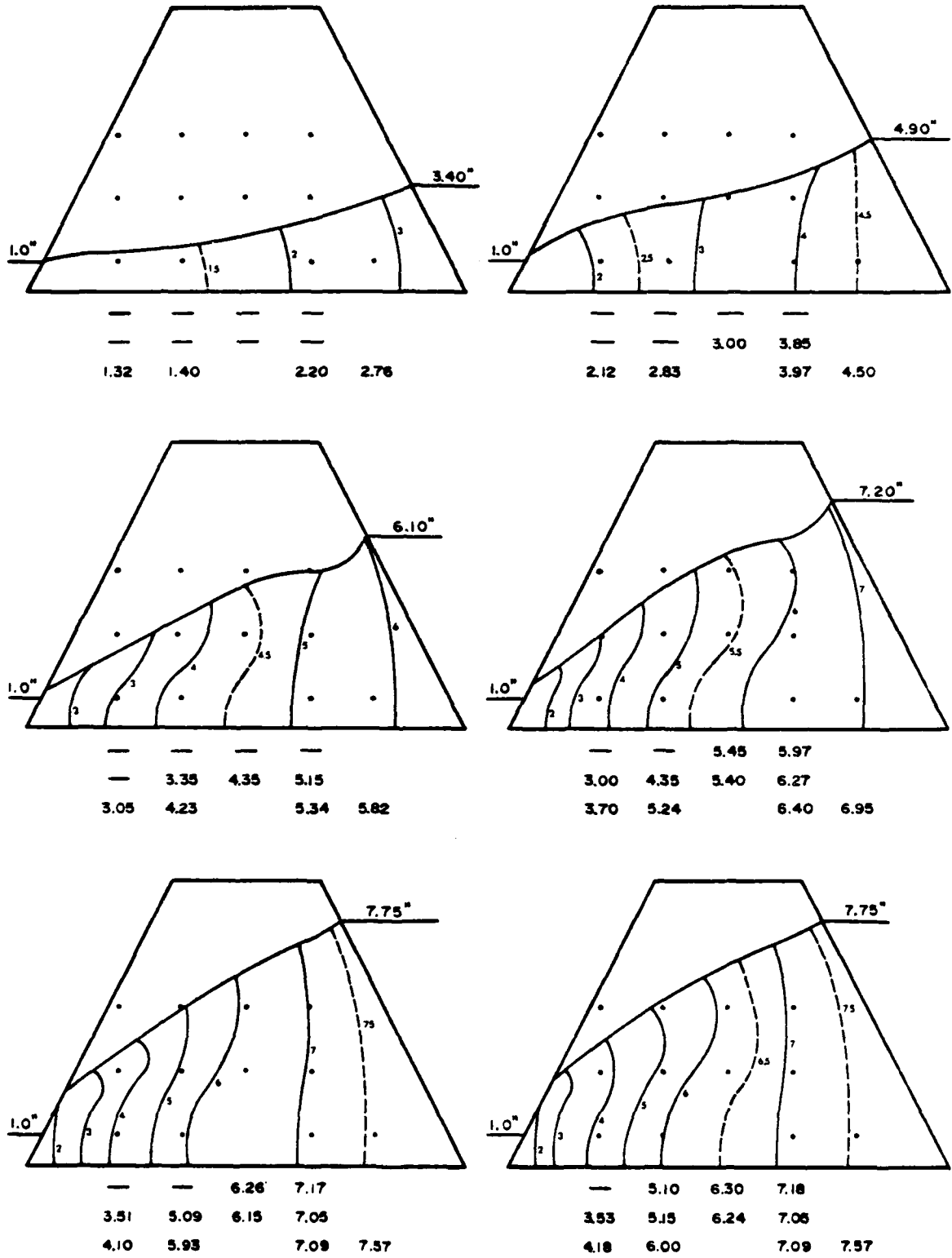
Figure A13.   Equipotentials during headwater rise for OR soil at 25 g.
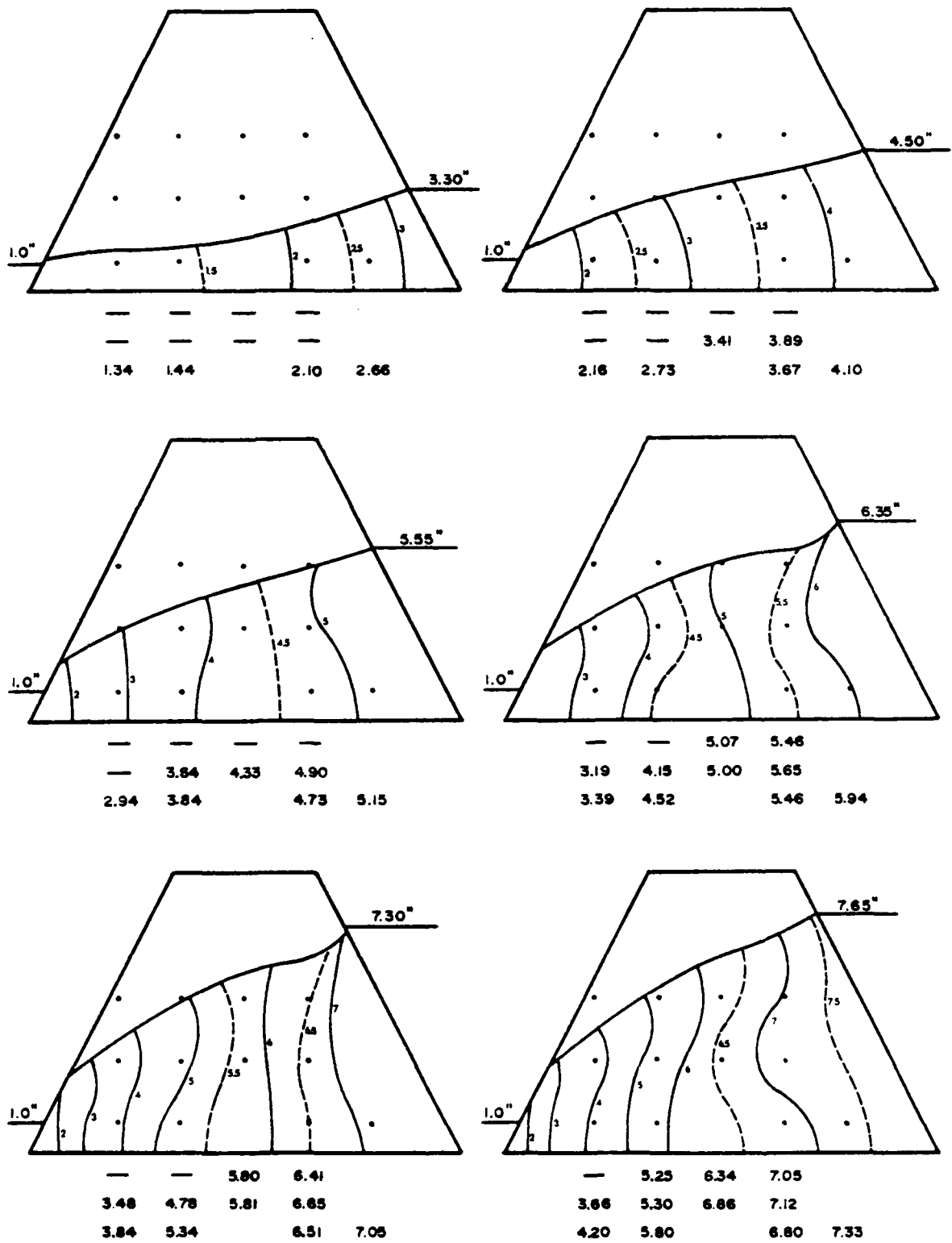
Figure A14. Equipotentials during headwater rise for OR soil at 37.5 g.
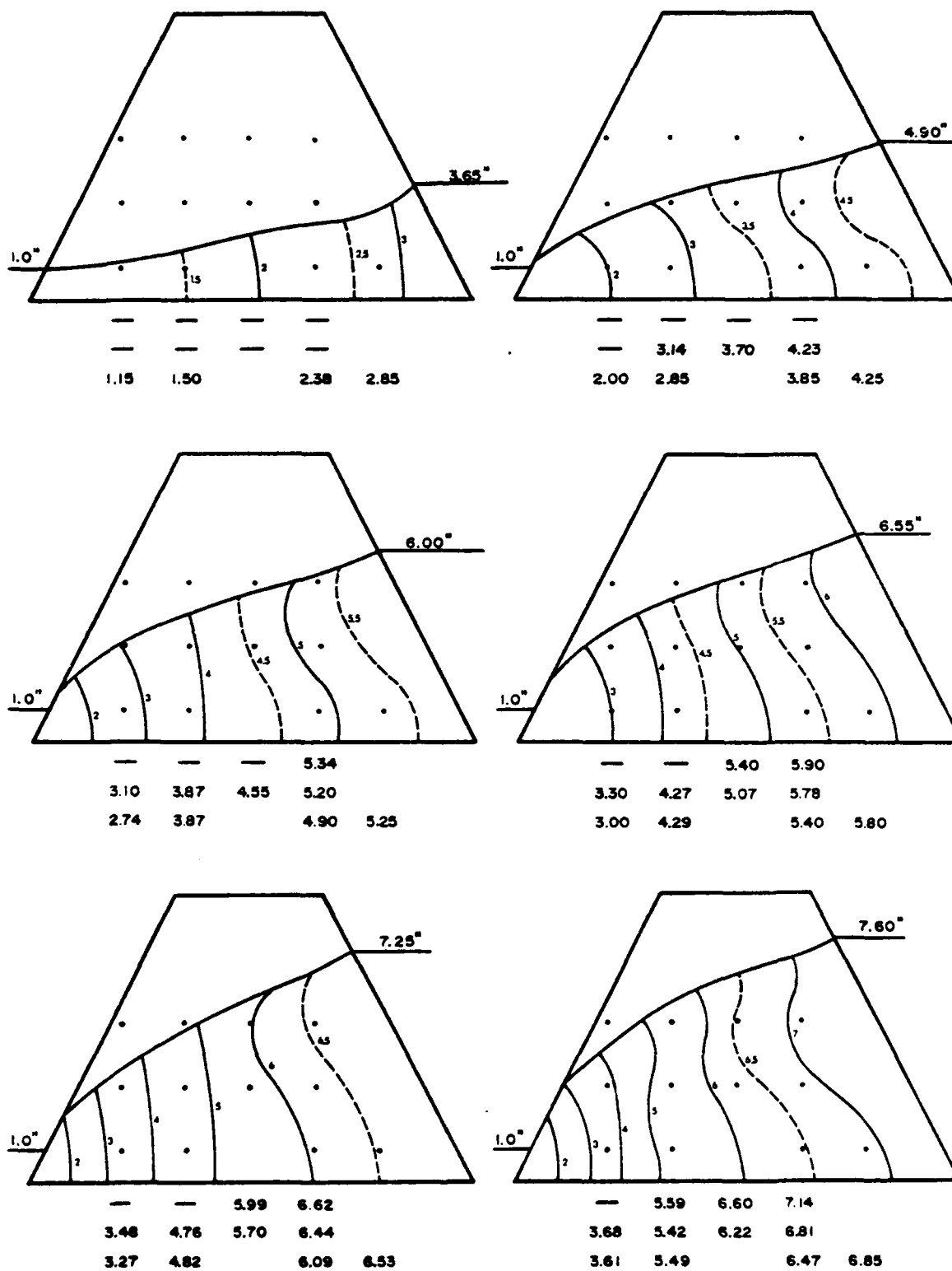
Figure A15. Equipotentials during headwater rise for OR soil at 50 g.
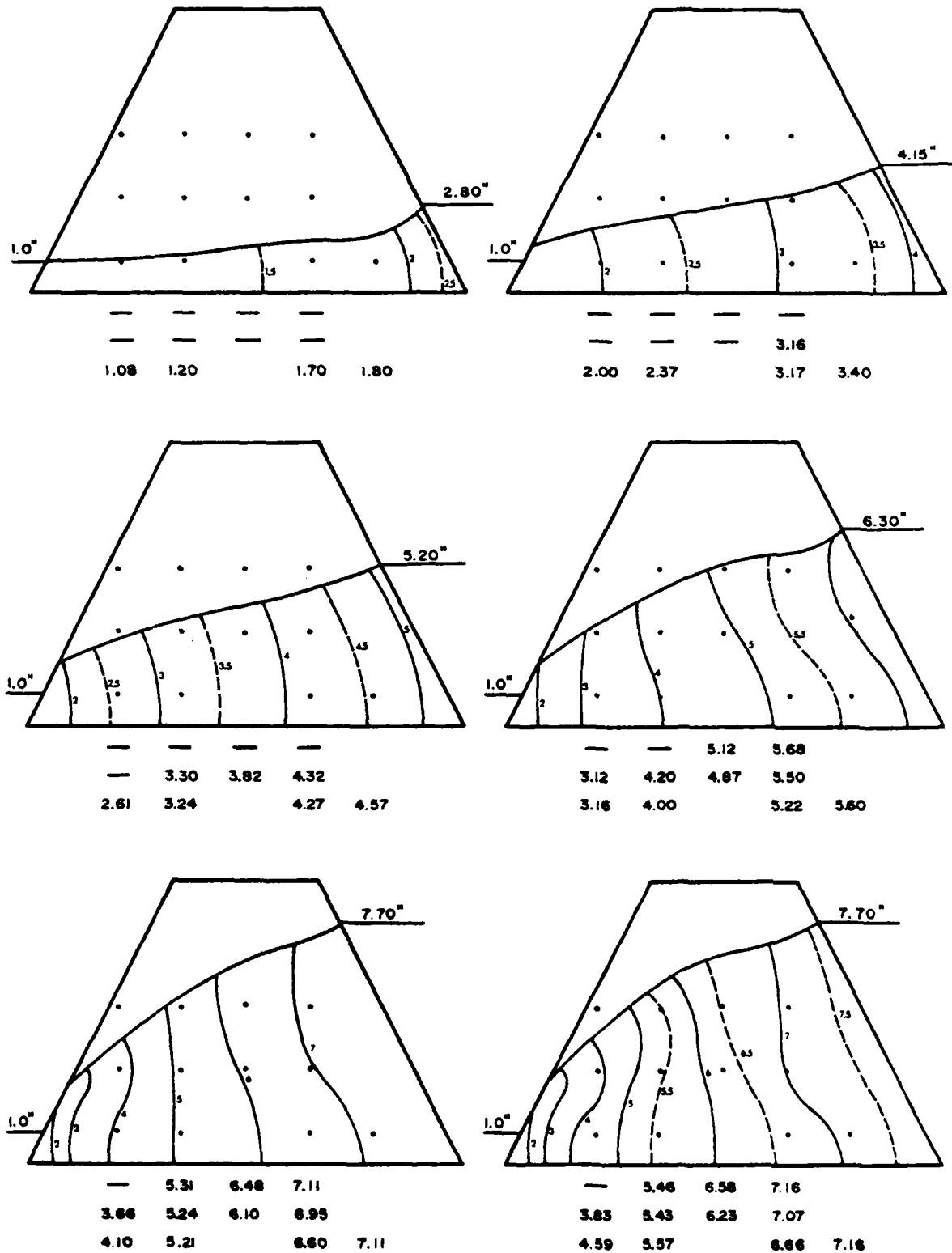
Figure A16. Equipotentials during headwater rise for CR soil at 25 g.
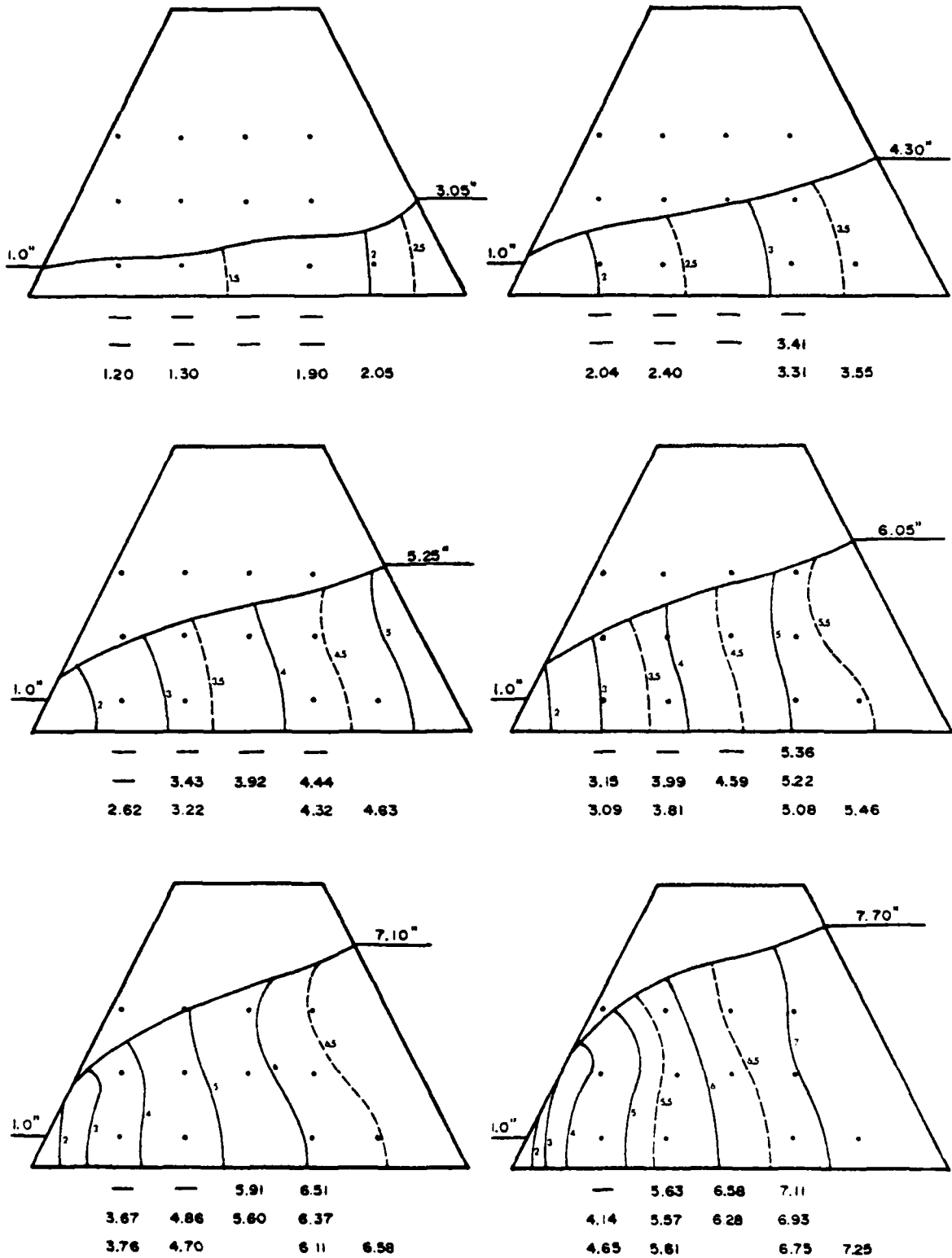
Figure A17. Equipotentials during headwater rise for CR soil at 37.5 g.
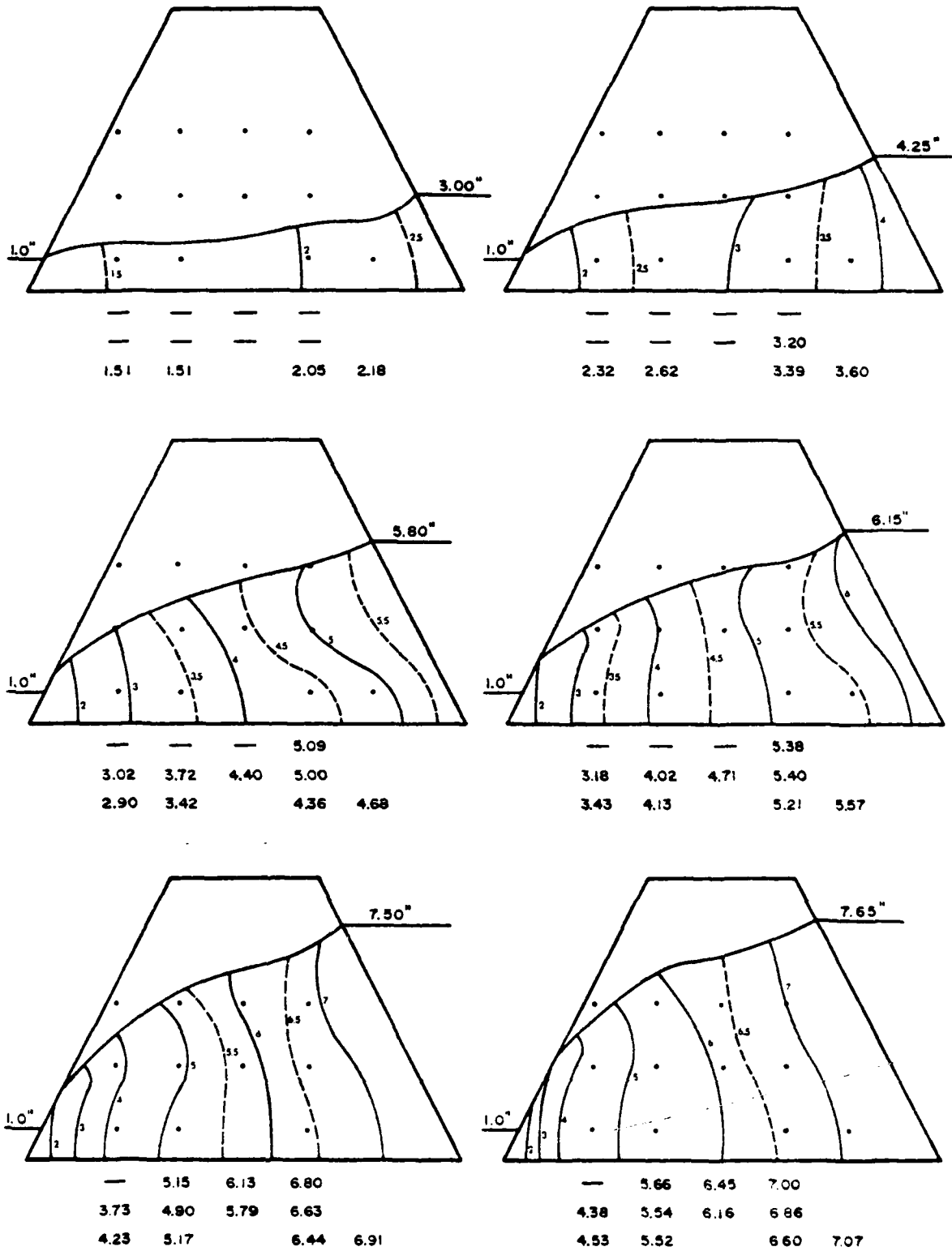
Figure A18. Equipotentials during headwater rise for CR soil at 50 g.
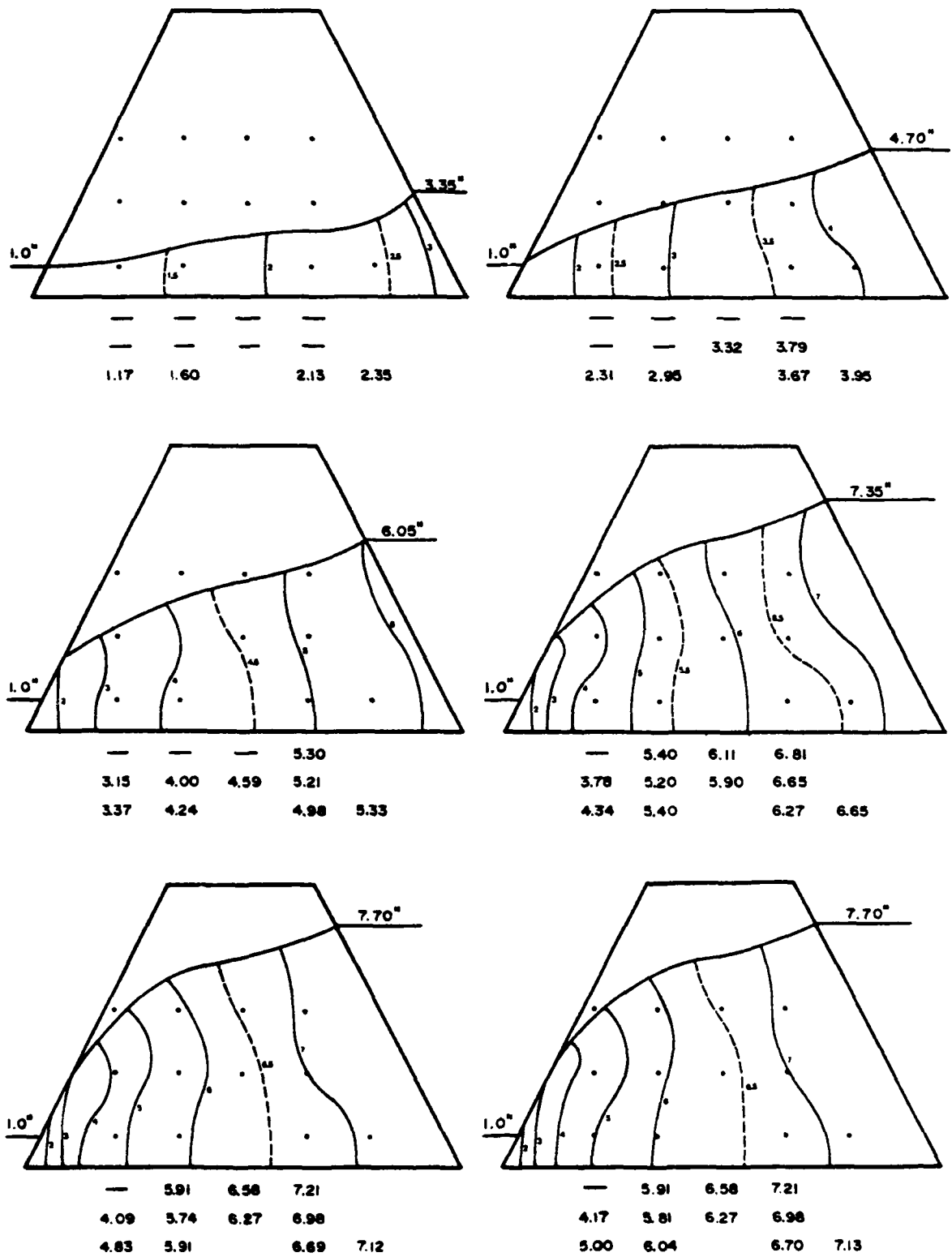
Figure A19. Equipotentials during headwater rise for D_{10} soil at 25 g.
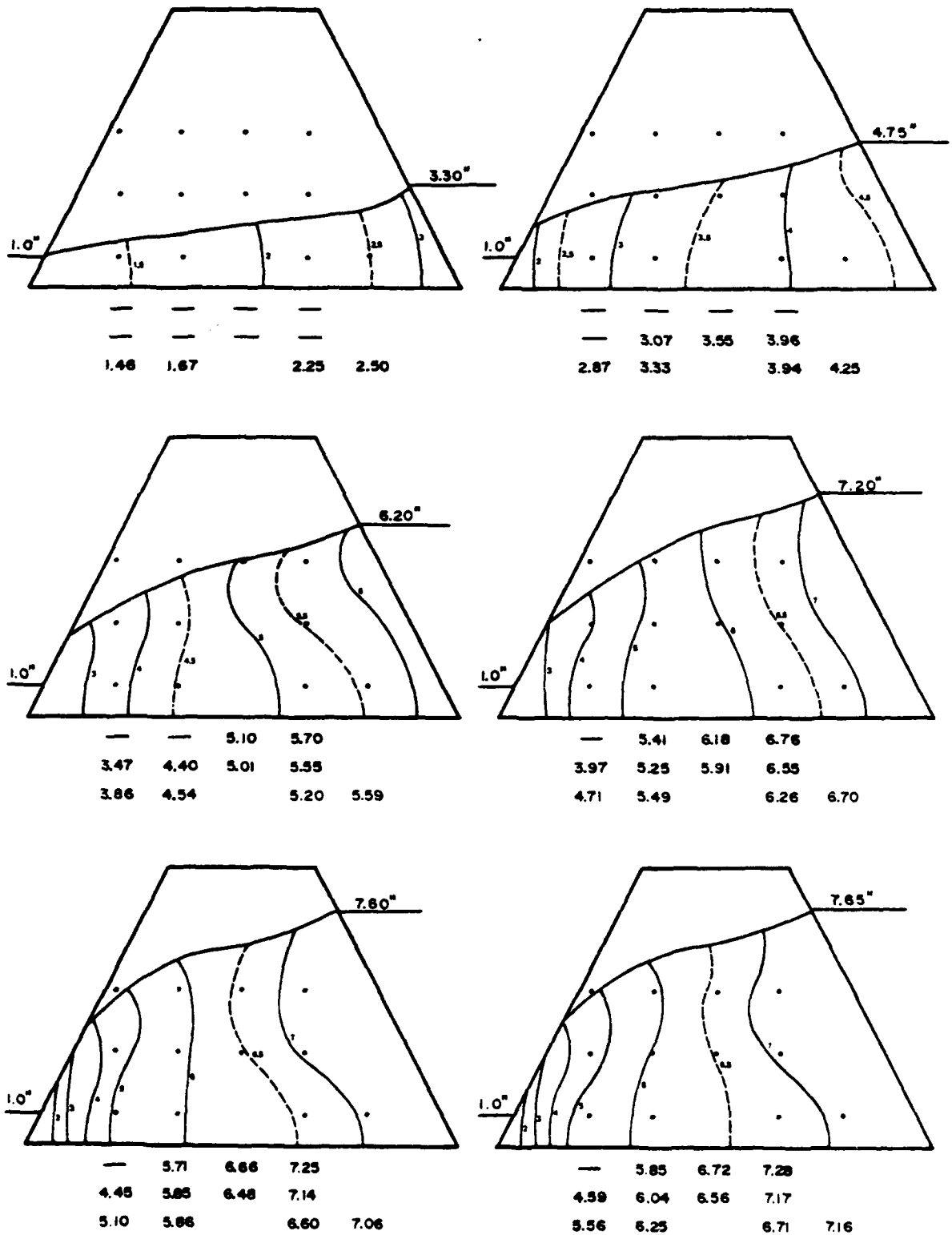
Figure A20. Equipotentials during headwater rise for D_{10} soil at 37.5 g.
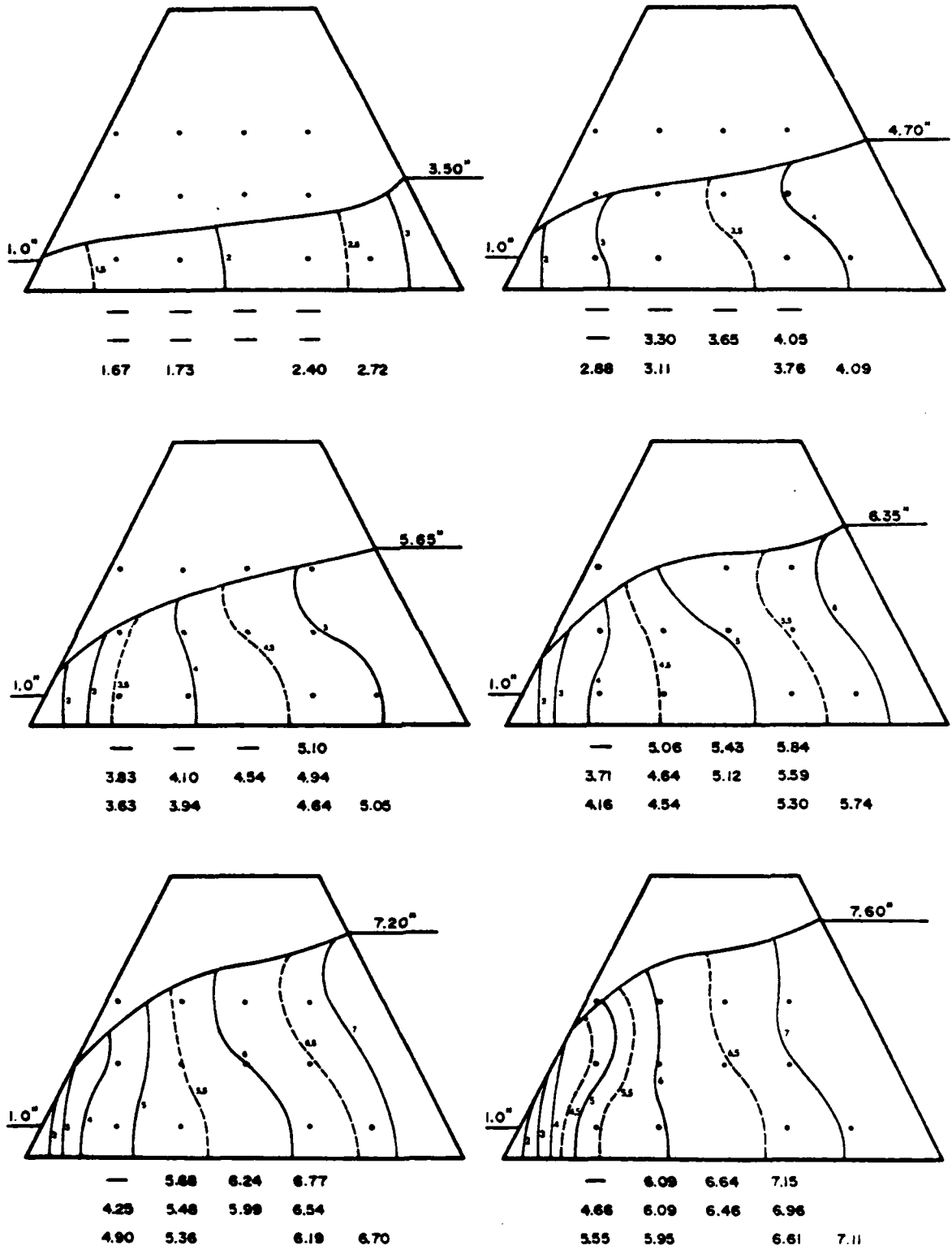
Figure A21. Equipotentials during headwater rise for D_{10} soil at 50 g.
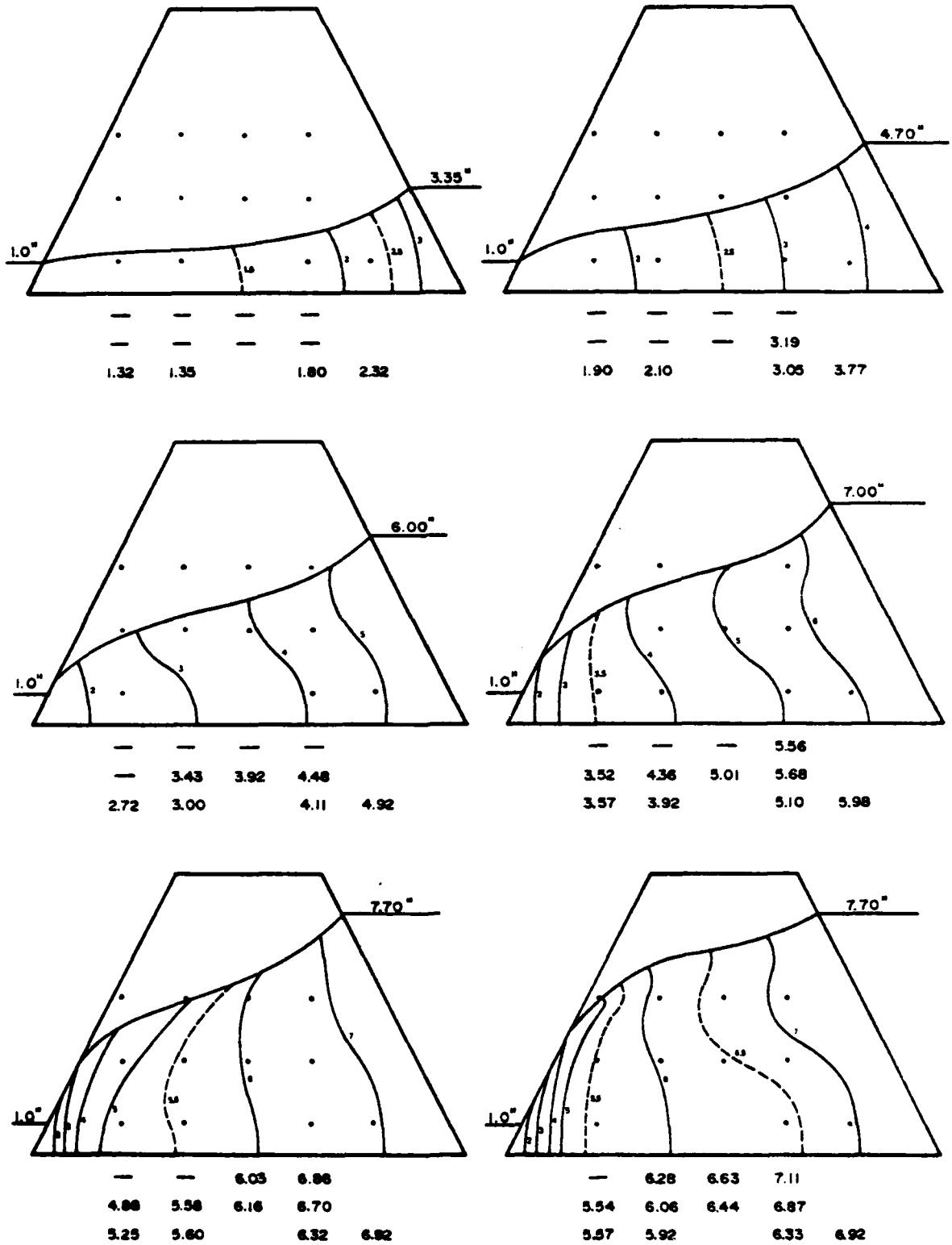
Figure A22. Equipotentials during headwater rise for CU soil at 25 g.
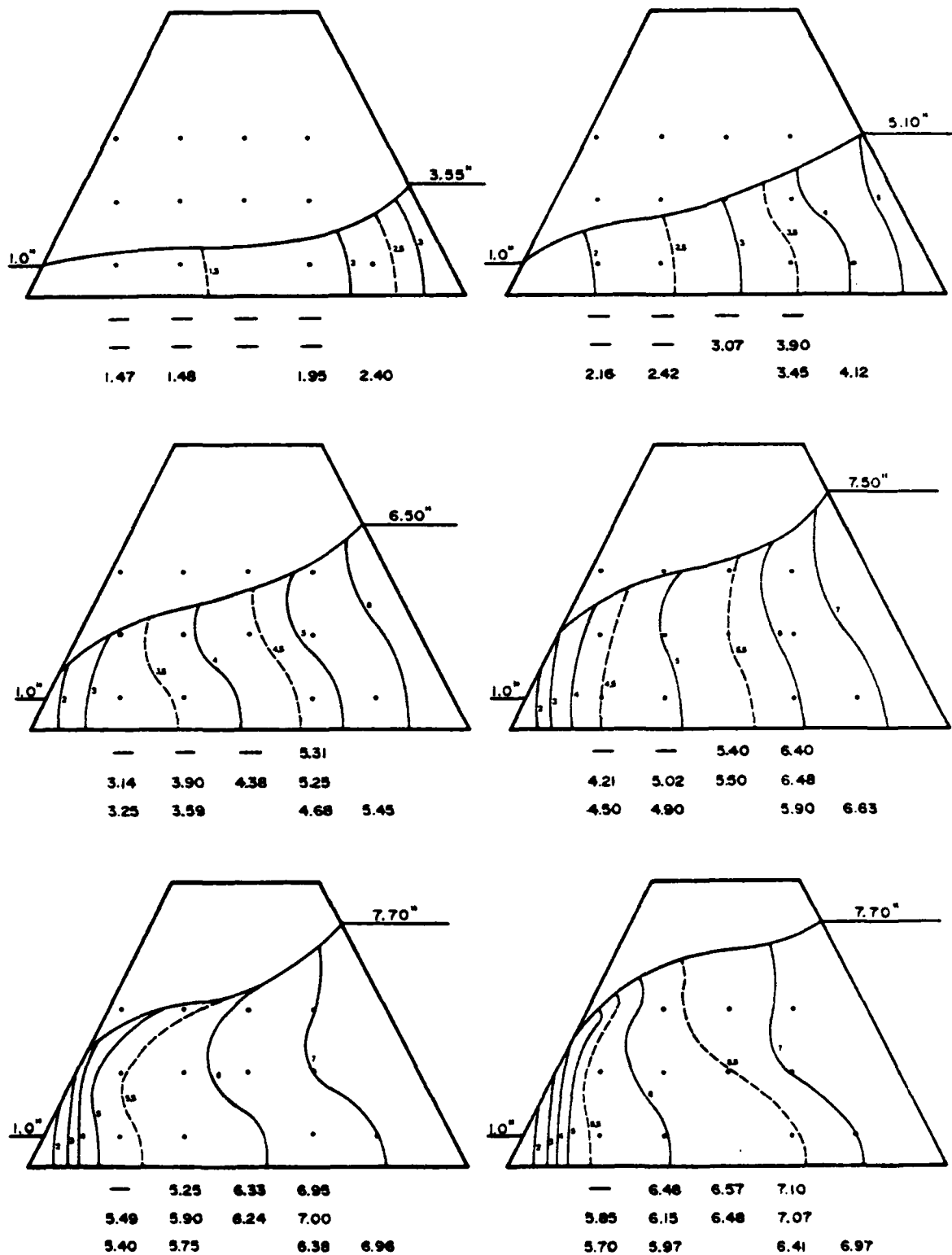
Figure A23. Equipotentials during headwater rise for CU soil at 37.5 g.
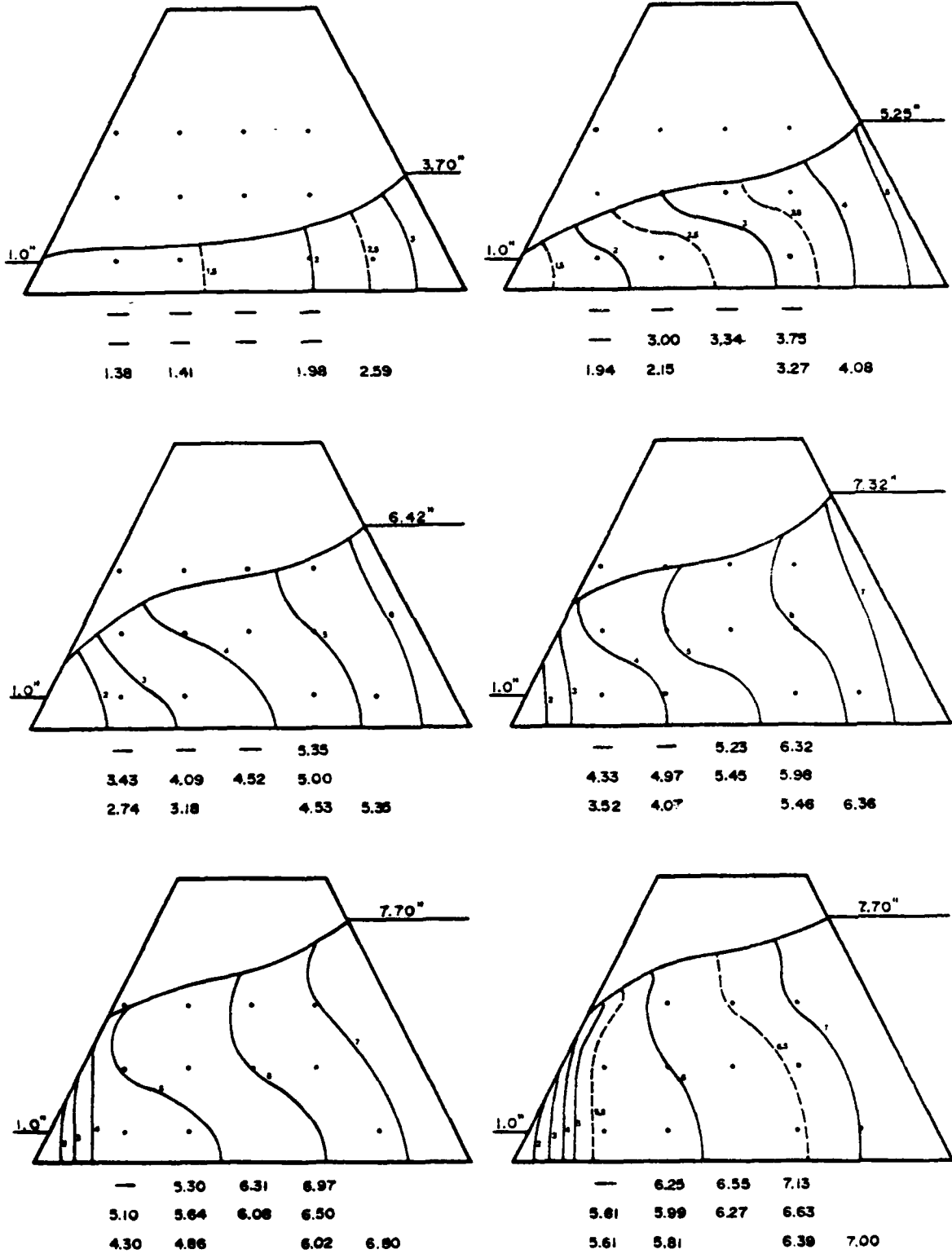
Figure A24.   Equipotentials during headwater rise for CU soil at 50 g.

150
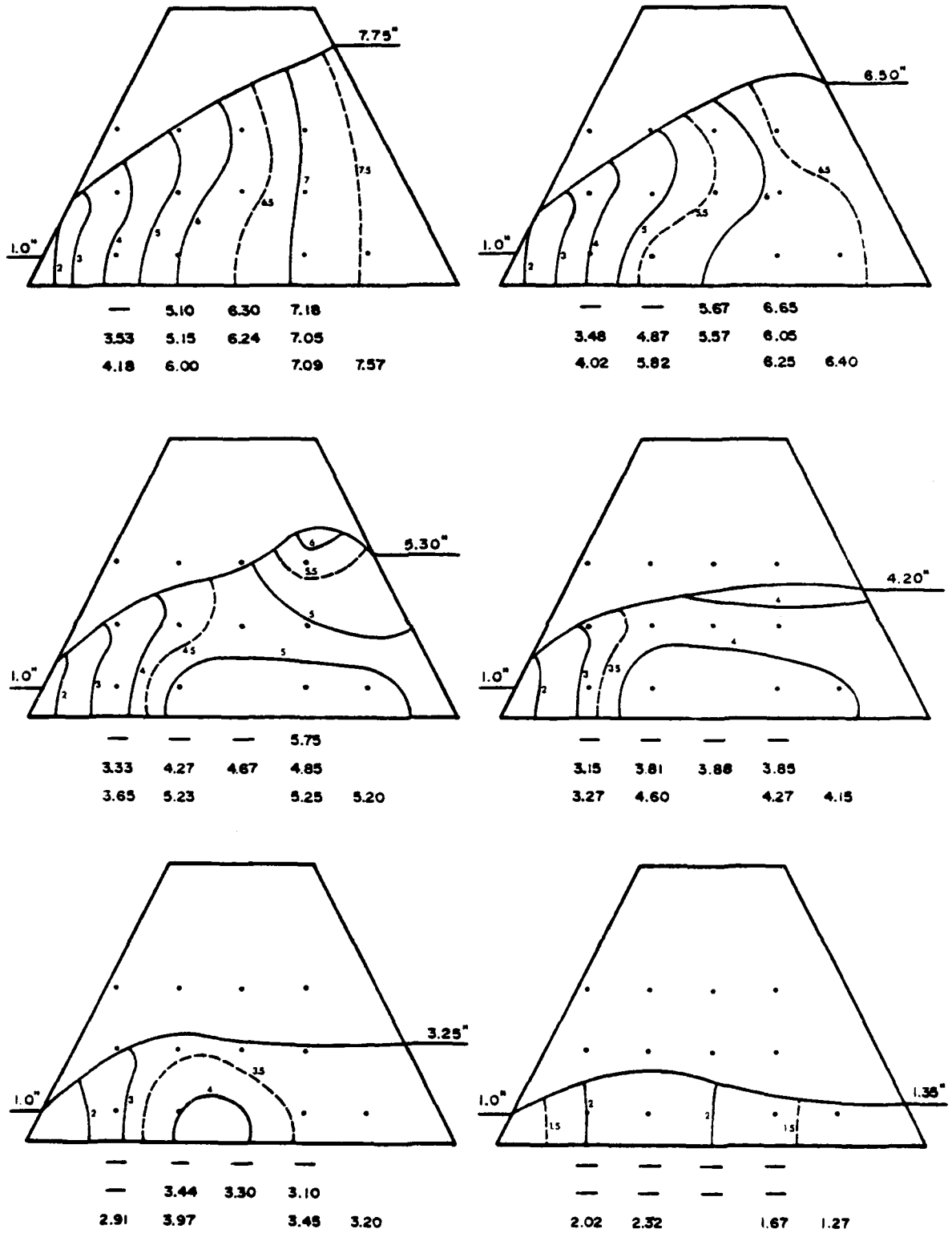

Figure A25. Equipotentials during drawdown for OR soil at 25 g.
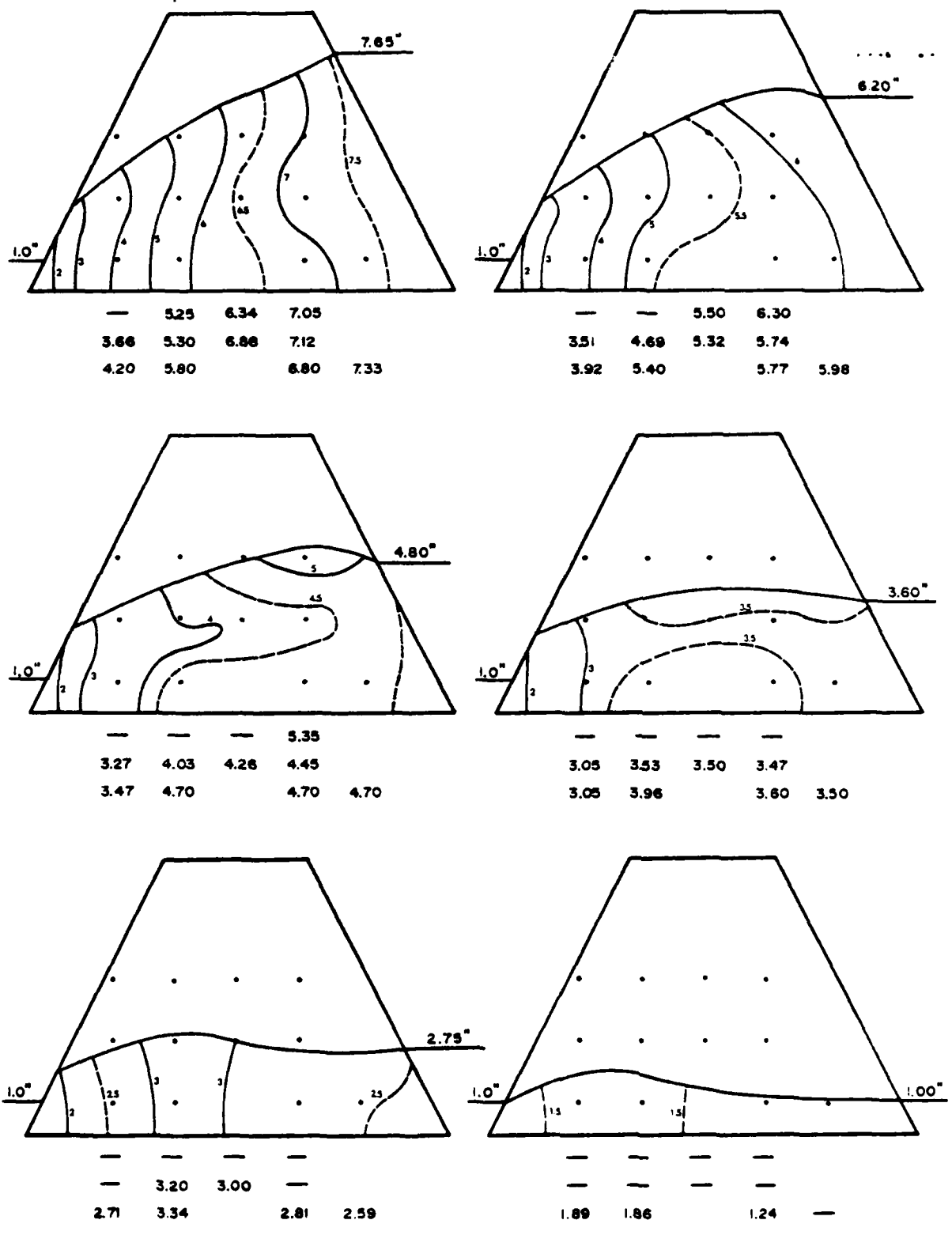
Figure A26. Equipotentials during drawdown for OR soil at 37.5 g.
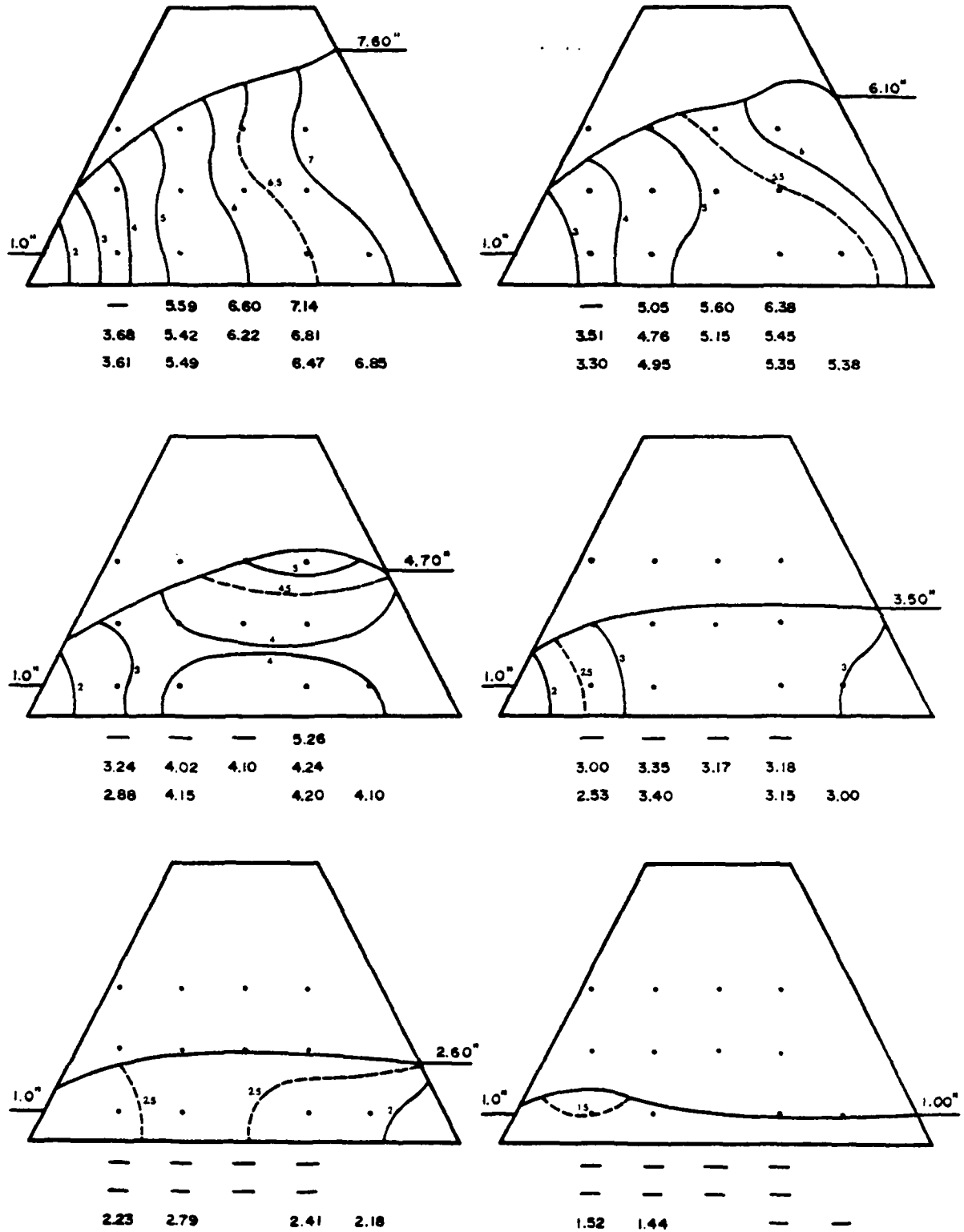
Figure A27. Equipotentials during drawdown for OR soil at 50 g.
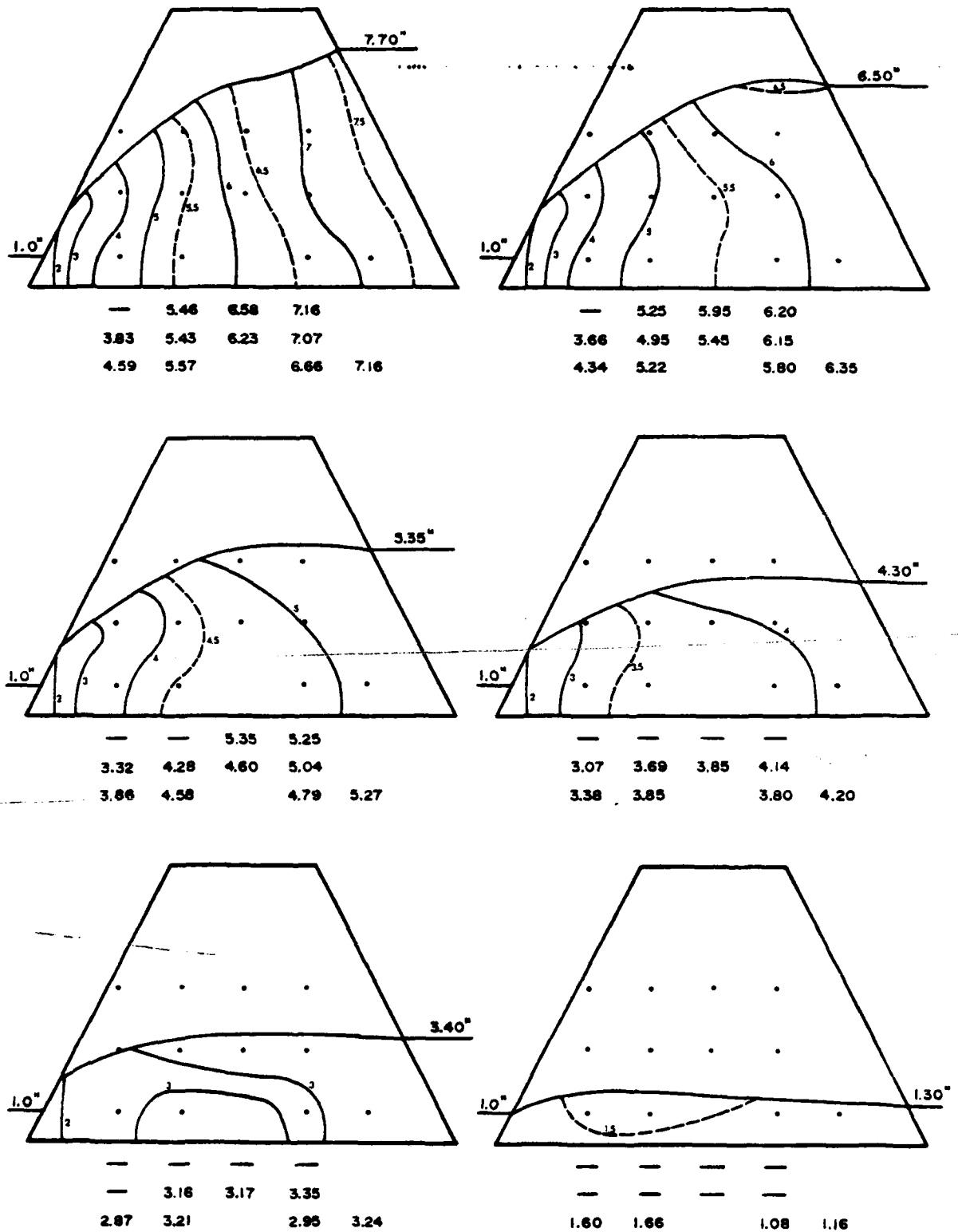
Figure A28. Equipotentials during drawdown for CR soil at 25 g.
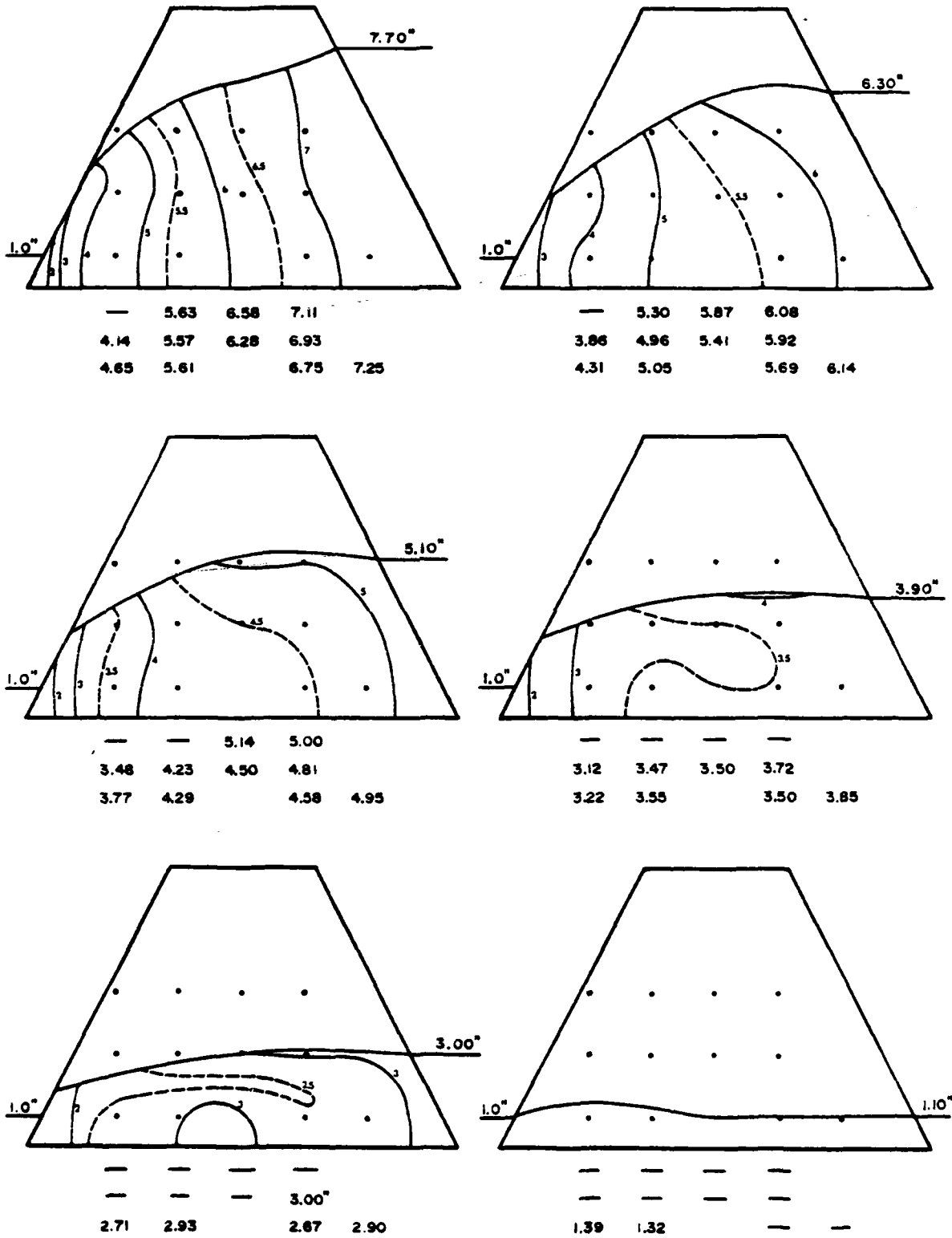
Figure A29. Equipotentials during drawdown for CR soil at 37.5 g.
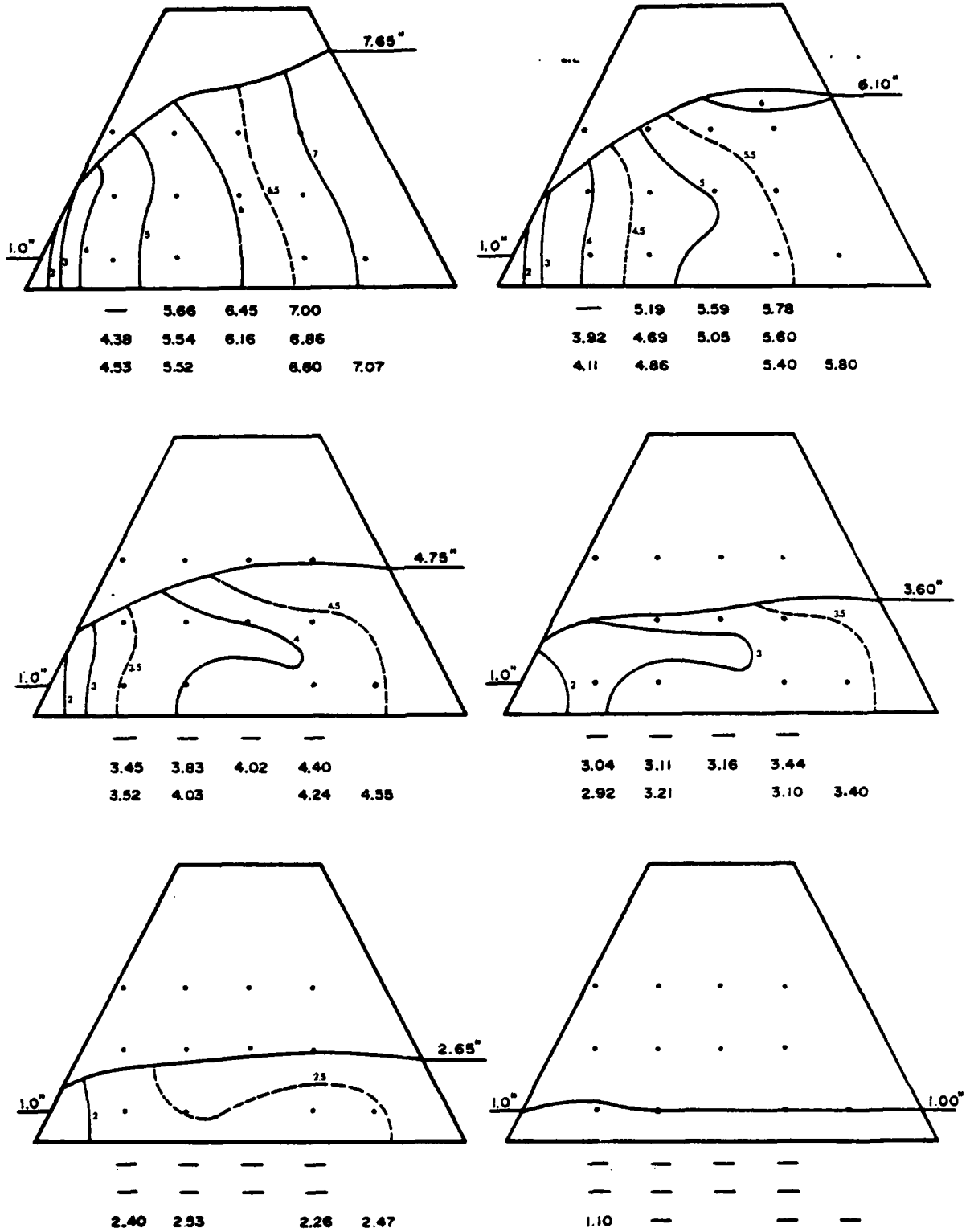
Figure A30. Equipotentials during drawdown for CR soil at 50 g.
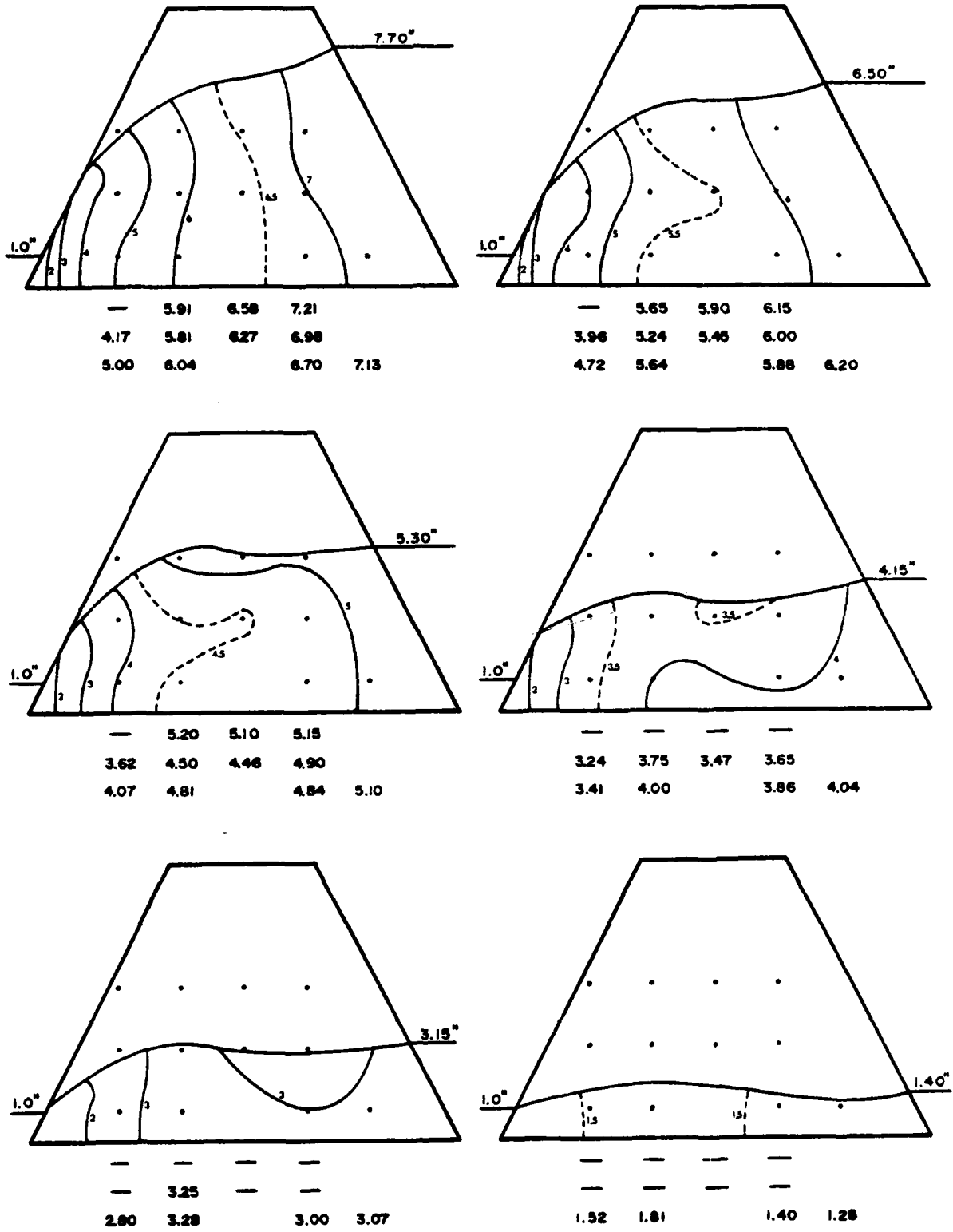
Figure A31. Equipotentials during drawdown for D_{10} soil at 25 g.
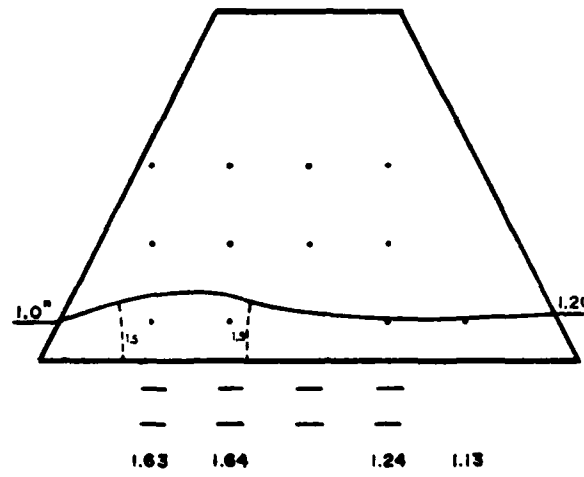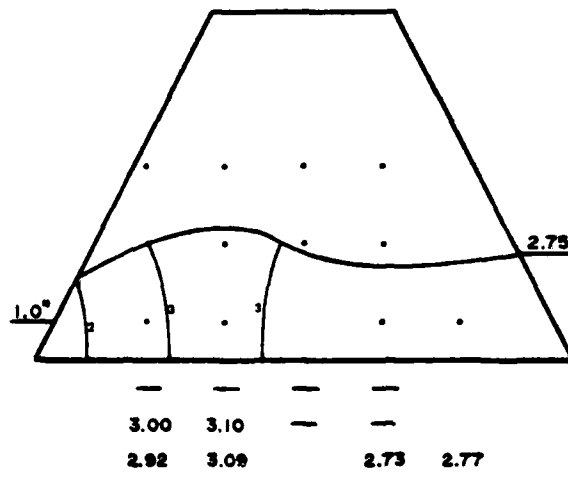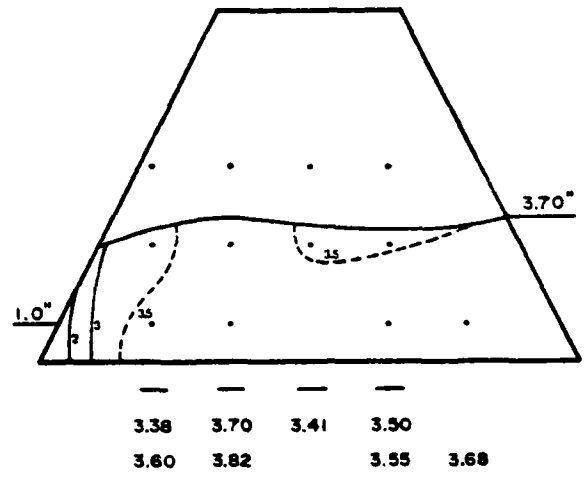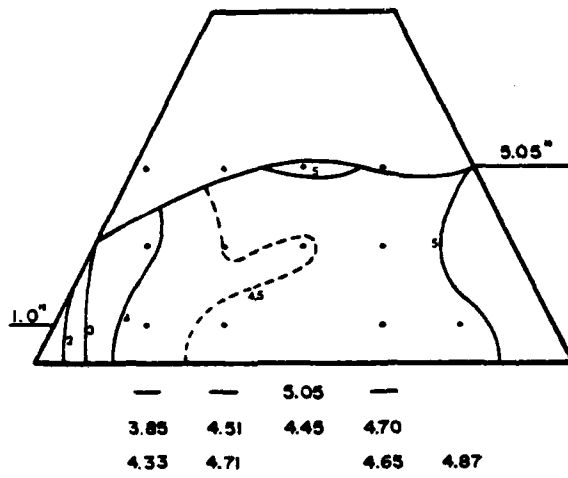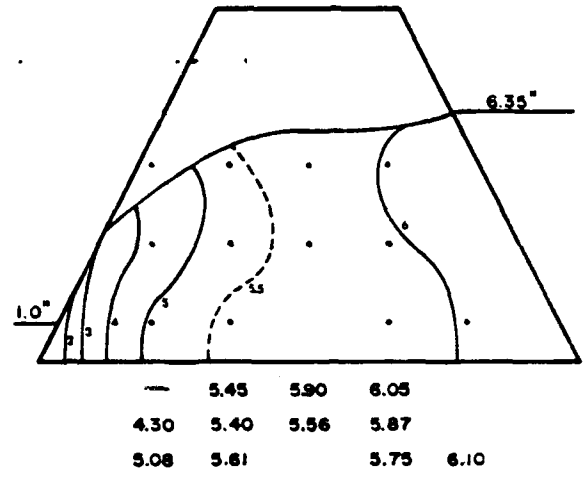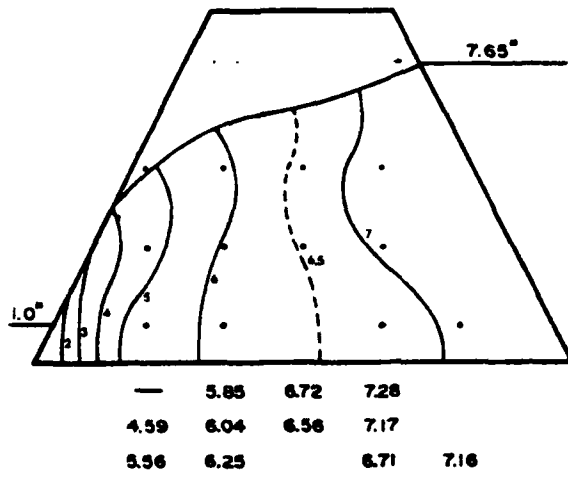
Figure A32. Equipotentials during drawdown for D_{10} soil at 37.5 g.
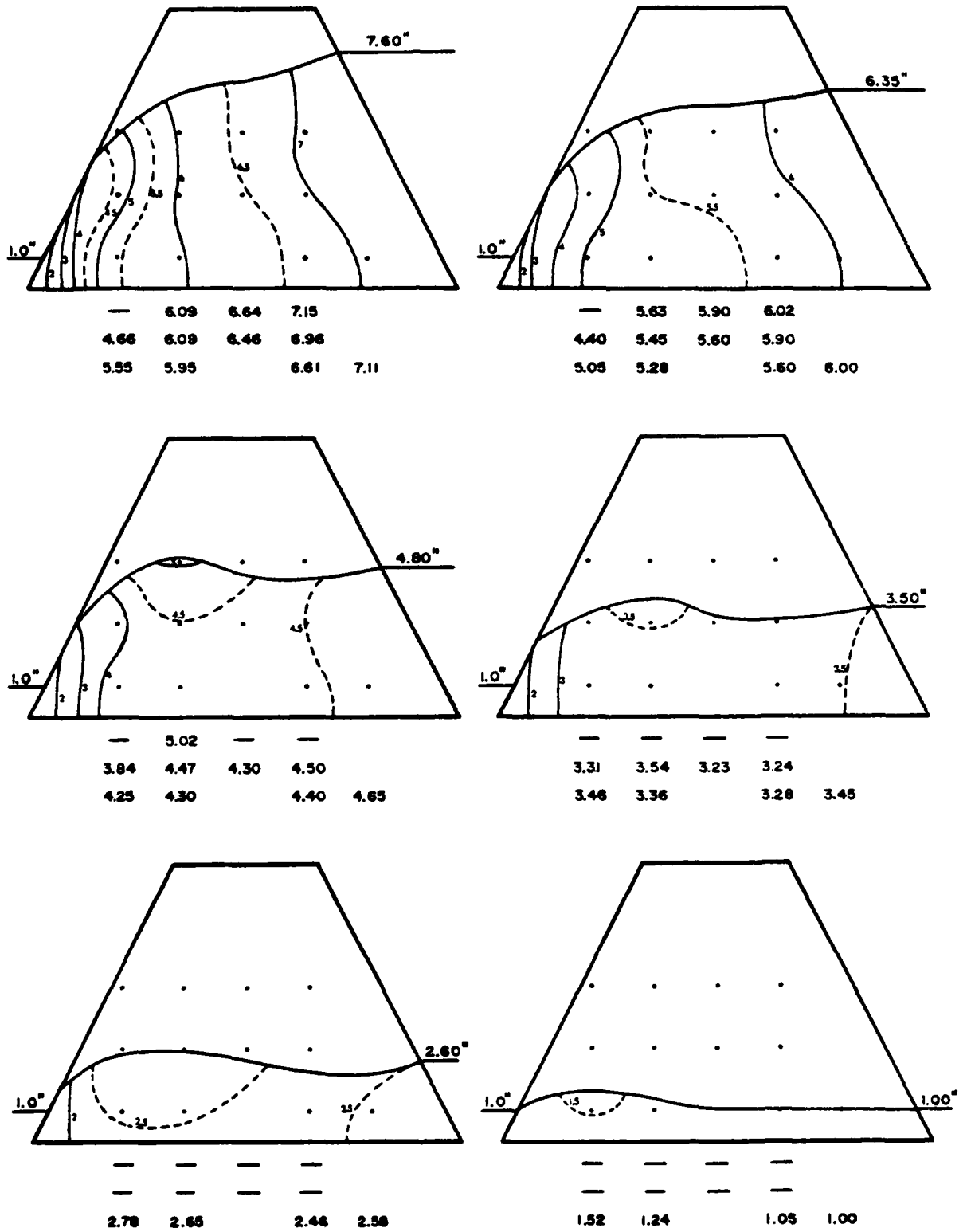
Figure A33. Equipotentials during drawdown for D_{10} soil at 50 g.
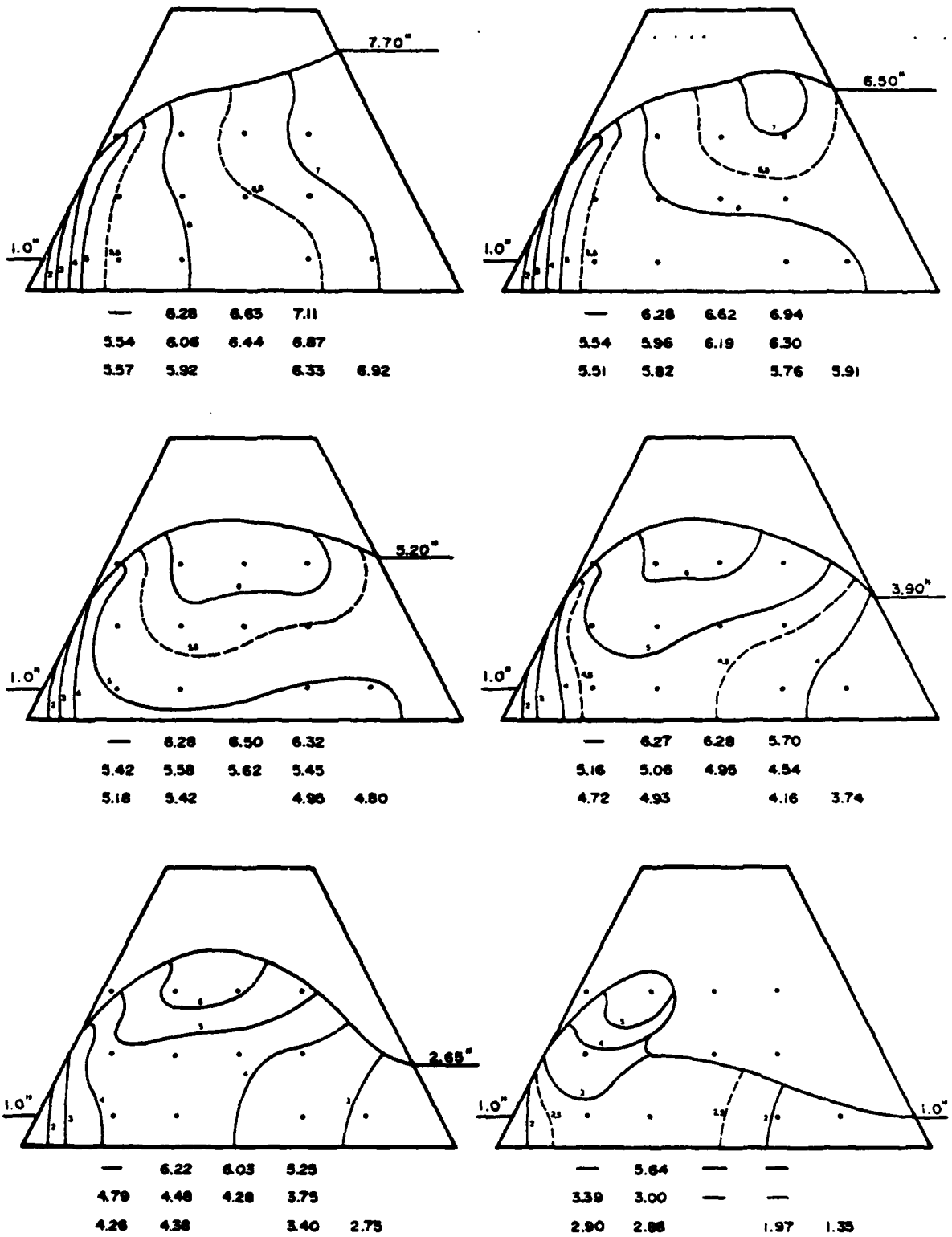
Figure A34. Equipotentials duirng drawdown for CU soil at 25 g.
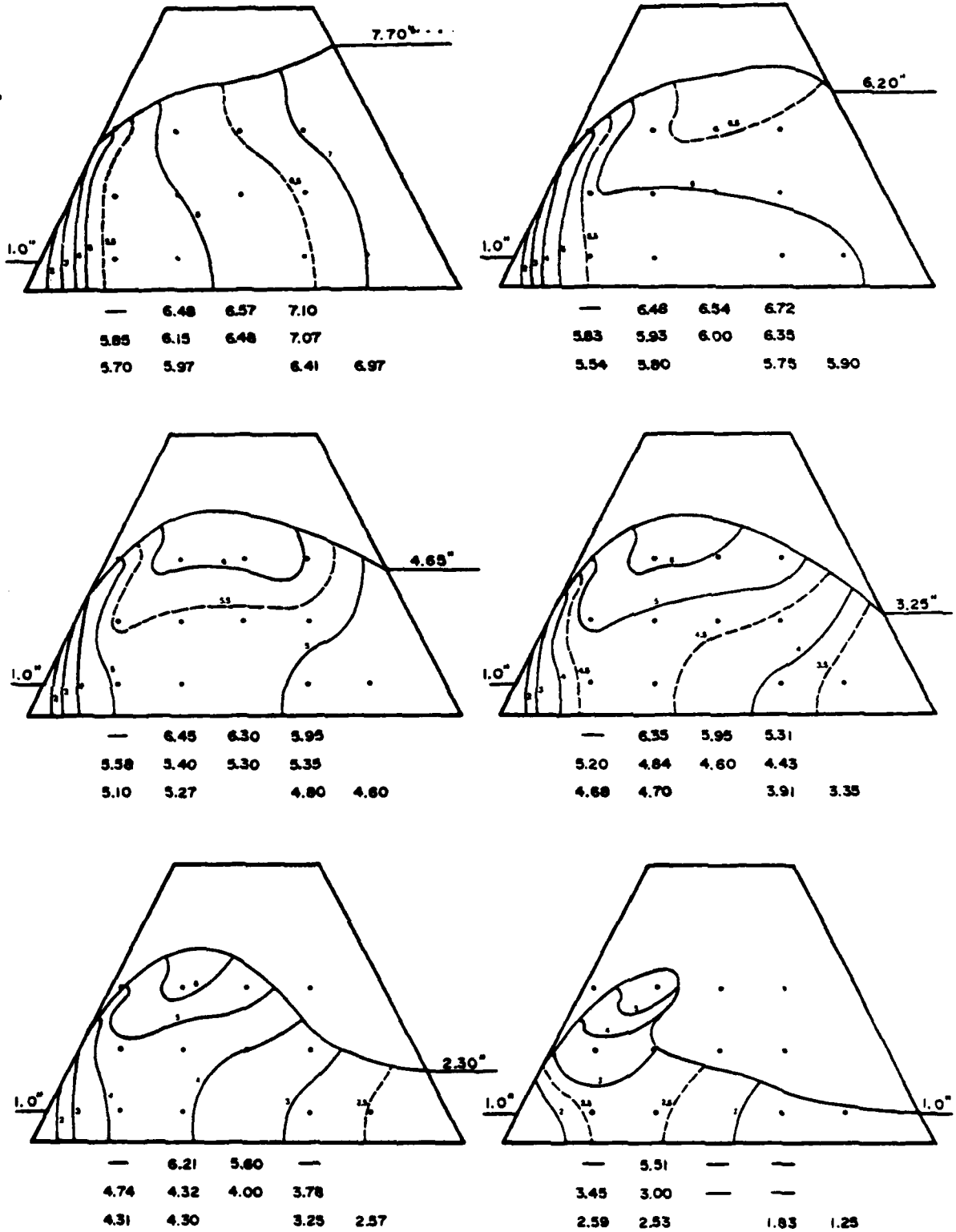
Figure A35. Equipotentials during drawdown for CU soil at 37.5 g.
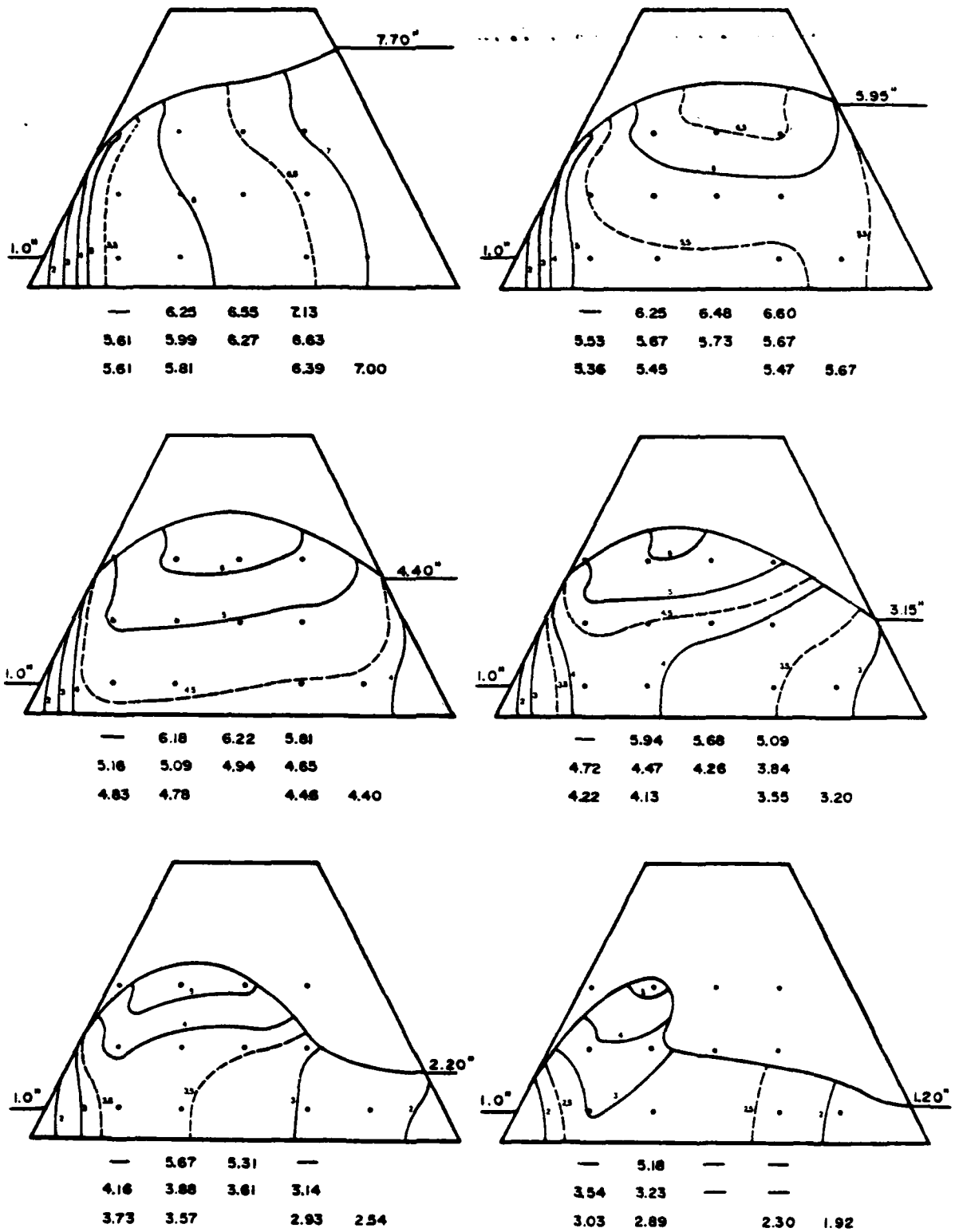
Figure A36. Equipotentials during drawdown for CU soil at 50 g.